Estimation of Radiated Emissions from Electrically large EUTs

Dissertation

zur Erlangung des akademischen Grades

Doktoringenieur

(Dr.-Ing.)

von **M. Sc. Xiaowei Wang**

geb. am 26.05.1987 in Qingdao, China

genehmigt durch die Fakultät für Elektrotechnik und Informationstechnik
der Otto-von-Guericke-Universität Magdeburg

Gutachter:

Univ.-Prof. Dr.-Ing. Ralf Vick

Univ.-Prof. Dr.-Ing. Heyno Garbe

Promotionskolloquium am 30. März 2021

„Stay positive and happy. Work hard and don't give up hope. Be open to criticism and keep learning. Surround yourself with happy, warm and genuine people."

Tena Desae

Abstract

With the increasing application of faster switching electronics and digital computers with high clock frequencies, a PC-size enclosure becomes electrically large, in comparison with the wavelength. The concept of 'electrically large' is characterized by the geometrical size and the considered frequency. Such devices radiate unintentional electromagnetic waves through slots, sockets and ventilation vents, which could be considered as 'unintentional radiators'. The focus of this work is to determine the radiated emission of an electrically large equipment under test (ELEUT). A rectangular slotted metallic enclosure was considered to be an ELEUT, which is comparable to personal computers or other electronic devices. Another configuration with connecting wires attached to the ELEUT has been also investigated.

In order to reduce the risk of interferences from these devices, the radiated emission can be measured via different EMC test methods. In general, these emission measurement methods can be classified to electric-field-based or total-power-based methods. The electric-field-based measurement method is denoted as the classical method, the corresponding measurement environments are e. g., open area test sites, semi-anechoic chambers and fully anechoic rooms. Typical total-power-based measurement methods are conducted in mode-stirred chamber (MSC)s and gigahertz transverse electromagnetic cells. The relation between these two methods is connected by the directivity, which allows the conversion of the total radiated power to the electric field strength.

The motivation in this work is to apply the MSC as the alternative test methods (ATM) to measure the total radiated power of the ELEUTs, which is irrelevant to the radiation patterns of the ELEUTs. The enhanced robustness of measurements in the MSC makes it a rigorous EMC test environment, which has been recognized as a suitable alternative measurement technique. The maximum electric field strength of ELEUTs can be determined by the combination of the total radiated power measurement in the MSC and the estimated directivity of the EUTs. The maximum directivity of the ELEUTs can be achieved by an analytical approximation or a numerical simulation.

In order to determine the radiated emission of ELEUT, three variants will be applied in this work. In variant 1, the conversion procedure introduced in CISPR 16-4-5 is applied to the ELEUTs, which can be compared with the existing limit of the FAR. In variant 2, the total radiated power can be converted to an equivalent electric field strength, with the help of the directivity. These two methods depends on the number of EUTs and could not be directly compared with the measured total radiated power, which is not very practical. Based on variant 3, the new power limit of the MSC is derived, which could directly compare with the measured total radiated power. This method is very helpful and could be applied for further research.

Kurzfassung

Durch die zunehmende Anwendung von leistungselektronischen Wandlern mit hohen Schaltfrequenzen bzw. durch Digitalschaltungen mit hohen Taktfrequenzen müssen entsprechend ausgestattete Geräte als elektrisch groß (also größer als die betrachtete Wellenlänge) aufgefasst werden. Der Begriff „elektrisch groß“ ist durch die geometrische Größe und die betrachtete Frequenz charakterisiert. Solche Geräte strahlen elektromagnetische Wellen durch Schlitze, Öffnungen und Durchführungen im Gehäuse ab und können als „unbeabsichtigte Strahler“ betrachtet werden. Der Schwerpunkt dieser Arbeit ist die Untersuchung der Abstrahlung von elektrisch großen, unbeabsichtigten Strahlern (englisch: electrically large equipment under test, ELEUT). Im Rahmen der Arbeit wurde ein quaderförmiges Metallgehäuse mit einem Schlitz als Prüfling eingesetzt, das mit einem Computergehäuse oder anderen elektronischen Geräten vergleichbar ist. Eine weitere Konfiguration eines ELEUT mit daran angeschlossenen Anschlussleitungen wurde ebenfalls untersucht.

Zur Sicherstellung der elektromagnetischen Verträglichkeit muss die Abstrahlung dieser Geräte in verschiedenen EMV-Testeinrichtungen gemessen werden. Allgemein können die Emissionsmessverfahren in Messungen der maximalen Feldstärke in einem bestimmten Abstand und in Messungen der Gesamtstrahlungsleistung eingeteilt werden. Das feldstärkebasierte Verfahren wird auch als das klassische Verfahren bezeichnet. Zugehörige Messumgebungen sind z. B. Freifelder, Halbabsorberhallen und Vollabsorberhallen. Typische gesamtstrahlungsleistung-basierte Messmethoden finden in Modenverwirbelungskammern (MVK) und GTEM-Zellen statt. Der Zusammenhang zwischen diesen beiden Methoden wird durch die Direktivität hergestellt, welche die Umrechnung der gesamten abgestrahlten Leistung in die elektrische Feldstärke erlaubt.

Das Ziel dieser Arbeit ist es, eine alternative Testmethode (ATM) zur Vereinfachung der Emissionsmessung anzuwenden, wobei Modenverwirbelungskammern als ATM verwendet wurden. Ein Vorteil dieser Messumgebung ist die bessere Reproduzierbarkeit und Robustheit der Messergebnisse. Die Messgröße ist dabei die gesamtabgestrahlte Leistung, die unabhängig von dem konkreten Abstrahldiagramm des Prüflings ist. Die maximale elektrische Feldstärke von Prüflingen kann durch die Kombination der gemessenen Gesamtstrahlungsleistung in einer MVK und über die Schätzung der Direktivität der Prüflinge bestimmt werden. Die maximale Direktivität der ELEUTs kann durch analytische Annäherung oder durch numerische Simulationstechniken bestimmt werden.

Um die abgestrahlte Emission von ELEUT zu bestimmen, werden in dieser Arbeit drei Varianten angewendet. In Variante 1 wird das im Standard CISPR 16-4-5 eingeführte Konversionsverfahren auf ELEUTs angewendet, die mit der bestehenden Grenze der FAR verglichen werden kann. In Variante 2 kann die gesamte abgestrahlte Leistung mit Hilfe der Direktivität in eine äquivalente elektrische Feldstärke umgewandelt werden. Diese beiden

Methoden hängen von der Anzahl der EUTs ab und können nicht direkt mit der gemessenen Gesamtstrahlungsleistung verglichen werden, was nicht sehr praktikabel ist. Basierend auf Variante 3 wird die neue Leistungsgrenze des MVKs abgeleitet. Außerdem könnte diese Grenze direkt angewendet werden, um mit der gemessenen Gesamtstrahlungsleistung zu vergleichen. Diese Methode ist sehr hilfreich und könnte für weitere Forschung angewendet werden.

Contents

1 Introduction

List of Acronyms

1D	One Dimensional
3D	Three Dimensional
AF	Antenna Factor
ATM	Alternative Test Method
CDF	Cumulative Distribution Function
CE	Conducted Emission
CF	Conversion Factor
CISPR	Comité International Spécial des Perturbations Radioélectriques
CM	Common Mode
DM	Differential Mode
DOF	Degrees of Freedom
ELEUT	Electrically Large Equipment Under Test
EM	Electromagnetic
EMC	Electromagnetic Compatibility
EMI	Electromagnetic Interference
ETM	Established Test Method
EUT	Equipment Under Test
FAR	Fully-Anechoic Room
FCC	Federal Communications Commission
FDTD	Finite Differences in Time Domain
FS	Free Space
GTEM	Gigahertz Transverse Electromagnetic Cell

IL	Insertion Loss
ITE	Information Technology Equipment
MCS	Monte Carlo Simulation
MIL-STD	Military Standard
MSC	Mode-Stirred Chamber
OATS	Open Area Test Site
PDF	Probability Density Function
PEC	Perfect Electrically Conducting
RE	Radiated Emission
SAC	Semi-Anechoic Chamber
SW	Spherical Wave
SWA	Standing Wave Antenna
TE	Transverse Electric
TEM	Transverse Electromagnetic
TL	Transmission Line
TM	Transverse Magnetic
TWA	Traveling Wave Antenna
US	United States
VDE	Verband Deutscher Elektrotechniker

List of Symbols

a	Effective radius
a_{EUT}	Dimension of the EUT
$a_{\mathrm{EUT+Wire}}$	Dimension of the EUT and the connecting wire
α	Phase angle
ε	Permittivity of the material
ε_0	Permittivity of the material in vacuum
$\mathbf{B}$	Magnetic flux density
β	Phase constant
c	Velocity of light
C_{E}	Element factor
$C_{\mathrm{group,v}}$	Group pattern for a vertical dipole antenna
$C_{\mathrm{group,h}}$	Group pattern for a horizontal dipole antenna
C_{Gr}	Array factor
Ci	Cosine integral
$C(\theta)$	Radiation pattern
$C_{\mathrm{total,v}}$	Total radiation pattern for a vertical dipole antenna
$C_{\mathrm{total,h}}$	Total radiation pattern for a horizontal dipole antenna
C_{total}	Total radiation pattern
d	Maximal geometrical dimension of the EUT
$\langle D \rangle$	Expectation value of the directivity
$D_{\mathrm{ATMi},i}$	Deviation by alternative test method for a certain EUT i
$\overline{D}_{\mathrm{ATM}}$	Mean value of the deviations for the alternative test method

D_{co}	Co-polarized directivity
D_{cross}	Cross-polarized directivity
$D^{\mathrm{C}}_{\max}$	Directivity obtained by the *Cylinder* method
$D_{\mathrm{ETM},i}$	Deviation by established test method for a certain EUT i
$\overline{D}_{\mathrm{ETM}}$	Mean value of the deviations for the established test method
$D_{\max}$	Maximum directivity
$\uparrow D_{\max}\uparrow$	Upper boundary of maximum directivity
D_{p}	Partial directivity
D_{ϕ}	Directivity in azimuth direction
$D^{\mathrm{R}}_{\max}$	Directivity obtained by the *Ring* method
$D^{\mathrm{S}}_{\max}$	Directivity obtained by the *Sphere* method
D_{θ}	Directivity in elevation direction
Δ	Uncertainty difference between alternative and established test methods
E	Electric field magnitude
$\mathbf{E}$	Electric field vector
$\mathbf{E}_{Q}$	Electric field strength vector for every small source
$\mathbf{E}_{Q_i}$	Electric field strength vector for small dipole source number i
$\mathbf{E}_{\mathrm{EUT}}$	Electric field strength vector of the EUT
$\overline{\mathbf{E}^2}$	Average of the squared electric field strength vector
$E_{\theta}(r)$	Electric field strength in θ direction at the observation distance r
$\mathbf{e}_r$	Unit position vector
η	Free space wave impedance
φ_i	position angle
$\mathbf{H}$	Magnetic field strength
$\mathbf{J}$	Electric current density vector
I_{CM}	Magnitude of common mode current

I_i	Magnitude of isotropic point source number i
I_m	Peak current
I_SWA	Current along the standing wave antenna
k	Wave number
ka	Electrical size
κ	Coverage factor
$\overline{K}$	Average conversion factor
K_i	Conversion factor for EUT number i
$\mathbf{K}_{smn}$	Spherical wave functions vector
λ	Wavelength
L_ATM	Limit for alternative test method
l_h	Length of a horizontally orientated standing wave antenna
l_v	Length of a vertically orientated standing wave antenna
M_ATM	Measured results by the alternative test method
M_ETM	Measured results by the established test method
μ	Permeability of the material
μ_0	Permeability of the material in vacuum
N_c	Number of sampling over a planar cut
N_6c	Number of sampling on three orthogonal planar cuts with 2 polarizations
N_m	Number of modes
N_MCS	Number of Monte Carlo Simulations
N_obs	Number of observation points
N_dp	Number of dipoles
N_s	Number of sampling over the sphere
ω	Angular frequency
Ω	Solid angle

ϕ	Azimuth angle
ϕ_0	Azimuth angle in a certain direction
ϕ_i	Phase of isotropic point source number i
p_τ	Shape parameter of the Gamma distribution
$p(\phi)$	Polarization efficiency
$\ddot{\mathbf{p}}$	Second derivative of the dipole moment
P_0	Radiated power in a certain direction
$P_{\mathrm{rec,EUT}}$	Received power by the EUT
$P_{\mathrm{rec,ref}}$	Received power by a reference source
$P_{\mathrm{rad,ref}}$	Radiated power by a reference source
P_{rad}	Radiated power of EUTs
$Q_{smn}^{(3)}$	Wave coefficients
R	Distance between the EUT and the receiving antenna
ρ	Volume charge density
$\mathrm{std}(D_{\mathrm{ATM}})$	Standard deviation of the deviations for the alternative test method
$\mathrm{std}(D_{\mathrm{ETM}})$	Standard deviation of the deviations for the established test method
$\Gamma(x)$	Gamma function
θ	Elevation angle
θ_{m}	Elevation angle at the direction of the maximum radiation
θ_0	Elevation angle in a certain direction
$u_{\mathrm{ATM,inherent}}$	Inherent uncertainty for the alternative test method
$u_{\mathrm{ETM,inherent}}$	Inherent uncertainty for the established test method
u_{ATM}	Uncertainty for the alternative test method
u_{ETM}	Uncertainty for the established test method
U_{ATM}	Expanded uncertainty for the alternative test method
U_{ETM}	Expanded uncertainty for the established test method

$U_{\max}$	Maximum radiated power flux density
U_ϕ	Radiated power flux density in ϕ direction
U_θ	Radiated power flux density in θ direction
$\mathrm{var}(D)$	Variance of the directivity
X	Reference quantity

List of Figures

List of Tables

1 Introduction

The increasing application of electronic devices into everyday life – TVs, mobile phones, PCs, etc. increases the risk of interferences between these devices. The currents and voltages in one equipment produce electromagnetic (EM) fields that reach into nearby equipment. These fields may induce unwanted currents and voltages on nearby equipment, which in turn may result in interference. If all equipment coexist without electromagnetic interference (EMI) problems, this circumstance is called electromagnetic compatibility (EMC). By this definition, two different physical phenomena are classified: EM emission and EM immunity. EM emission is the generation and propagation of the unintentional and unwanted electromagnetic energy from an electronic device, which should be suppressed as far as possible so that other components are less affected as possible. EM immunity is the ability that an electronic or electrical device or system works without failure up to a certain level of electromagnetic interference. Thus, malfunctions of the device that might occur within the electromagnetic environment can be avoided. Thus, the EMC has become a quality measure of products. The products have to meet EMC regulations before put into the market.

The electromagnetic emission of electronic devices is strongly limited to protect radio communication services. In general, these emissions can be divided into two major categories – conducted emission (CE) and radiated emission (RE). The conducted emissions treat all signals transmitted via the power cord and connecting wires. The connected wires can behave like antennas, and the resulting radiated signal may cause interference with radio devices. According to the federal communications commission (FCC) Part 15 requirements and international special committee on radio interference (CISPR) standards, the considered frequency range for conducted emissions is from 150 kHz to 30 MHz [Pau06].

On the other hand, a device can directly emit energy via the electromagnetic field, which is called radiated emissions. The electromagnetic fields created by the electrical device may propagate through air, away from the device. Therefore, there is a potential risk of interference especially with radio services. For radiated emissions, the considered frequency range varies between 30 MHz and 40 GHz. Most digital devices are not intended to emit EM waves and can be considered to be unintentional radiation sources.

The protection of radio services is enforced by setting limits of maximum electromagnetic emission of electronic devices. The conformity to the regulations can be shown by comparing the measured maximum radiated emission from an Equipment under Test (EUT) to the applicable limits. Those limits can be found in in different worldwide standards, e. g., nonmilitary standards – FCC in United States (US), European standards (EN) in Europe and Verband Deutscher Elektrotechniker (VDE) standards in Germany as well as military standard (MIL-STD). The emission measurements could be carried out in different EMC test facilities.

At lower frequencies, when the geometrical size of the EUT is small compared to the wavelength, the EUT radiates power in a broad, dipole pattern. In this case, it is relatively simple to detect the maximum radiated E-field strength due to its simple radiation pattern. However, as frequency increases and the EUT becomes comparable or even larger in size with regards to the wavelength, the device becomes an 'electrically large' radiator and the radiation pattern becomes more irregular with multiple lobes in different directions. Herein 'electrically large' is related to the physical size as well as the considered frequency range. The radiation characteristic of electrically large equipment under test (ELEUT)s is more complicated, in comparison to 'electrically small' EUTs. It can be very difficult to find the maximum field strength during an emission measurement due to multiple lobes. Also, the directivity is usually unknown and difficult to measure.

Due to the trends of faster switching electronics and digital computers with high clock frequencies, even a PC-size enclosure may become an electrically large radiator. Because of the increasing number of such equipment, this work is exclusively focused on the radiated emissions of unintentional ELEUTs.

1.1 EMC measurement environments

The radiated emission measurements can be performed in a number of deterministic test facilities, such as an open area test site (OATS), a semi-anechoic chamber (SAC), a fully-anechoic room (FAR) and a gigahertz transverse electromagnetic cell (GTEM). Here, 'deterministic' field means that the radiated emission of an EUT are assumed to be as a plane electromagnetic wave with a certain direction, a certain polarization and a fixed amplitude. These conditions lead to the concept of deterministic fields. On the other hand, there exist test facilities like a mode-stirred chamber (MSC), where due to a resonant environment with numerous multiple reflections and a stronger coupling of the test object with its surroundings, the field conditions can be described under the concept of statistical fields [Mag12]. It is of general interest to develop applicable procedures to compare or convert measurement results obtained in these different test facilities in respect to the reference value for the limits of radiated emission.

The emission measurement facilities can be grouped into two main categories, in terms of the measured quantities (electric-field-based or power-based) [Har00]. The electric-field-based methods are usually denoted as classical methods, e. g., the E-field strength at a certain distance would often be measured in a SAC, with the EUT horizontally rotated and vertically scanned, in order to measure the maximum emission. But this kind of measurements are very time-consuming and expensive. Furthermore, not all information is necessary and relevant, e. g., in most cases the minimum emission level is not a quantity of interest. The measured field strength would be compared with the established limit. If the emission level is lower than the established limit, implying that the EUT passes the emission test. Vice versa, a higher emission level than the limit means the test is failed.

In comparison, the power-based methods, e. g., a GTEM cell and a MSC, indirectly and directly measure the total radiated power of an EUT. In this work, the MSC method is applied as the alternative test method (ATM), taking the advantage of avoiding the physical rotations of EUTs. This method could simplify the measurement procedures, which is more convenient for radiated emission tests at higher frequencies. The reason lies in the fact that in a MSC, the radiation patterns of the EUT is irrelevant, and the polarization properties are not preserved for characterizing an EUT. The total radiated power measured in a MSC, is converted to the equivalent E-field strength using the directivity of the EUT. In other words, the conversion between the classical method and the alternative method could be connected by the directivity. This is necessary, because there are no established emission limits in terms of the total radiated power.

1.2 Motivation and objective of this thesis

The motivation is to accurately determine the radiated emission of electrically large EUTs. In this work, the MSC is selected as the ATM. The total radiated power of the EUT measured in the MSC can be converted to the E-field strength with the help of the directivity. Therefore, the quantity of the directivity turns out to be an important factor for application of the alternative measurement method. Nevertheless, it is still a problem to reliably estimate the directivity of arbitrary EUTs. For an electrically small test object, the directivity is well known. However, electrically large test objects may have emission patterns that differ from those of electrically small antennas. Besides, the directivity is difficult to measure, due to the fact that the directivity measurement requires a time-consuming 3D measurement, which is usually not practicable. Consequently, a numerical simulation technique can be used to estimate the directivity. In order to generalize the directivity for arbitrary ELEUTs, a statistical analysis of the directivity is presented in this work. The results of the calculated directivity of ELEUTs can be applied to most test objects above 1 GHz. Furthermore, the directivity of ELEUTs with cabling wires is also important, which will be analyzed using numerical simulations.

The whole problem could also be solved, if there would be well-accepted power-based emission limits. Generally, there are two methods. One is to compare the measured total radiated power in a MSC directly with an established power limit. Another approach is to convert the measured total radiated power to an equivalent electric field strength E_{MSC} and to compare it with the established CISPR class B limit. However, the CISPR class B limit takes the directivity of the EUT of 1.7, which results from the approximation of the test EUT as a dipole. This assumption is not valid for ELEUTs. Therefore, it is necessary to modify the emission limit.

The aim of this work is the reliable determination of the directivity of ELEUTs to allow the application of the MSC as an alternative measurement environment. The final objective of this thesis is to provide a profitable methodology for radiated emission test of the ELEUTs, which may be generalized and expanded in the emission standards. A comprehensive analysis of this methodology [CIS06b] will be carried out, using the simulated values of the directivity and the total radiated power P_{rad} of the EUT measured in a MSC to obtain the equivalent E-field strength. The equivalent E-field strength obtained using this conversion method has to be compared with the E-field strength measured by the established method, where the uncertainty has to be taken into account.

A diagram of the conversion procedures is shown in Fig. 1.1. The procedures are carried out as followed: The E-field strength can be directly measured in FAR or SAC. However, the measurement procedures are much too complicated and not advantageous for electrically large EUTs. Instead, the total radiated power P_{rad} of the EUT is measured in a MSC and then converted to the equivalent electric field strength E_{MSC} depending on the directivity D, the frequency f and the effective radius a. Based on the conversion procedure in CISPR 16-4-5, it seems also feasible to convert the limit E_{limit} to a power limit P_{limit}. The radiated power of other EUTs can be measured and directly compared with this limit P_{limit}. Different radii a_1, a_2, a_3 could be used to convert the radiated power P_{rad} of the EUT to the equivalent E-field strength and then compare with E_{limit}.

1.3 Outline

In this thesis, a rectangular metallic box with slots was investigated as an ELEUT. The emission source was placed inside the enclosure, radiating energy through the slots to the outside enclosure. The radiated emission was measured and simulated using different methods.

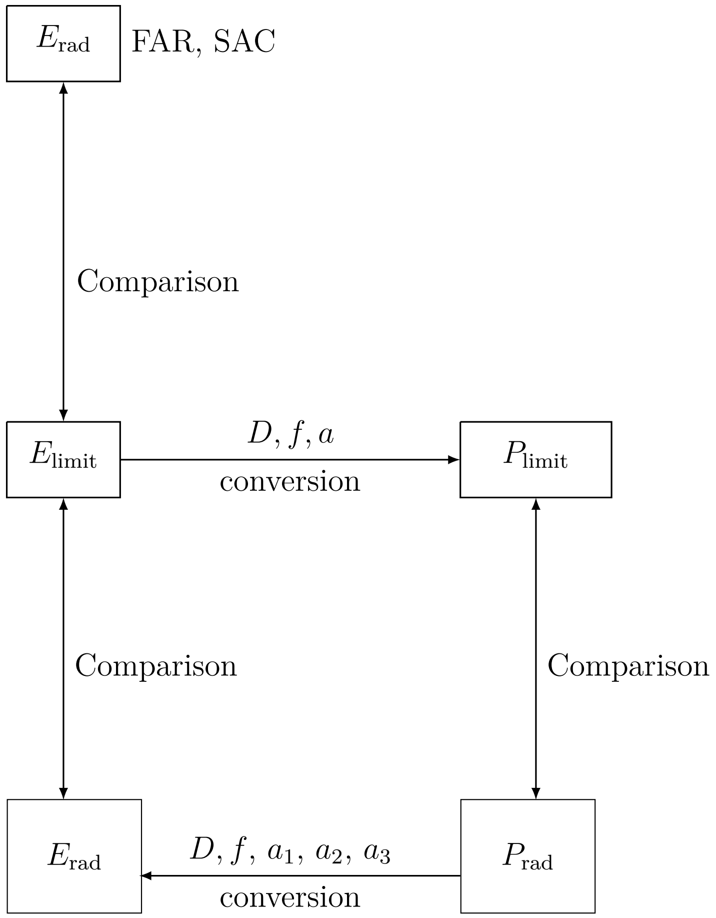

Figure 1.1: Conversion procedures carried out in this thesis

Chapter 2 provides the necessary theoretical backgrounds for the following chapters. Three main parts are introduced. The first part describes the EM theory, wave propagation and polarization, the concept of common mode (CM) and differential mode (DM) currents and the electrical size of EUTs.

In the second part, the fundamental radiators are described. As a complex radiator, the transmission line (TL) is also described. The traveling wave antenna (TWA) and standing wave antenna (SWA) theory are presented. The analytical formulas to describe the directivity of the antennas can be straight-forward applied later. The directivity of EUTs can be described with analytical methods or numerical simulation technique.

In the third part, different radiated emission measurement methods and the conversion procedure between these test facilities are described.

Chapter 3 provides a comprehensive analysis of ELEUTs. Several relevant cases are taken into account. The radiation patterns of a slotted enclosure with and without cables are compared between measurement and simulation results. Then the numerical simulation is used for statistical analysis, to derive the directivity of EUTs. Also an analytical approach is described, to determine the directivity of EUTs with cables based on the simulated current distribution.

In Chapter 4, the influencing factors on the maximum directivity are investigated. Analytical and numerical methods can be use to determine the directivity of EUTs. The results of the maximum directivity based on statistical analysis including randomly changing of the wire length and the size of the enclosure are obtained, which can be used for the conversion procedure in the next chapter.

Finally, in Chapter 5, three methods are applied in order to determine the emission levels of EUTs and simplify the measurement procedures. The first method is to apply the conversion procedure described in CISPR 16-4-5. The second method is to convert the total radiated power to an equivalent E-field strength by using the directivity. The third method is to derive a new power-based limit. The disadvantages and advantages are compared.

In Chapter 6, a final summary and an outlook to future work complete the thesis.

2 Fundamentals of Radiated Emission

In this chapter, the fundamentals of the radiated emission are introduced. From Maxwell's equations, the EM plane wave characteristics in terms of wave propagation and polarization can be analytically described. The transmission line, as a specific type of antennas, is investigated with regards to the common mode and differential mode currents. For EMC analysis, it is important to identify the quantity of electrical size, which is related to quasi stationary process and high frequency process. As followed, the radiation behavior and directivity of fundamental radiators is described. It is also of great interest to derive the directivity of transmission lines, which is based on the directivity of SWAs and TWAs. In order to obtain the directivity of EUTs, not only an analytical solution is possible, but also a numerical simulation could be applied.

2.1 EM theory

Maxwell's equations are the theoretical fundamentals of the electromagnetic phenomena, which consist of four equations.

Gauss' laws for the electric fields:

$$\nabla \cdot \mathbf{D} = \rho \tag{2.1}$$

Here, symbols in bold represent vector quantities. The vector **D** represents the electric flux density, ρ is the electric charge density.

Ampere's law:

$$\nabla \times \mathbf{H} = \mathbf{J} + \frac{\partial \mathbf{D}}{\partial t} \tag{2.2}$$

Here, **H** represents the magnetic field strength and **J** represents the electric current density.

Gauss' laws for the magnetic fields:

$$\nabla \cdot \mathbf{B} = 0 \tag{2.3}$$

Here, **B** represents the magnetic field flux density.

Faraday's law of induction:

$$\nabla \times \mathbf{E} = -\frac{\partial \mathbf{B}}{\partial t} \tag{2.4}$$

Here, **E** represents the electric field strength. In the absence of free charges and current densities, the simplified form of Maxwell's equations are expressed by:

$$\begin{aligned} \nabla \cdot \mathbf{D} &= 0 \\ \nabla \times \mathbf{H} &= \frac{\partial \mathbf{D}}{\partial t} \\ \nabla \cdot \mathbf{B} &= 0 \\ \nabla \times \mathbf{E} &= -\frac{\partial \mathbf{B}}{\partial t} \end{aligned} \tag{2.5}$$

Besides, the constitutive relations are defined by:

$$\begin{aligned} \mathbf{D} &= \varepsilon \mathbf{E} \\ \mathbf{H} &= \frac{1}{\mu} \mathbf{B} \end{aligned} \tag{2.6}$$

where ε is the permittivity and μ is the permeability.

Assuming monochromatic waves, which are characterized by a single frequency with harmonic time dependence $\mathrm{e}^{-\mathrm{j}\omega t}$, so that with the real part of the complex quantity: $\mathbf{E}(r,t) = \Re\{(\mathbf{E}(r)\,\mathrm{e}^{-\mathrm{j}\omega t})\}$ and $\mathbf{B}(r,t) = \Re\{(\mathbf{B}(r)\,\mathrm{e}^{-\mathrm{j}\omega t})\}$, then the Helmholtz wave equation can be obtained:

$$\nabla^2 \mathbf{E} + \varepsilon\mu\omega^2 \mathbf{E} = 0 \tag{2.7}$$

$$\nabla^2 \mathbf{B} + \varepsilon\mu\omega^2 \mathbf{B} = 0 \tag{2.8}$$

where ω is the angular frequency. Based on Maxwell's equations, the EM fields can be classified into: static fields, stationary fields, quasi stationary fields and high frequency fields, according to the considered frequency range [GV09]. The high frequency fields are related to the complete set of Maxwell's equations, which can be applied to the EM radiation, EM coupling and the antenna theory. Physically, all the coupling models in terms of EMC are due to the EM fields. The capacitive coupling between two conductors is due to the electric fields. The currents produce the magnetic fields around itself, which results in inductive coupling between two current-carrying conductors. The electric field strength and the magnetic field strength are considered as dependent fields forming the EM coupling.

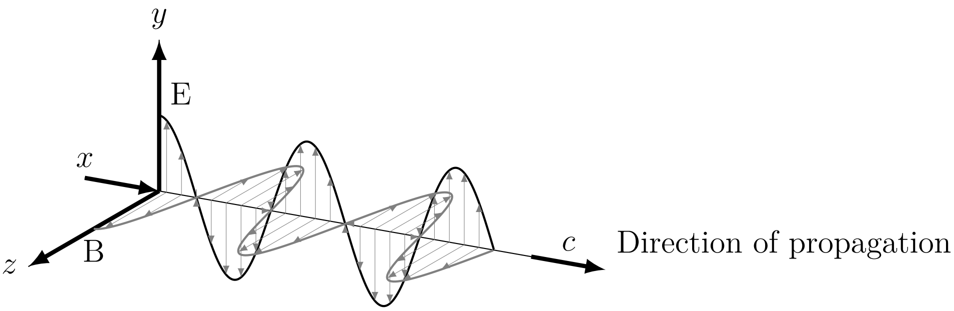

$$c = \frac{E}{B}$$

$E =$ electric field amplitude
$B =$ magnetic field amplitude (instantaneous values)
$c =$ velocity of light ($2.998 \times 10^8\,\mathrm{m/s}$)

$$c = \frac{1}{\sqrt{\mu_0 \varepsilon_0}}$$

$\mu_0 =$ magnetic permeability in vacuum, $\mu_0 = 4\pi \times 10^{-7}\,\mathrm{H/m}$
$\varepsilon_0 =$ electric permittivity in vacuum, $\varepsilon_0 = 8.85 \times 10^{-12}\,\mathrm{F/m}$

Figure 2.1: Electric field, magnetic field and wave propagation formed by the electromagnetic waves [Men15]

2.2 Wave propagation and polarization

The EM fields are mutually dependent fields forming EM waves. The most simple and fundamental EM waves are transverse plane waves, which have both a spatial and temporal dependence. The electric component of an EM plane wave can oscillate in any direction perpendicular to the direction of the wave propagation, see Fig. 2.1.

The direction of the field's rotation is called polarization. Both the electric field and magnetic field are oscillating but in different directions. Conventionally, the polarization refers to the polarization of the electric field, as shown in Fig. 2.1. The oscillation of the electric field may be in a single direction (linear polarization), or the field may rotate (circular or elliptical polarization). For a horizontally polarized wave, the electric field lies in a horizontal direction. For a vertically polarized wave, the electric field lies in a vertical direction. As an example, for a search antenna of a missile guidance radar, the maximum pickup occurs only when the receiving antenna is oriented in the same direction and has the same polarization as the transmitting antenna. Thus, a horizontal antenna can be applied for the efficient receiving of horizontally polarized waves and a vertical antenna can be used to receive vertically polarized waves.

However, other polarizations are also possible, as shown in Fig. 2.2. If two linearly polarized waves with equal amplitude, one polarized in the x-direction, and another in the y-direction, that has 90° phase difference, then a circularly polarized wave could be obtained. When two perpendicular electric field components are not in phase, either with

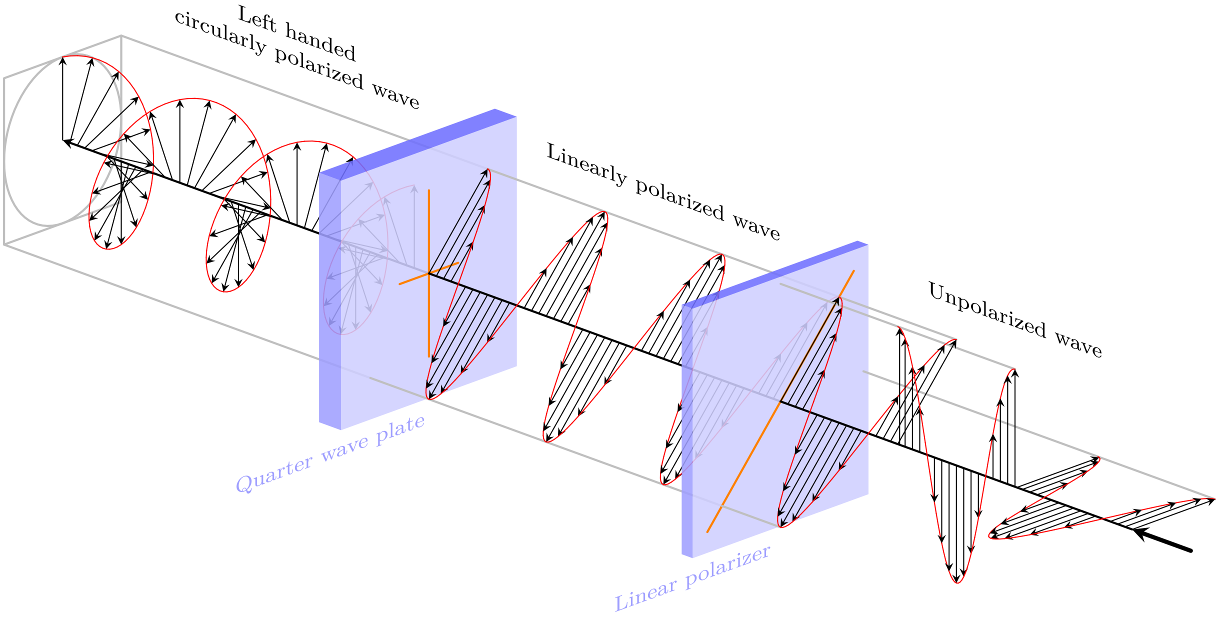

Figure 2.2: Polarization of electromagnetic waves [Bom13]

different amplitudes or out of phase, the resulting state of the complete polarization is elliptical [Wik].

If the electric field $\mathbf{E}(x)$ varies in only one dimension, say the x-direction, which is independent of y and z, then the combination of Eq. (2.7) and (2.8) becomes:

$$\frac{\mathrm{d}^2\mathbf{E}(x,t)}{\mathrm{d}x^2} + k^2\mathbf{E}(x,t) = 0 \tag{2.9}$$

where k is the wave number, which has the relation: $k = {}^{2\pi}/_{\lambda} = {}^{2\pi f}/_{c} = {}^{\omega}/_{c} = \omega\sqrt{\mu\varepsilon}$, with the wavelength denoted by λ. This equation is mathematically the same as the harmonic oscillator equation. For a wave traveling in the $+x$ direction, the solution of (2.9) can be derived:

$$e(x,t) = E \cdot \cos\left(\omega t - \beta x + \varphi\right) \tag{2.10}$$

For a wave traveling in the -x direction, the following solution can be derived:

$$e(x,t) = E \cdot \cos\left(\omega t + \beta x + \varphi\right) \tag{2.11}$$

where β is the space constant, φ is the phase shift and E is the magnitude of the wave.

Likewise, the radiation behavior of general radiating structures – antennas and slots can be also analytically described, based on the Maxwell's equations. However, unintentional antennas have more complicated radiation patterns, which cannot be analytically described. It is more useful to perform numerical simulation procedures.

2.3 Common mode and differential mode currents

Another common type of unintentional antennas are transmission lines, whose radiation behavior can be analyzed based on the Maxwell's equations. The obtained equations are called the classical transmission line equations [Pau94]. As shown in Fig. 2.3, for the current-carrying two-conductor transmission lines (T1 and T2) with a common ground, the EM disturbances can be classified into two categories, CM currents and DM currents. A CM current is defined as the current flowing along the transmission line in the same direction and return via the ground, denoted by the red arrow. The DM currents are represented by the two currents of same magnitude and phase flowing in opposite directions, expressed by the green arrow in Fig. 2.3.

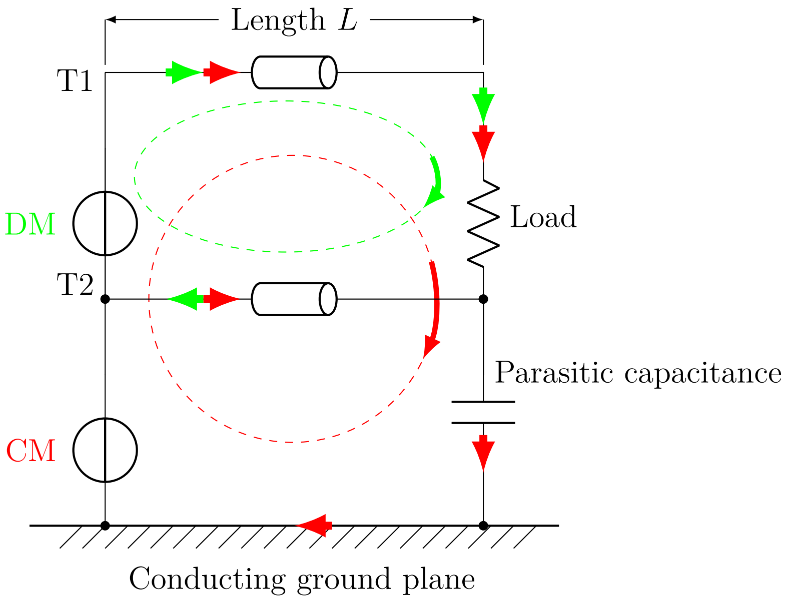

Figure 2.3: Schematic of common mode and differential mode disturbances

The EMI caused by the CM and DM currents are investigated in detail in [Pau94]. The CM currents are not necessary for the functional performance of the electronic devices. The CM currents will also not be predicted by ideal transmission line models. CM currents are undesired currents, which are generally much smaller than the DM currents. However, their loop area is much larger than for the DM so that the CM radiation often dominates [Pau94]. The reason lies in the fact that the DM currents have the same magnitude but opposite direction. Therefore, the radiated fields tend to cancel each other. On the other hand, the CM currents flow in the same direction and their radiated fields will add up, producing a larger radiation.

2.4 Electrical size of equipment

Generally, any cables and electrical device can act as an antenna system [Kar14] and can be the source of unintentional radiated emission. In this case, the analysis process is complicated because the full set of Maxwell's equation has to be treated. For an EMC analysis, it is important to know at what circumstances the system can be analyzed using methods applicable for quasi-stationary processes and when this is not possible any longer, transmission line theory and wave propagation have to be considered. The answer to this question depend on the geometrical size of the equipment and the wavelength of the considered signal. A general rule of thumb states, that a system is considered to be electrically small as long as the following condition is valid [GV09]:

$$d < {}^{\lambda}\!/_{10} \tag{2.12}$$

In this equation, d is the maximal geometrical dimension of the EUT and λ is the wavelength of the exciting source. From an EMC point of view, it can be assumed, that an electrical small device does not radiate directly, only the conducted emission needs to be considered. For an electrically large device, the radiated emission has to be considered and the conducted emission can be neglected.

If only a cable is considered, the maximal geometrical dimension d is just the length of the cable. Also the maximum geometrical dimension of the housing of an EUT could be assumed as d. It is not obvious if the electrical wires or the cables of a product will be the dominant source of radiated emissions. Therefore, standards for emission measurements require to measure the maximum field strength by different cable orientations when defining the measurement setup.

For the model of an EUT with a connecting wire in Fig. 2.4, the total RE level is the superposition of the wire radiation and the enclosure radiation. In general, at lower frequencies, the emission level of the attached cables dominates due to multiple resonances when compared to the radiation level due to the modes inside the enclosure. In contrast, at higher frequencies, the higher order modes of the enclosure dominate the emission level compared to the radiation of wires [Mar01].

Trying to apply the mode stirred chamber for radiated emission measurements, the models to predict the directivity are needed. If considering the the directivity of an structure, the term electrical size is normally referred to the product of the wave number k and the effective radius a. A structure is assumed to be electrically large if the condition satisfies:

$$ka > 1 \tag{2.13}$$

Otherwise, the structure is electrically small. The effective radius represents the smallest radius of a sphere bounding the EUT. Examples are shown in Fig. 2.4. If the equipment has no cables connected to the housing, like battery powered systems, the radius a only corresponds to a spherical-shaped test object, likewise is shown in Fig. 2.4.

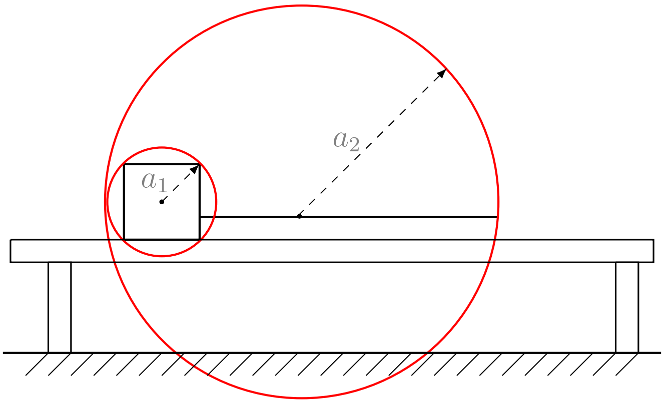

Figure 2.4: Effective radius of different spheres enclosing the EUT

In practice, the test objects are usually cuboid shaped or other more complex geometries. The effective radius a is herein defined as the radius of the smallest sphere containing the radiating systems including the EUT ($a = a_1$). It is reasonable to take the half-diagonal of the enclosure as the effective radius. This assumption is mostly used for theoretical approaches to determine the directivity of objects, such as the spherical wave theory, which will be introduced later.

These approaches neglect the radiation of the attached cabling. Therefore, the consideration of a second effective radius is suggested in this work, a radius which includes the attached cable and the EUT ($a = a_2$), as shown in Fig. 2.4. However, it is still not clear, what length of the attached cable needs to be included into the dimension as the effective radius, and how large the effective radius is to be determined based on the directivity estimation. It gives a worst-case estimation if the half of the dimension including the EUT and the wire is taken as the effective radius and the total RE level may be overestimated.

Previous work on similar subjects has been reported in [GB08, ZHGG11]. An EUT with cables was investigated up to 1 GHz in [GB08]. But still there are questions arising:

- how is the behavior in an extended frequency range from 1 GHz to 6 GHz,
- what is the effect of slotted metallic enclosures, e. g., with visible internal resonances of the enclosure,
- what cable length has to be considered with symmetrical and common mode excitation of the attached wires,

- what is the effect of the wires orientation e. g., straight wires (parallel to the ground plane) and bent wires (consisting of a horizontal part and a vertical part over the ground plane).

A solution for this problem will be suggested in the subsequent content in Chapter 3 and Chapter 4.

2.5 Fundamental radiators

Here, the radiation behavior of fundamental radiators is described. An isotropic antenna is a theoretical point source antenna with omnidirectional radiation patterns, which radiates the same intensity in all directions. Therefore, the corresponding directivity is equal to 1 for all directions. It is usually used as a reference radiator. Other radiators can be compared with an isotropic antenna. For example, a Hertzian dipole antenna with a directivity of 1.5 receives 1.5 times the power of an isotropic antenna in the main beam direction.

The maximum electric field strength in the far field can be calculated for intentional radiators from the radiated power if the directivity is known [Wil04, Wil10, GB08]:

$$E = \sqrt{\frac{D \eta P_{\mathrm{rad}}}{4 \pi r^2}} \tag{2.14}$$

In this equation, E is the calculated field strength at a distance r from the EUT, D is the directivity of the EUT and η is free space wave impedance. Through this equation, it is convenient to convert the measured P_{rad} in a MSC to the corresponding electric field strength in free space. In this case, a direct comparison with the limits would be possible. Unfortunately, the directivity of the investigated EUT is normally not known. For electrically small devices, a dipole characteristic can be assumed, as it is done for the determination of the field strength measured in the GTEM. Hence, it is important to investigate the directivity of EUTs. Therefore, the directivity of exemplary fundamental radiators is investigated progressively as followed.

A Hertzian dipole is very thin, with its length much smaller than the wavelength. This approximation and the assumption of a top load restricts the current along the Hertzian dipole as constant. The radiation pattern can be observed in Fig. 2.5.

Unlike an isotropic antenna, the radiation pattern of a Hertzian dipole is not uniform in all directions. It shows a preferred direction, which has the maximum radiation at right angles to the Hertzian dipole and becomes zero along the axis of the antenna. As it is shown in Fig. 2.5, the Hertzian dipole has a maximum directivity of 1.5.

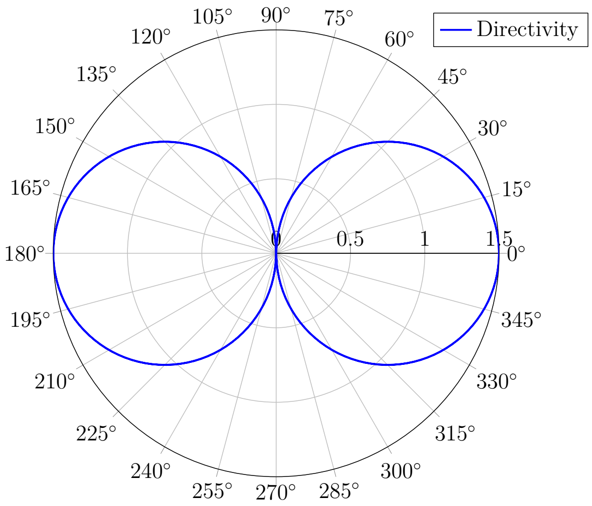

Figure 2.5: Symmetrical radiation pattern of a Hertzian dipole with a directivity value of 1.5 (in linear scale)

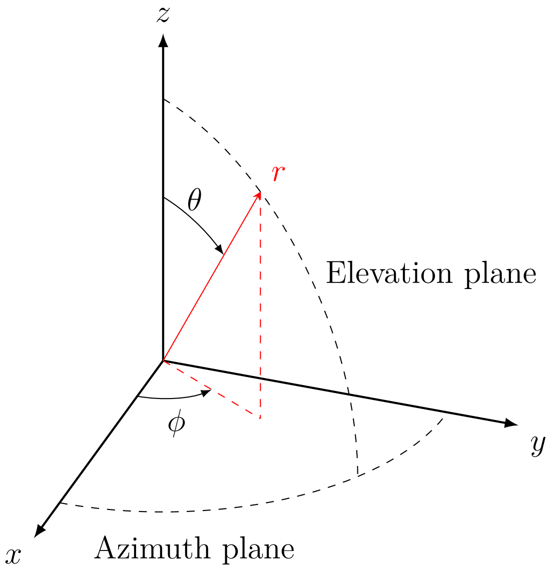

Figure 2.6: Typical antenna coordinate system

Here, it is necessary to introduce some terminologies related to the directivity. It is a measure of how directional the radiation pattern is. A higher directivity implies a more directional antenna. The directivity is usually defined for the far field only, which could be defined as the ratio of the radiated power flux density $U(\phi_0, \theta_0)$ in a certain direction (ϕ_0, θ_0) over the radiated power flux density averaged in all radiation directions. A definition of the corresponding spherical coordinate system is shown in Fig. 2.6, where ϕ is the azimuth angle and θ is the polar angle. The averaged radiated power flux density is equal to the total radiated power divided by the total solid angle (4π steradians) over the whole sphere.

$$D(\phi_0, \theta_0) = \frac{U(\phi_0, \theta_0)}{\frac{1}{4\pi}\int_0^{2\pi}\int_0^{\pi} P(\phi, \theta)\sin(\theta)\,\mathrm{d}\theta\,\mathrm{d}\phi} \tag{2.15}$$

Through (2.15), it is straightforward to calculate the directivity of antennas.

The concept of the directivity describes how much energy is concentrated in one direction compared to other directions. An isotropic spherical radiator that radiates equally in all directions has a directivity value of 1. In most cases, the most interesting quantity is the maximum directivity $D_{\max}$, which is the ratio of the maximum radiated power flux density over the average radiated power flux density.

$$D_{\max}(\phi_0, \theta_0) = \frac{U_{\max}(\phi_0, \theta_0)}{\frac{1}{4\pi}\int_0^{2\pi}\int_0^{\pi} P(\phi, \theta)\sin(\theta)\,\mathrm{d}\theta\,\mathrm{d}\phi} \tag{2.16}$$

For the case of the antenna above ground, which corresponds to a half space environment, the total radiated power has to be integrated over the upper hemisphere with θ ranged from 0 to $\pi/2$ and normalized to the total solid angle of 4π.

$$D_{\mathrm{HS},\max}(\phi_0, \theta_0) = \frac{U_{\max}(\phi_0, \theta_0)}{\frac{1}{4\pi}\int_0^{2\pi}\int_0^{\pi/2} P(\phi, \theta)\sin(\theta)\,\mathrm{d}\theta\,\mathrm{d}\phi} \tag{2.17}$$

2.5.1 Short dipole antenna

The following procedure can be carried out to calculate the directivity in the far field: As long as the current distribution is known, then the electric field strength can be deduced. Correspondingly, the radiated power can be calculated if the electric field strength is known. Based on the definition, the directivity is obtained by taking the ratio of the power in a certain direction over the average power over the whole sphere. It is important to realize that the flowing current I along the antenna is the reason of the electromagnetic field. If the electric field is known, the radiated power P_{rad} of an antenna can be obtained by the integral of the electric field over the solid angle:

$$P_{\mathrm{rad}} = \frac{1}{2\eta}\iint |E_\theta|^2 r^2 \sin\theta\,\mathrm{d}\theta\,\mathrm{d}\phi \tag{2.18}$$

Here, E_θ is the electric field strength in θ direction. Take a short dipole antenna as an example: A short dipole is the simplest physical antenna, which is shown in Fig. 2.7.

When the length of the dipole L is less than a tenth of wavelength (see also Eq. (2.12)), it is said to be a short dipole antenna. The voltage source is very small compared to the wire length. If the short dipole is oriented along the z-axis with center at $z = 0$, the current distribution is given by:

$$I(z) = I_m\left(1 - \frac{2|z|}{L}\right) \tag{2.19}$$

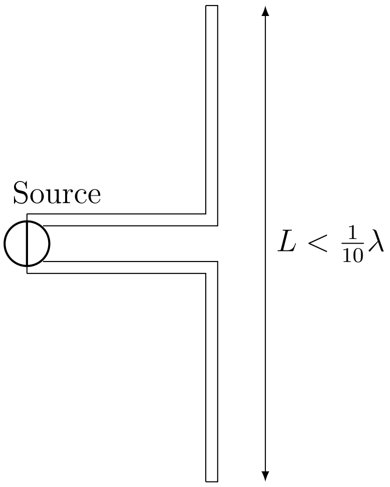

Figure 2.7: Schematic of a short dipole antenna of length L

where I_m is the peak current. The far field radiation is given by [GV09]:

$$\begin{aligned} E_\theta &= \frac{j\eta k I_0 L\, \mathrm{e}^{-jkr}}{8\pi r}\sin\theta \\ H_\phi &= \frac{E_\theta}{\eta} \\ E_r &= H_r = E_\phi = H_\theta = 0 \end{aligned} \tag{2.20}$$

In the above equations, only the E_θ and H_ϕ fields exist and they are perpendicular to the propagation direction (in the r direction). This implies that in the far field region the fields are propagating like a plane wave. Then the radiated power of a short dipole can easily be calculated:

$$P_{\text{rad}} = \frac{1}{2\eta}\iint |E_\theta|^2 r^2 \sin\theta\, \mathrm{d}\theta\, \mathrm{d}\phi \tag{2.21}$$

Based on Eq. (2.15) and Eq. (2.18), the directivity can be calculated by taking the ratio of the power in one direction over the mean power over the whole sphere. In this way, the obtained directivity of a short dipole is: $D_{\text{short,dipole}} = {}^{U_{\max}}/_{P_{\text{rad}}/4\pi} = 1.5$.

2.5.2 Half-wave dipole antenna

A dipole antenna is similar to a short dipole except that the length is not required to be small compared to the wavelength. A schematic view is shown in Fig. 2.8. If a dipole antenna with a length of $L = \lambda/2$ (half-wave dipole) is oriented along the z-axis and centered at $z = 0$, the current distribution is as follows:

$$I(z) = I_m \cos kz \tag{2.22}$$

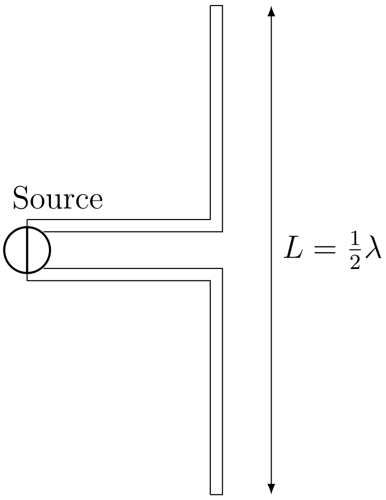

Figure 2.8: Schematic of a half-wave dipole antenna of length L

The current distribution shows a standing wave pattern, with a sinusoidal distribution along the half-wave dipole. The far field radiation pattern in terms of the electric field is given by [Stu81]:

$$E_{\theta,\text{dipole}} = \frac{j\eta I_m \, \mathrm{e}^{-jkr} \cos\left(\frac{\pi}{2}\cos\theta\right)}{2\pi r \sin\theta} \tag{2.23}$$

Through Eq. (2.18) and Eq. (2.15), the directivity of a half-wave dipole antenna can be obtained with the magnitude of 1.64. In a similar manner, the derivation of the directivity for the connecting wire is investigated as followed.

2.6 Analytical treatment of cable radiation

The attached cables of an EUT can unintentionally radiate electromagnetic energy. The radiation can be analytically treated using the antenna theory. According to [Stu81], a standing wave antenna is a resonant structure with a standing-wave current distribution, which is generated by a forward current wave away from the feeding point and a backward current wave due to the complete reflection at the end. An open-ended long wire can be considered as a simple SWA. If a matched load at the end prevents reflections, the current wave propagates only in the forward direction and one gets a traveling wave antenna. In other words, a SWA is a guiding for standing waves and a TWA supports traveling waves. A standing wave antenna can be modeled by two TWAs, whereby the waves are traveling in opposite directions.

2.6.1 Standing wave antenna

To some extent, a standing wave antenna could be considered as a long dipole. It is important to note that the radiation of an antenna is determined by the current distribution.

According to [Stu81], the current distribution of a SWA with a length of l_{SWA} oriented along the z-axis is given by the following equation:

$$I_{\mathrm{SWA}} = I_{\mathrm{m}} \sin\left[\beta\left(\frac{l_{\mathrm{SWA}}}{2} - z\right)\right] = \frac{I_{\mathrm{m}}}{2j}\,\mathrm{e}^{j(\beta l_{\mathrm{SWA}}/2)}(\mathrm{e}^{-j\beta z} - \mathrm{e}^{j\beta z}) \tag{2.24}$$

The current distribution of a SWA can be considered to be sinusoidal, which can be expressed by the first term representing the forward traveling current wave and the second term denoting the reflected wave. Here β denotes the phase constant, I_{m} describes the peak current flowing in the SWA.

According to Eq. (2.25), the radiation patterns of a horizontally or vertically oriented dipole antenna in free space is a function of the elevation angle θ, the wave number k and the length of the antenna l_{SWA}.

$$C(\theta) = \frac{\left|\cos\left(\frac{k l_{\mathrm{SWA}}}{2}\cos\theta\right) - \cos\left(\frac{k l_{\mathrm{SWA}}}{2}\right)\right|}{\sin\theta} \tag{2.25}$$

If a standing wave antenna is placed over an infinite extended, perfectly electrically conducting (PEC) ground plane, the wave is reflected due to the ground plane. It is assumed that the ground plane doubles the maximum E-field through the constructive interference due to the reflected path. The total radiation of an antenna in the presence of a PEC ground consists of a direct path from the antenna and a reflected path from the PEC ground. Therefore, a SWA over a ground plane can be analyzed as a two-element array of a dipole and its image. As is introduced in [Kar14], the total radiation patterns can be calculated by the product of the group pattern and the antenna pattern. For a vertically oriented SWA with the length of l_{v} above a ground plane, with the distance $l_{\mathrm{v}}/2$ from the center of wire and the ground plane, the group pattern $C_{\mathrm{group,v}}$ has a mathematical description of the following expression:

$$C_{\mathrm{group,v}} = \left|\cos k\frac{l_{\mathrm{v}}}{2}\cos\theta\right| \tag{2.26}$$

The radiation pattern of a vertical SWA can be obtained by the product of (2.25) and (2.26):

$$C_{\mathrm{total,v}} = C(\theta)\cdot C_{\mathrm{group,v}} = \frac{\left|\cos\left(\frac{k l_{\mathrm{SWA}}}{2}\cdot\cos\theta\right) - \cos\left(\frac{k l_{\mathrm{SWA}}}{2}\right)\right|}{\sin\theta}\cdot\left|\cos\frac{k l_{\mathrm{v}}}{2}\cdot\cos\theta\right| \tag{2.27}$$

Here, l_{v} is the same as l_{SWA}.

For comparison, according to [Kar14], the group pattern $C_{\mathrm{group,h}}$ for a horizontal dipole with the length of l_h can be expressed by:

$$C_\mathrm{group,h} = |\sin kl_\mathrm{h} \cos\theta \sin\varphi| \tag{2.28}$$

The resulting total radiation pattern of a horizontal SWA with the length of l_h could be obtained by the product of (2.25) and (2.28):

$$C_\mathrm{total,h} = C(\theta) \cdot C_\mathrm{group,h} = \frac{\left|\cos\left(\frac{kl_\mathrm{SWA}}{2}\cos\theta\right) - \cos\left(\frac{kl_\mathrm{SWA}}{2}\right)\right|}{\sin\theta} \cdot |(\sin kl_\mathrm{h} \cos\theta \sin\varphi| \tag{2.29}$$

Here, l_h is the same as l_TWA.

As an example, the radiation patterns of an open-ended long wire with the length of 3λ and radius of 0.5λ at the height of λ above ground is depicted in Fig. 2.9. It can be seen that the elevation patterns are rotationally symmetrical. As the wire length increases, the main beam becomes sharper because the angle of the main lobe direction moves slightly towards the axis of the antenna (end-fire direction).

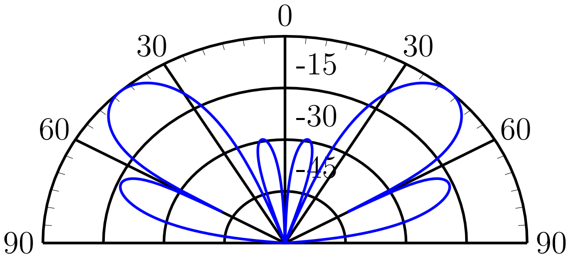

Figure 2.9: Radiation pattern (radiated power flux density, unit: dB) of a SWA with the length of 3λ and the radius of 0.5λ at the height of λ above a perfect electrically conducting ground

A long wire behaves like a SWA, which could be analyzed as two TWAs with forward and backward waves propagating in opposite. According to [Bal97], Eq. (2.30) can be used to calculate the directivity of a long wire above ground behaving like an SWA:

$$D_\mathrm{max} \approx 2 \cdot \frac{9.1\frac{l_\mathrm{SWA}}{\lambda} - 1.7}{2.1 + \ln\frac{l_\mathrm{SWA}}{\lambda}} \tag{2.30}$$

where l_SWA is the length of the SWA and λ is the wavelength. The detailed derivation of the directivity was shown in Chapter C.

2.6.2 Traveling wave antenna

When the transmission line is terminated with a matched impedance, the current wave flows only in the direction from the source to the load. It can be assumed that only the traveling wave exist. Correspondingly, the TL can be considered as a TWA. The radiation pattern for a TWA with the length of 3λ and the radius of 0.5λ at the height of λ above a perfect electrically conducting ground as shown in Fig. 2.10 has only a major lobe in the propagating direction.

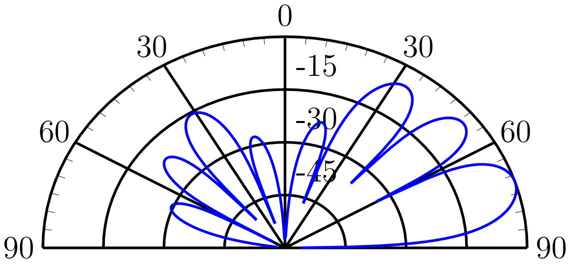

Figure 2.10: Radiation patterns (radiated power flux density, unit: dB) of a TWA with the length of 3λ and the radius of 0.5λ at the height of λ above a perfect electrically conducting ground

2.7 Determination of the directivity of EUTs

To determine the directivity of EUTs, different methods can be used. For electrically small EUTs, it is simple to apply analytical methods to describe the directivity. For electrically large EUTs, it depends on the complexity of the EUT. For long transmission lines, it is straightforward to apply the analytical formulas in Section 2.6. The directivity of an electrically large enclosure with slots has no analytical solutions due to the fact that the radiation patterns cannot be analytically described.

When the statistical properties of the directivity are of interest, it is useful to apply statistical models. Given an example, the average value and the quantiles of the directivity can be obtained based on the statistical model through the random variation of the electrical size of the EUT.

2.7.1 Analytical expression for the directivity

The analytical expression for the directivity of fundamental radiators as well as TWAs and SWAs have been derived in Section 2.5 and Section 2.6. First of all, the current along the radiator can be analytically described. Then the radiated electric field can be obtained directly. The radiated power is calculated by the integral of the electric field over the whole solid angle. As followed, the directivity is obtained directly by taking the ratio of the maximum radiated power flux density and the average radiated power flux density. The directivity expression can be applied later, which can be used to compare with the directivity obtained by numerical simulations.

2.7.2 Spherical wave theory

Besides the analytical solution of the directivity for fundamental radiators and transmission lines, it is also important to investigate the directivity of unintentional antennas, which could be described by the spherical wave (SW) theory. The SW theory has been well developed for spherical field antenna measurements [Han88]. It is assumed that the radiated field of unintentional emitters can be described by spherical functions with particular spherical wave expansion coefficients. The real part and the imaginary part of the wave coefficients are independent Gaussian distributed variables with zero mean. Under this assumption, the distribution of the field components and the directivity can be estimated. The background and a detailed formulation of the SW theory has been described in [Han88] and only a brief description will be given here. In this work, the relevant quantities to describe the unintentional emitters are summarized. These quantities include the radiated E-field strength, the total radiated power and the directivity of the EUT, which would be mathematically described in details.

The far-field of an unintentional emitter can be expressed by spherical waves with special expansion coefficients. The electric field strength of an EUT under the far-field conditions can be expressed by:

$$\mathbf{E}(r,\theta,\varphi) = k\sqrt{\eta}\frac{1}{\sqrt{4\pi}}\frac{\mathrm{e}^{jkr}}{kr}\sum_{smn} Q^{(3)}_{smn}\mathbf{K}_{smn}(\theta,\varphi) \tag{2.31}$$

In the above equations, $Q^{(3)}_{smn}$ are the wave coefficients, and $\mathbf{K}_{smn}(\theta,\varphi)$ are the far field forms of the power-normalized SW functions [Han88]. In fact, (2.31) is the solution of the spherical wave equation. The number of spherical wave modes can be expressed by: $\sum\limits_{smn} = \sum\limits_{s=1}^{2}\sum\limits_{n=1}^{N}\sum\limits_{m=-n}^{n}$, where s defines either a transverse electric (TE) or a transverse magnetic (TM) mode, and $N \approx ka$, where ka is the electrical size, a is the radius of the smallest sphere enclosing the EUT, which is the same as defined in Fig. 2.4, and k is the wave number. Theoretically the summation over n goes to infinity when considering all the modes, however, the SW functions propagates in the far field under the condition that

$n \leq ka$. The number of modes N_m for the truncated series is:

$$N_\mathrm{m} = 2\sum_{n=1}^{N}(2n+1) = 2(N^2+2N) \tag{2.32}$$

The number of samples of the total wave coefficients N_s are twice of N_m since the coefficients includes independent real and imaginary parts. The field components are turned out to be χ^2 distributed with two degrees of freedom (DOF). The total radiated power of an EUT is described by the square of the coefficients of the SW modes and can be expressed by:

$$P_\mathrm{rad} = \frac{1}{2}\sum_{smn}|Q^{(3)}_{smn}|^2 \tag{2.33}$$

It is obvious that the radiated power is independent of the distance r between the source and the observation point. In [Han88], it is shown that the far-field power is χ^2 distributed with 2 DOF. For an unintentional emitter, the maximum directivity D_max can be expressed by [WHH02]:

$$D_\mathrm{max} \approx \begin{cases} 3 & ka \leq 1 \\ (ka)^2 + 2ka & ka > 1 \end{cases} \tag{2.34}$$

where the effective radius denoted by a is the smallest radius of a sphere bounding the EUT (see also Fig. 2.4) and k is the wave number. For electrically small EUTs, the maximum directivity D_max is equal to 3. Under the condition of $ka > 1$, the EUT becomes electrically large, whose D_max is a function of the electrical size ka. Equation (2.34) estimates the D_max for an unintentional emitter, providing a good upper boundary. A statistical investigation of the directivity of unintentional emitters is more suitable. If the probability density function (PDF) is denoted as $f(x)$, and the cumulative distribution function (CDF) is denoted by $F(x)$, then the probability over N samples is called $\lceil f(x) \rceil_N$. If the mean and standard deviation of x are taken to have a value $2\sigma^2$, then the PDF and CDF can be expressed by [WHH02]:

$$f(x) = (1/2\sigma^2)\,\mathrm{e}^{-\,x/2\sigma^2} \tag{2.35}$$

$$F(x) = 1 - \mathrm{e}^{-\,x/2\sigma^2} \tag{2.36}$$

The expected value of $\lceil f(x) \rceil_N$ is expressed by $\langle \lceil f(x) \rceil_N \rangle$, which has the form:

$$\begin{aligned} \langle \lceil f(x) \rceil_N \rangle &= \int_{x=1}^{\infty} xN\left[1-\mathrm{e}^{-\,x/2\sigma^2}\right]^{N-1}\frac{1}{2\sigma^2}\,\mathrm{e}^{-\,x/2\sigma^2}\,\mathrm{d}x & (2.37)\\ &= N2\sigma^2\sum_{m=0}^{N-1}(-1)^m\begin{pmatrix} N-1 \\ m \end{pmatrix} \times \int_0^{\infty}\mu\,\mathrm{e}^{-(m+1)\mu}\,\mathrm{d}\mu & (2.38)\\ &= N2\sigma^2\sum_{m=0}^{N-1}(-1)^m\begin{pmatrix} N-1 \\ m \end{pmatrix}\frac{1}{(m+1)^2} & (2.39) \end{aligned}$$

$$= 2\sigma^2 \sum_{n=1}^{N} (-1)^{n-1} \begin{pmatrix} N \\ n \end{pmatrix} \frac{1}{n} \tag{2.40}$$

$$= \langle f(x) \rangle \sum_{n=1}^{N} \frac{1}{n} \tag{2.41}$$

Herein, $N \begin{pmatrix} N-1 \\ m \end{pmatrix} \frac{1}{m+1} = \begin{pmatrix} N \\ m+1 \end{pmatrix}$ and in the last step in Eq. (2.41), a binomial summation result is applied, which has the form of $\sum\limits_{k=1}^{n} \frac{(-1)^{k+1}}{k} \begin{pmatrix} n \\ k \end{pmatrix} = \sum\limits_{m=1}^{n} \frac{1}{m}$. In fact, the total maximum directivity is the summation of any two orthogonal components. Here, the two orthogonal polarization terms can be denoted as D_{co} and D_{cross}. Cross polarization means the polarizations are orthogonal to each other. Co polarization means the polarizations are parallel to each other. For example, if the fields of an antenna are horizontally polarized, then the cross polarization means the vertical polarization and the co polarization means the horizontal polarization. Correspondingly the total directivity is the summation of these two terms: $D = D_{\mathrm{co}} + D_{\mathrm{cross}}$. The mean values of the co- and cross-polarized terms are equal, thus the expected value of the co- and cross-polarized directivity is: $\langle D_{\mathrm{co}} \rangle = \langle D_{\mathrm{cross}} \rangle = 1/2$. Then Eq. (2.41) could be applied to obtain the expectation value of the maximum co-polarized directivity:

$$\langle D_{\mathrm{co,max}} \rangle = \langle D_{\mathrm{co}} \rangle \sum_{n=1}^{N_{\mathrm{s}}} \frac{1}{n} \approx \frac{1}{2} \cdot \left[0.577 + \ln\left(N_{\mathrm{s}}\right) + \frac{1}{2N_{\mathrm{s}}} \right] \tag{2.42}$$

From the above discussions, it follows that a complete form of the expected directivity of electrically small and electrically large unintentional emitters is given by:

$$\langle D_{\mathrm{max,s}} \rangle \approx \begin{cases} 1.55, & ka \leq 1 \\ \frac{1}{2} \cdot \left[0.577 + \ln\left(N_{\mathrm{s}}\right) + \frac{1}{N_{\mathrm{s}}} \right] & ka > 1 \end{cases} \tag{2.43}$$

Here, N_{s} denotes the number of sampling points over the whole sphere, which can be referred to Table 2.1, with the parameter: $N = ka$ [Kra07a].

In Table 2.1, the number of sampling points for the particular cases in terms of different sampling planes are summarized and presented. The unified form $\langle D_{\mathrm{max}} \rangle$ was used to represent the expectation value of the maximum directivity. Equation (2.43) corresponds to the appropriate number of sampling points over a full sphere (refer to Fig. 2.12). For a one-dimensional (1D) sampling of the radiation patterns over a planar cut (refer to Fig. 2.17), the number of independent samples should take N_{c}, whose value is shown

Table 2.1: Required number of sampling points at different sampling planes

Category	**Polarization**	**Number of sampling points**
Full sphere	1	$N_\mathrm{s} = 4 \cdot (N^2 + 2N)$
Full sphere	2	$N_\mathrm{s} = 8 \cdot (N^2 + 2N)$
Planar cut	1	$N_\mathrm{c} = 2 \cdot (2N + 1)$
Planar cut	2	$N_c = 4 \cdot (2N + 1)$
3 Orthogonal planar cuts	1	$N_\mathrm{6c} = 2 \cdot (6N - 3)$
3 Orthogonal planar cuts	2	$N_\mathrm{6c} = 4 \cdot (6N - 3)$

in Table 2.1. The maximum directivity for planar sampling becomes [WHH02]:

$$\langle D_\mathrm{max,c} \rangle \approx \begin{cases} 2.45, & ka \leq 1 \\ 0.577 + \ln\left(N_\mathrm{c}\right) + \dfrac{1}{2N_\mathrm{c}} & ka > 1 \end{cases} \tag{2.44}$$

If the sampling data is taken on three orthogonal planar cuts with two orthogonal polarizations, the number of the sampling points is denoted by N_6c. The expectation value of the maximum directivity in this case is equal to:

$$\langle D_\mathrm{max,6c} \rangle \approx \begin{cases} 3.10, & ka \leq 1 \\ 0.577 + \ln\left(N_\mathrm{6c}\right) + \dfrac{1}{2N_\mathrm{6c}} & ka > 1 \end{cases} \tag{2.45}$$

Various contributions to the subject of unintentional emitters were published earlier [Han88, WHH02, Buc12]. The theoretical background for describing unintentional emitters has been investigated by Hansen [Han88]. The unintentional emitter radiates energy randomly, not at a preferred direction, therefore the direction of maximum emission is not known a priori by design. Most electronic devices are constructed not to radiate energy intentionally. According to Menssen [MBG14], the maximum directivity of an unintentional radiator is given by Eq. (2.46).

Based on the spherical wave theory, this formula provides the expression for the expectation of the maximum co-polarized directivity over a full sphere:

$$\langle D_\mathrm{co,max} \rangle = \begin{cases} 1.55, & ka \leq 1 \\ \frac{1}{2} \cdot \left[\ln(4(ka)^2 + 8ka) + \frac{1}{8(ka)^2 + 16ka} + 0.577 \right], & ka > 1 \end{cases} \tag{2.46}$$

where ka denotes the electrical size of the EUT. The complete form in the above mentioned equation (2.46) includes two cases. The electrically small ($ka < 1$) objects have a constant directivity of 1.55, while the directivity of electrically large ($ka > 1$) test objects is a function of ka [KHL00].

The unintentional emitters has been described by developing three different models. These models could be constructed based on the analytical model using the SW theory, or a monte carlo simulation (MCS) method based on a large number of stochastic point sources randomly located on a sphere or a MCS method based on the stochastic Hertzian dipole sources. As followed, the MCS method will be described in details.

2.7.3 Numerical determination by Monte Carlo simulations

The unintentional emitter could be simulated by a set of small emitters consisting of the EUT. A Monte Carlo method is a statistical method, which can be used to evaluate the related statistics, e. g., the expectation value, the standard deviation and quantiles by changing randomly parameters of the model, such as the the location or the phase of the emitter.

In order to develop a simulation model of a statistical test object, the selected emitters must be randomly superimposed to form a random EUT. Therefore, it is important to know the positions of the sources and how they are distributed, whether they have different phase angles and in which direction radiates. The positions of the sources can be determined by the coordinates x, y and z:

$$\begin{aligned} x &= a \sin\theta \cos\varphi \\ y &= a \sin\theta \sin\varphi \\ z &= a \cos\theta \end{aligned} \tag{2.47}$$

While the radius a of the sphere keeps constant, the azimuth angle φ uniformly distributed in the range of $(0, 2\pi)$, and the polar angle θ with $\cos\theta$ uniformly distributed in the range of (0, 1) (refer to Fig. 2.6):

$$\begin{aligned} a &= \text{const.} \\ \varphi &= U(0, 2\pi) \\ \cos\theta &= U(0, 1) \end{aligned} \tag{2.48}$$

With randomly changing these parameters of small source emitters, a number of Monte Carlo simulations can be carried out. Then the average value of all Monte Carlo simulations can be derived and compared with the analytical expression. As followed, the procedures of Monte Carlo simulation using point sources and Hertzian dipoles are described.

2.7.3.1 Monte Carlo simulation using point sources

The unintentional emitter could be simulated as a set of stochastic isotropic point sources randomly placed on the surface of a sphere of radius a, as shown in Fig. 2.11. The isotropic spherical radiator radiates EM energy uniformly in all directions. Each small source has a random magnitude ranging from $[0, 1]$ and a randomly distributed phase in the range from 0 to 2π.

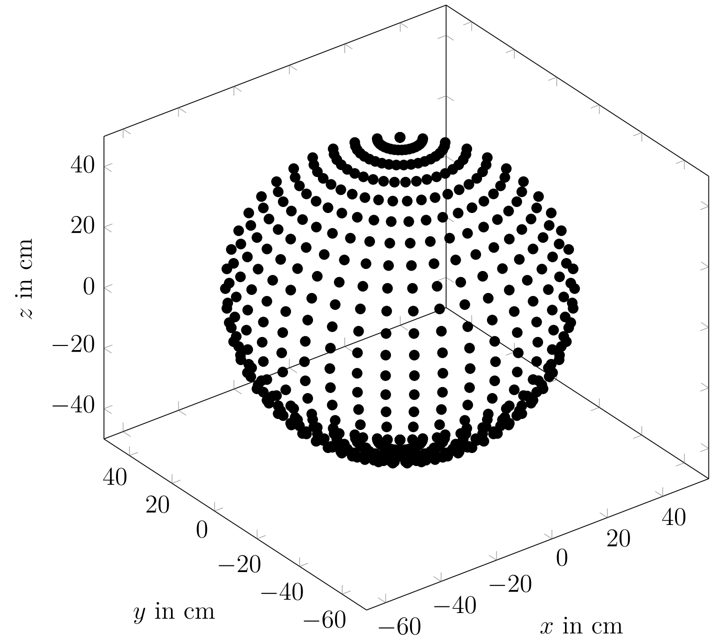

Figure 2.11: A spherical surface consisting of 500 randomly distributed isotropic point sources, with a radius a ($a = 25\,\mathrm{cm}$), a magnitude $I_i \in [0, 1]$, phase $\alpha_i \in [0, 2\pi]$, elevation angle $\theta_i \in [0, \pi]$ and azimuth angle $\phi_i \in [0, 2\pi]$

The electrical size ka of small elements with the magnitude of I_i and the position angle φ_i could be integrated into the equation to obtain the E field:

$$E(\theta, \varphi) = \sum_{i=1}^{N_\mathrm{q}} I_i\, \mathrm{e}^{j(ka \cos \varphi_i + \phi_i)} \tag{2.49}$$

The number of small point sources is here designated as N_q. Each source has a random location (θ_i, ϕ_i) on the sphere. The elevation angle is denoted by $\theta_i \in [0, \pi]$ and the azimuth angle is denoted by $\phi_i \in [0, 2\pi]$. The position of the EUT enters into the equation only by a phase shift φ_i, where (θ_i, φ_i) is the location of ith source, and with the relation: $\cos \phi_i = \cos\theta \cos\theta_i + \sin\theta \sin\theta_i \cos(\varphi - \varphi_i)$ [WHH02]. This model could simulate an enclosure with various electrically small surface sources, due to apertures, slots, etc. It was shown that a good agreement was achieved between the MCS results and the theoretical values according to the spherical wave theory by Hansen [WHH02]. However, the eccentricity of the radiator is not sufficiently described in this model. However, the eccentricity of the radiator is included in the MCS model using Hertzian dipoles, which will be described as followed.

2.7.3.2 Monte Carlo Simulation using Hertzian dipoles

An isotropic spherical radiator cannot be completely physically realized, only described by a postulated model. The most simple physically describable source is a Hertzian dipole. An approach introduced in [Buc12] deals with a MCS model assuming a large number of Hertzian dipoles randomly placed on the surface of a sphere.

The field strength $\mathbf{E}_{\mathrm{Q}_i}$ for every small source can be expressed by:

$$\mathbf{E}_{\mathrm{Q}_i} = \frac{1}{4\pi\varepsilon_0}\left(\frac{\mathbf{e}_r \times (\mathbf{e}_r \times \ddot{\mathbf{p}})}{rc^2}\right) \tag{2.50}$$

In this equation, Q stands for every small source. The second derivative of the dipole moment is denoted by $\ddot{\mathbf{p}}$, $\mathbf{e}_r$ is the unit position vector and r is the distance between the source and the observation point. The field strength of the EUT is obtained by the summation of the field strength of all Hertzian dipole sources, $\mathbf{E}_{\mathrm{EUT}} = \sum\limits_{i=1}^{N_{\mathrm{dp}}} \mathbf{E}_{\mathrm{Q}_i}$.

Based on the MCS model of a set of small Hertzian dipoles, Appendix Chapter D summarizes the most important influencing factors on the directivity evaluation.

2.8 Overview of radiated emission measurement methods

The maximum electric field generated in the far field of the EUTs has to be evaluated to make a safe assessment of the EMC in respect to the interference with radio services. For electrical small equipment, the established method, e. g., the open area test site, gives reliable results. At higher frequencies, the radiation pattern can be very complex and the determination of the maximum electric field strength would need a three-dimensional (3D) spherical sampling in free space, as shown in Fig. 2.12.

The distance of the sampling points would need to be selected according to the wavelength of the measured signal. It is obvious that this approach is very time-consuming for electrically large radiators due to the complex radiation pattern. A full 3D sampling is also not performed in the standardized test method.

Consequently, the knowledge of the measured quantities and the possible conversion of measurement results is necessary. A crucial impact on the conversion process (transforming the radiated power of the EUT into the equivalent electric field strength) is the directivity of the EUT. Therefore, this part gives a short overview over standardized measurement

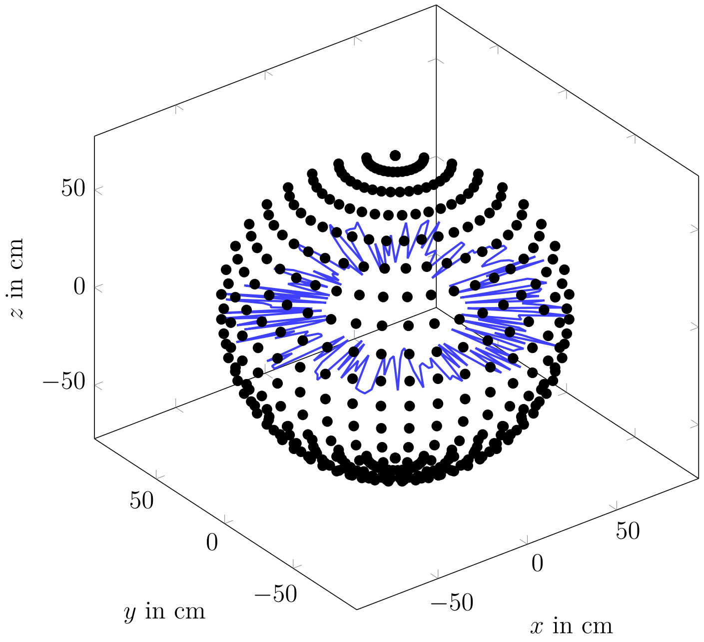

Figure 2.12: Spherical sampling of the EUT in the radiated emission measurements, with the radiation pattern of the EUT (blue curve)

environments, explains the procedure of CISPR 16-4-5 to convert test results and provides three methods to describe the electrically large EUTs as unintentional emitters.

In electric-field-based methods, such as an OATS, a SAC, or a FAR, the E-field strength is directly measured. While the power-based methods, like a GTEM cell and the MSC, measure the radiated power of the EUT. In the following, the radiated emission measurement methods are described explicitly to provide the necessary background to have an interpretation of the different measurement results.

2.8.1 Open area test site

The detailed measurement procedures in an OATS are stated in [CIS06a]. A schematic of the OATS can be observed in Fig. 2.13. The OATS method is the most universally accepted approach for measuring the RE from EUTs. With the help of the antenna factor (AF), the reading of the measuring instrument is associated with the electric field strength in volts per meter, or the magnetic field strength in amperes per meter. By scanning the antenna in the vertical direction (height scan), it is possible to compensate the destructive interference due to the ground plane reflection. The EUT is mounted on a table and the measurement antenna is placed at a specified distance (3 m, 10 m or 30 m). The height of the antenna (h_2 in Fig. 2.13) is varied between 1 m and 4 m (or between 2 m and 6 m for the 30 m range) and the EUT is rotated 360° in the azimuth in order to determine the maximum emission. The test is repeated both for vertical and horizontal polarizations.

Therefore, a cylindrical scan surface is formed due to the horizontal rotation of the EUT and the vertical scan of the antenna, as shown in Fig. 2.14.

In the diagram of the radiation pattern representation (the blue curve in Fig. 2.14), it is obvious that the radiation lobes may occur at different directions, which may not be on the cylindrical surface. This implies that the maximum emission may not be found outside the cylindrical surface. If the maximum E-field strength occurs at the top and bottom surface of the cylinder, the maximum E-field strength cannot be determined. In addition to the height scan and the rotation of the EUT around an axis perpendicular to the ground plane, this would be correct if an additional rotation around an axis parallel to the ground plane would be done. However, this is not the case in the OATS measurement.

In comparison, for electrically small EUTs, it is normally sufficient to test the emission on the cylindrical surface. For electrically large EUTs, it may miss the maximum emission due to its complicated radiation patterns. Besides, the emission measurement in the OATS is very time consuming for electrically large EUTs. In order to obtain a quasi-truly maximum emission, a very fine angle resolution in azimuth and antenna height scan is necessary, which is usually not practicable for an EMC test.

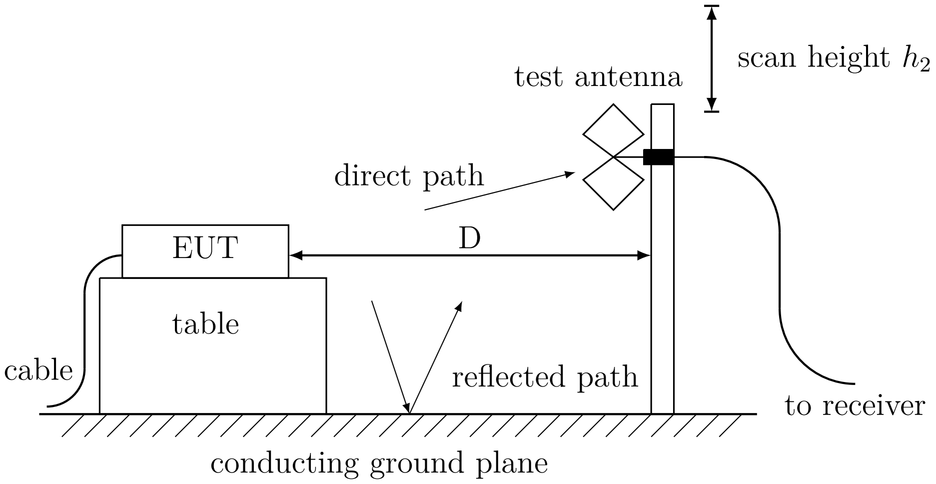

Figure 2.13: Schematic of the side view of the radiated emission measurement in an OATS.

2.8.2 Semi-anechoic chamber

Although the OATS is a reference facility to measure the radiated emission from EUTs, it is not always convenient. In order to be independent of weather conditions, environment or noise influences, most OATS emission measurements are carried out in a SAC (as shown in Fig. 2.15) in a similar manner, realizing indoor shielded laboratory measurement instead of outdoor sites measurement.

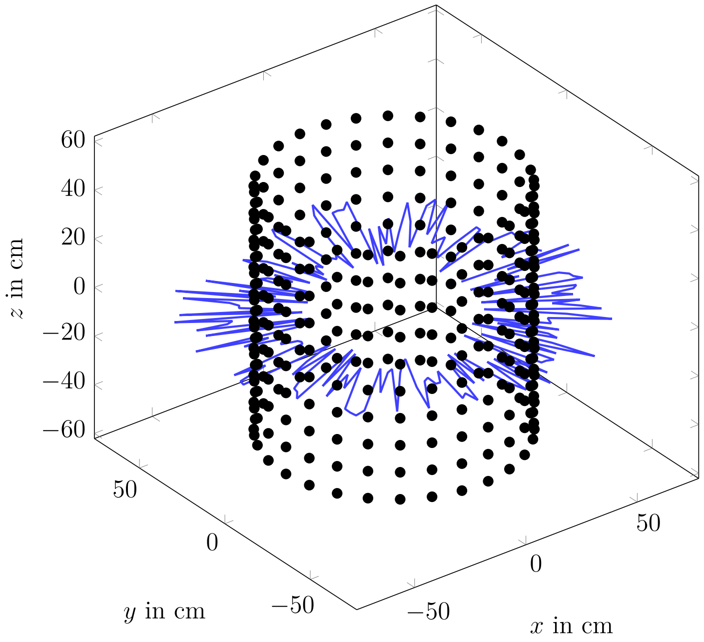

Figure 2.14: Cylindrical scanning of the EUT in the radiated emission measurements in a SAC, with the radiation pattern of the EUT (blue curve)

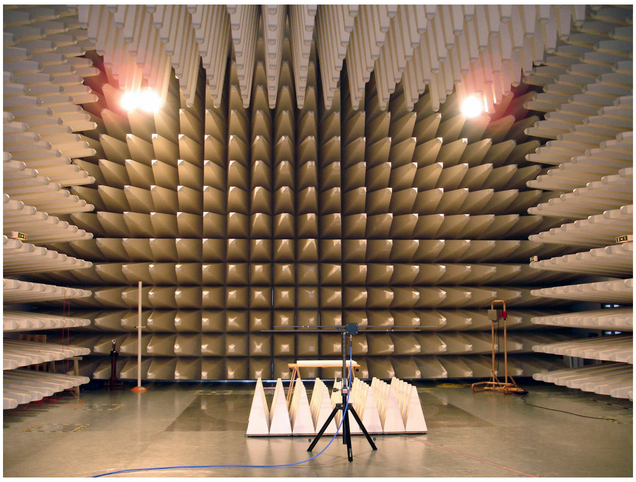

Figure 2.15: SAC at the Otto von Guericke university in Magdeburg

The internal walls and the ceiling are lined with absorbers in order to prevent reflections of the electromagnetic waves. However, the disadvantages are that this facility is relatively expensive and the measurement procedure is complicated. The test space available in a SAC is limited by the size of the „quiet zone“, where the generated electric field is highly uniform. Accordingly, the size of the EUT is limited by the size of the SAC and the applied frequency range. Similar to the OATS measurement, the associated mechanical facilities for locating the position and orientation of the EUT and measuring antennas are also a somewhat costly approach for the RE measurements. The receiving antenna measures the RE level on a cylindrical surface (as shown in Fig. 2.14) as the antenna scan is performed in both horizontal and vertical directions.

2.8.3 Fully-anechoic room

The detailed measurement procedures in the FAR are defined in [CIS06c]. The FAR is constructed as a shielded room, covered with absorber materials on all walls, ceiling and floor. Compared to a SAC, there is no conducting ground plane. The application of the FAR as an alternative to the SAC for RE measurements has been a topic for some time, with the concept of „inexpensive and relatively smaller“ and better reproducibility. The elimination of the ground reflected signal realizes a better reproducibility. A free space (FS) environment can be replicated in a FAR, as shown in Fig. 2.16.

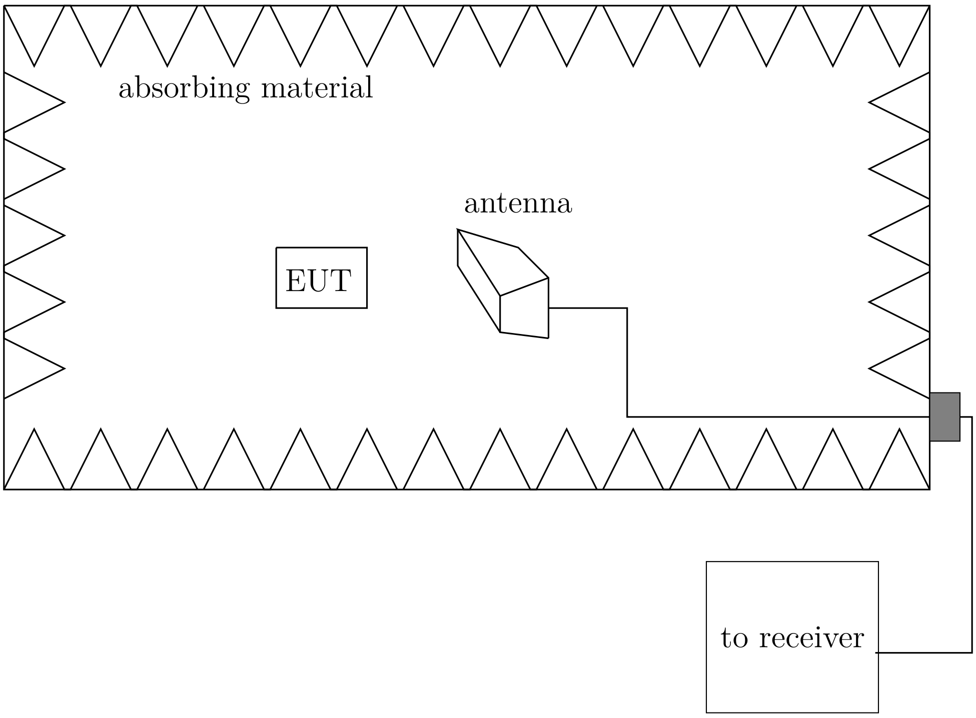

Figure 2.16: Schematic of the side view of the radiated emission measurement in a FAR.

The receiving antenna is usually centered on the test volume at one antenna height and the EUT rotates in the horizontal direction over a complete revolution in order to determine the maximum field strength. This corresponds to a single planar scanning of the EUT, which can be schematically displayed in Fig. 2.17 by the black dotted pointed line. This implies that the RE at other antenna heights may not be measured. This may cause inaccuracies in order to determine the maximum emission. This effect can be observed in the work [BG08]. The deviation due to a coarser angle resolution (19.25°) of the azimuth scan is 3.5 dB compared to a finer angle resolution 2.75° (assumed as the true maximum). Besides, the deviation of the angle resolution increases with increasing the frequency. This implies for electrically large EUTs, with a coarser angle resolution of the whole 360° azimuth scan, that the probability to detect the maximum becomes lower. The deviation of the measured maximum using this measurement method and the true maximum becomes larger with increased frequency. This effect can be also observed in the diagram for the directivity in Fig. 2.17 by the blue curve, it is visible that the maximum emission is not always located at the circumference of the planar cut at one antenna height. Thus, the EUT might be reoriented to other heights so that other planar cuts can be measured.

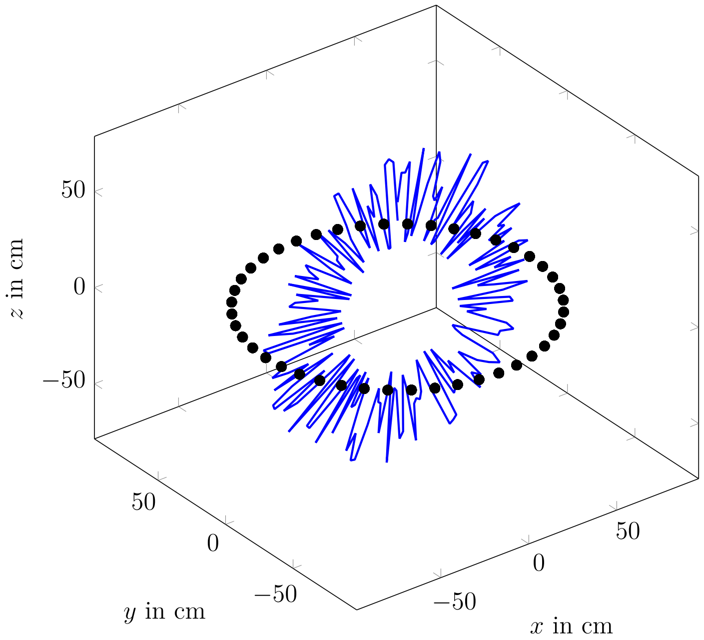

Figure 2.17: Planar sampling of the FAR method, with the radiation pattern of the EUT (blue curve)

2.8.4 Gigahertz transverse electromagnetic cell

The detailed measurement procedures in the TEM/GTEM cell are defined in [Int10]. In a GTEM cell (as shown in Fig. 2.18), the measured voltage readings from three orthogonal positions of an EUT can be employed to estimate the radiated power P_{rad} for each orientation. The fact is that the coupling to the fundamental waveguide mode is considered in a GTEM, and the test object can be conceptually replaced by an equivalent system of electric and magnetic moments. The radiated power of the EUT inside a GTEM cell is propagated in the transverse electromagnetic (TEM) mode and coupled to the ports of the GTEM cell. The EUT needs to be rotated and measured by a sufficient number of different orientations in order to ensure that the RE is properly coupled to the transmission mode [Kod01]. This implies that it will also be very time-consuming to measure the emissions of an electrically large EUT inside a GTEM cell, just as in the SAC or FAR.

Figure 2.18: GTEM cell at the Otto von Guericke University in Magdeburg

2.8.5 Mode–stirred chamber

A mode-stirred chamber is used to measure the total radiated power of EUTs, as is shown in Fig. 2.19. The detailed measurement procedures in the MSC are defined in [CIS02]. In the MSC, a uniformly statistically homogeneous and isotropic field within a local region is generated by rotating a mode stirrer or tuner either continuously or in steps. The correction of antennas-loss effects are avoided by a comparable measurement with a reference source of a known power, while keeping the chamber conditions the same. The measured total radiated power in a MSC includes the 3D radiation information of the EUT and there is no need to perform a height scan or to rotate the EUT, providing an efficient simplification of measurement procedures. Therefore, the MSC is specially advantageous to be used for electrically large EUTs. The measured P_{rad} cannot be directly compared to the limiting values of the electric field of emission standards. It would need to be converted to an equivalent E-field strength, which can only be realized, if the directivity of the EUT is known. Therefore, a power-based emission limit that could directly be applied would be more convenient to use.

2.8.6 Comparison of measurement methods

Three different measurement environments can be used for the determination of the radiated electric field of EUTs. The Semi-anechoic chamber, the OATS and the FAR could be applied for almost all radiated emissions, to directly measure the E-field strength of EUTs. The obtained radiated emission results will depend on the observation methods. In order to measure the maximum emission of an EUT, one would have to apply the *Sphere* method, by sampling the observation points on a spherical surface around the EUT, which is shown in Fig. 2.12. One would obtain the 3D information of the electric field, both in

Figure 2.19: Mode stirred chamber (MSC with dimensions of 7.9 m × 6.5 m × 3.45 m) with a lowest usable frequency (LUF) of 200 MHz at the Otto von Guericke University in Magdeburg. Copyright © Chair of Electromagnetic Compatibility, University of Magdeburg, Germany

vertical and horizontal directions. However, this sampling method is not implemented in standardized EMC measurement procedures.

In the FAR, the *Ring* sampling method is applied, as shown in Fig. 2.17. For a certain number of observation points on a ring surface around the EUT, the E-field strength can be evaluated. The directivity can be determined by: $D(\mathbf{r}) = |\mathbf{E}^2(\mathbf{r})|/|\overline{\mathbf{E}^2}|$, which is the ratio of the position-dependent E-field strength and the average E-field strength over all directions. For most emission measurements, only the maximum E-field strength is of interest, therefore the maximum directivity of an EUT can be determined by the ratio of the maximum and average E-field strength: $D_{\text{max}} = |\mathbf{E}^2_{\text{max}}|/|\overline{\mathbf{E}^2}|$. However, it is possible to miss the maximum emission of the EUT, if the main radiation lobe does not lay on the sampled ring surface.

In the SAC and OATS, the *Cylinder* sampling is used, as shown in Fig. 2.14. The electric field strength is determined on a cylindrical surface around the EUT. The reflection of the ground plane is taken into account by a height scan in the vertical direction. However, with coarser scan either on a cylindrical surface (OATS and SAC) or a planar cut (FAR) there is always a potential possibility to miss the maximum emission of electrically large EUTs. Only a spherical scan with a dense sampling mash could deliver the maximum emission.

Additionally, there are power-based measurement methods which directly determine the radiated power. The direct comparison of the field and power based measurement results is difficult and only possible, if the directivity of the EUT is known. The measurement in the MSC includes the 3D information of the field and could increase the accuracy of the emission measurement at higher frequencies.

2.9 Comparing results of different measurement methods

As it was shown in the section before, the measurement quantities obtained by the possible emission measurement methods differ from each other and a direct comparison of the results is limited. For example, if varying number of lobes are measured due to the scanning methods or the measurement facility, one may observe different radiation patterns of the EUT and different emission levels. Two common ways to convert measured quantities with different measurement methods, especially referring to converting the radiated power to electric field strength, are described in the following:

1. Conversion of the results by conversion factor (CF) according to CISPR
2. Calculation the electric field strength from the radiated power, knowing the directivity of the EUT

2.9.1 CISPR method to calculate conversion factors

In previous works [CIS06b, KH99, Kap03], a conversion method was described, which is aimed to compare the emission results for established test methods and alternative test methods. The established test method is normally the open area test site. The conversion method described in CISPR 16-4-5 can be used to develop emission limits for an ATM and can be summarized as followed:

1. Selecting the reference quantity
2. Describe the test methods and the corresponding measurand
3. Determine the deviations from the reference quantity
4. Determine the conversion factors CF
5. Determine the final emission limit of alternative test methods

This procedure is based on a round robin test conducted with a number N of different EUTs. The number N must be large enough in order to obtain a stochastic representation of typical devices.

In the first step, the reference quantity X is chosen, which is normally the maximum E-field strength of an EUT at a certain distance. Then, the frequency-dependent deviations between the reference value and the results obtained with the test methods are defined, normally in a logarithmic scale. The measured values might have a deviation to the reference quantity, e. g. if the sampling procedure does not guarantee the measurement of the maximum emission. The deviations have to be computed for both the established and alternative test methods. This frequency dependent deviation is given by:

$$D_{\mathrm{ATM},i}(f) = X_i(f) - M_{\mathrm{ATM},i}(f) \tag{2.51}$$

for the ATM and given by:

$$D_{\mathrm{ETM},i}(f) = X_i(f) - M_{\mathrm{ETM},i}(f) \tag{2.52}$$

for the ETM. The quantities $M_{\mathrm{ATMi}}(f)$ and $M_{\mathrm{ETMi}}(f)$ are the measured results obtained by the ATM and ETM for each EUT i. The deviations may depend on different characteristics of EUTs and the specific characteristic of the measurement procedures. For a number N of tested EUTs, the mean value of the deviations for the ATM and ETM can be determined by:

$$\overline{D}_{\mathrm{ATM}} = \frac{1}{N}\sum_{i=1}^{N} D_{\mathrm{ATM},i} \tag{2.53}$$

$$\overline{D}_{\mathrm{ETM}} = \frac{1}{N}\sum_{i=1}^{N} D_{\mathrm{ETM},i} \tag{2.54}$$

Furthermore, *inherent uncertainty* is equivalent to the standard deviation, can be calculated by:

$$u_{\mathrm{ATM,inherent}} = \mathrm{std}(D_{\mathrm{ATM}}) = \sqrt{\frac{\sum_{i=1}^{N}(D_{\mathrm{ATM},i} - \overline{D}_{\mathrm{ATM}})^2}{N-1}} \tag{2.55}$$

$$u_{\mathrm{ETM,inherent}} = \mathrm{std}(D_{\mathrm{ETM}}) = \sqrt{\frac{\sum_{i=1}^{N}(D_{\mathrm{ETM},i} - \overline{D}_{\mathrm{ETM}})^2}{N-1}} \tag{2.56}$$

The inherent uncertainty ($u_{\mathrm{ATM,inherent}}$ and $u_{\mathrm{ETM,inherent}}$), the uncertainty contributed by measurement instrumentation ($u_{\mathrm{ATM,m}}$ and $u_{\mathrm{ETM,m}}$) and the intrinsic uncertainty ($u_{\mathrm{ATM,intrinsic}}$ and $u_{\mathrm{ETM,intrinsic}}$) can be combined into the total uncertainty:

$$u_{\mathrm{ATM}} = \sqrt{u^2_{\mathrm{ATM,m}} + u^2_{\mathrm{ATM,inherent}} + u^2_{\mathrm{ATM,intrinsic}}} \tag{2.57}$$

$$u_{\mathrm{ETM}} = \sqrt{u^2_{\mathrm{ETM,m}} + u^2_{\mathrm{ETM,inherent}} u^2_{\mathrm{ETM,intrinsic}}} \tag{2.58}$$

The total uncertainty can be used to obtain the expanded uncertainty U_{ATM} or U_{ETM} using a coverage factor κ. The coverage factor κ depends on different probability distributions, different number of experiments and different confidence levels, which is usually taken 95 %. Here, it is assumed that $\kappa = 1.96$.

$$U_{\mathrm{ATM}} = \kappa \cdot u_{\mathrm{ATM}} \tag{2.59}$$

$$U_{\mathrm{ETM}} = \kappa \cdot u_{\mathrm{ETM}} \tag{2.60}$$

For each individual EUT i, the frequency dependent conversion factor $K_{\mathrm{i}}(f)$ can be calculated by the subtraction of the deviations between the alternative and established methods.

$$K_i(f) = D_{\mathrm{ATM},i}(f) - D_{\mathrm{ETM},i}(f) \tag{2.61}$$

Correspondingly, the average conversion factor $\overline{K}(f)$ for all EUTs can be calculated by:

$$\overline{K}(f) = \overline{D}_{\mathrm{ATM}}(f) - \overline{D}_{\mathrm{ETM}}(f) \tag{2.62}$$

Inserting Eq. (2.53), (2.54), using the reference quantity X_{i} yields:

$$\overline{K}(f) = \frac{1}{N}\sum_{i=1}^{N}(X_i - M_{\mathrm{ATM},i}) - \frac{1}{N}\sum_{i=1}^{N}(X_i - M_{\mathrm{ETM},i}) = \frac{1}{N}\sum_{i=1}^{N}(M_{\mathrm{ETM},i} - M_{\mathrm{ATM},i}) \tag{2.63}$$

As the next step, the emission limit for the ETM can be converted into the emission limit for the ATM:

$$L_{\mathrm{ATM}}(f) = L_{\mathrm{ETM}}(f) - \overline{K}(f) \tag{2.64}$$

This equation does not take into account the uncertainty of the test methods. Thus, a difference Δ between the uncertainty of the ETM U_{ETM} and the uncertainty of ATM U_{ATM} can be calculated:

$$\Delta = U_{\mathrm{ATM}} - U_{\mathrm{ETM}} \tag{2.65}$$

If the ETM has a higher uncertainty than the ATM, e. g., $U_{\mathrm{ATM}} > U_{\mathrm{ETM}}$, the deducted emission limit for ATM has to be corrected as follows:

$$L_{\mathrm{ATM,U}}(f) = \begin{cases} L_{\mathrm{ATM}}(f) - \Delta(f) & \text{if } \Delta(f) > 0 \\ L_{\mathrm{ATM}}(f) & \text{if } \Delta(f) \leq 0 \end{cases} \tag{2.66}$$

The conclusion from the Eq. (2.66) is that if the alternative method is better, which delivers a smaller uncertainty, then Δ is not taken into account. That is to say, there is always only penalties for ATMs on this method, even if the uncertainty is mainly caused by the ETM. This method is limited to the measurement procedures determining the same quantity, e. g., the electric field strength. Besides, by extending this method, it could also be applied to obtain a limiting value for the radiated power as measured in the mode stirred chamber.

2.9.2 Convertion using the directivity

As was introduced in Section 2.5, the maximum electric field strength can be obtained from the radiated power with the directivity according to Eq. (2.14). This effect was investigated in different studies. In the works [Kra11, WHK04], the conversion between different measurement methods – FAR, SAC, (G)TEM cell and MSC was analyzed. A dipole antenna with a directivity value of 1.5 was investigated as the EUT. It is assumed that the total radiated power from the EUT is the same for each case and the conversion could be derived in a straightforward manner. In the study [Kra11], the conversion of the measured quantities in different RE measurement sites was discussed, taking the uncertainty due to the polarization mismatch μ and the directivity effect from the statistical point of view into account. Besides, the statistical properties of the directivity is analyzed. However, the directivity depends strongly on the geometry, the size and the frequency. Consequently, more realistic values for the directivity of ELEUTs have to be used. This thesis would investigate the directivity of ELEUTs by numerical simulations. With the simulated directivity values, it is straightforward to convert the total radiated power in a MSC to an equivalent E-field strength.

In the work [Dij07], the conversion method between different measurement facilities was numerically analyzed for several EUTs. First of all, the conversion algorithm was applied to a simple model. A set of isotropic point sources representing an EUT was used to obtain the emission limit for MSC. The RE limits in the MSC were obtained assuming a directivity equal to one, due to the equal radiation in all directions of the isotropic point source. Special consideration were done to deal with the conversion of the RE between the 10 m OATS/SAC and the MSC methods. It was concluded that approximately 5 dB lower results in a MSC was observed, compared to the 10 m OATS/SAC method and approximately 4 dB lower results in relation to 3 m OATS/SAC method. A similar result can be observed for a tuned dipole with a well-known directivity of 1.65. However, for electrically large EUTs, the directivity is much higher than one and further investigations will be done in this thesis. Furthermore, the procedures were carried out for a long dipole antenna with an analytically calculable directivity. The conversion of the emission results was performed using the 3 m SAC method, the 3 m FAR method and the MSC method. It was concluded that the deviation from the reference quantity due to the directivity of EUTs for these three measurement methods is approximately the same, however, the deviation considerably depends on the polarization of the emission source. The uncertainty contributed by measurement instrumentation are almost equivalent, when comparing the FAR method, the OATS/SAC method and the MSC method. In this research, the directivity of a long dipole antenna was investigated, which was simply calculable through analytical formulas. However, the directivity for other electrically large EUTs is normally impossible to be analytically describable, because the radiation patterns of the ELEUTs cannot be analytically handled. In this case, numerical simulations are required.

The results in [Dij07] show that the conversion factors depend on the frequency and polarization. These dependencies reflect the significant influence of the radiation characteristics of EUTs. The statistical radiation characteristics are generated by stochastically varying the parameters of a number of elementary radiators inside a certain volume [KH99, Kap03]. The basic idea is that the emission of every EUT can be modeled by superposing the radiated fields of a set of elementary radiators with a random amplitude, phase angle and position. Statistical variations of these parameters of the set of small radiators correspondingly provides the field strength of all kinds of EUTs. For each EUT i, the E-field strength was directly compared for FAR and OATS and the conversion factor was calculated straightforward by taking the ratio of the E-field strength in an OATS and FAR.

The calculation of the E-field strength based on the described statistical model at different test sites in [Dij07] is expected to provide conversion factors that are presented as probability distribution functions. Each variation leads to one conversion factor. The simulations result in n conversion factors (see the definition in (2.61)) at every frequency. For the calculation of the n conversion factors, the parameters (position, amplitude and phase angle) of the model are viewed as being uniformly distributed. Correspondingly, the expectation value and standard deviations are calculated. The expectation values interpret the system deviation between two measurement methods. The standard deviation corresponds to the uncertainty of the evaluation. The results show that for the horizontal polarization, the expected value of the conversion factor has higher values and wider borders of 95 % probability, compared to the vertical polarization of the antenna. In the above work, merely the ELEUTs were investigated.

In comparison with the models discussed above, a conversion method for an ELEUT and ELEUT with connecting wires is investigated in this thesis. Combined with the electrically small EUTs studied in the above work [Dij07], the conversion method would be generalized for electrically small and large EUTs as well as large EUTs with connecting wires. The directivity of the ELEUT is investigated by numerical simulations in this thesis. Furthermore, in Section 3.5, a new analytical approximation is derived to describe the directivity of electrically large EUTs with connecting wires. Because it is difficult to access the real values from statistical models, the ELEUTs investigated in this thesis are not purely based on statistical models. However, the statistical model in [KH99, Kap03] provides a good approach to determine the conversion factors between different measurement methods, providing a comparison in the later investigations.

2.10 Chapter conclusion

In this chapter, first of all, the theoretical backgrounds of radiated emission are introduced. As followed, the radiation behavior and the directivity of fundamental radiators are outlined. Then, the analytical formulas based on the TWA and SWA theory were derived, in order to describe the directivity of electrically large test objects. This theory will be applied in Section 3.3. Then the radiated emission measurement methods are described.

To describe the unintentional emitters, three different approaches were interpreted. The first method – spherical wave theory assumes the electric field strength of unintentional emitters could be expressed by spherical wave modes with specific spherical mode coefficients. Later, Wilson developed a MCS model with a set of isotropic point sources randomly distributed on a sphere to obtain the statistical properties of the EUT [WHH02]. In a similar manner, another statistical model consisting of a set of small Hertzian dipoles with stochastic magnitudes and phases as well as polarizations was considered to effectively model the unintentional emitters. This model takes into account the simplest physically described small antennas – Hertzian dipoles. In short, the first approach is based on the spherical wave theory and the second approach shows a MCS model based on point sources, and the third method demonstrates a MCS model based on Hertzian dipole antennas.

The three different observation methods – *Sphere* method, *Cylinder* method as well as *Ring* method correspond to the quasi-real measurement environments, OATS/SAC and FAR. The conversion of measured values can be done using the procedure reported in CISPR 16-4-5. In extension, this procedure could be applied to develop a limiting value for the mode stirred chamber as the alternative measurement environment.

3 Simulation of Electrically Large EUTs

For a reliable conversion of the total radiated power of the EUT to the equivalent electric field strength, the quantity of the directivity must be known. However, the analytical models based on the spherical wave theory are applicable only for EUTs without cabling. Now the question is to know how real EUTs behave and how the cables could be included. One approach is to adopt the effective radius to approximate the directivity. Use an estimate based on measurements of the radiated emission is another approach, but this is very time consuming and needs a wide measurement campaign. Fortunately, numerical simulations are feasible to validate directivity models.

Different simulation models of EUTs [WV14, WV15a, WHV16] are suggested and verified in this chapter. A slotted box was physically constructed as an artificial EUT and an appropriate simulation model was created. The simulation results were compared with the measured radiation patterns of the EUT in different measurement facilities and the model was refined in order to give a sufficient agreement between measurements and simulations. Finally, the model was extended to an EUT with a connecting cable [WV15b]. Additionally, an analytic approach to determine the directivity of EUTs with cabling based on simulated current distribution on the cables is proposed.

3.1 Basic model of a slotted enclosure as an EUT

A first numerical simulation model of an artificial EUT was developed, which allows investigation of the directivity in the frequency range between 1 GHz to 6 GHz. A PC-size equipment should be simulated to represent the radiated emissions from a typical electronics enclosure. To validate the simulation results, a real EUT was constructed, as shown in Fig. 3.2. In order to place the radiating source inside the box, the front plate could be removed and reinstalled.

3.1.1 EUT modeling

All the simulations of EUTs are done using CST Microwave Studio, based on a finite differences in time domain (FDTD) technique [Com09].

An enclosure with a rectangular slot and two straps on its front plane is simulated. The model is shown in Fig. 3.1. As for real EUTs, the enclosure provides shielding efficiency over a wide frequency spectrum but enhances the emissions at certain frequencies due to resonance effects. The dimensions of the enclosure are 0.4 m × 0.3 m × 0.2 m, in the x, y and z direction, respectively. The considered frequency range was 1 GHz to 6 GHz for both simulations and measurements, at which the EUT is supposed to be electrically large due to the electrical size ka larger than 1. The structure was internal excited by a discrete port (with an input power 1 W) driven by a Gaussian signal for the simulations. In order to agree with the measurement setup, a comb generator was also included in the simulation model as shown in Fig. 3.1b. The boundary condition was chosen to be 'open and space' in order to simulate the free space condition and comply with the measurement environment. In Fig. 3.1, the corresponding spherical coordinate is shown, where (Phi, Theta) are the elevation and azimuth angle respectively. It is to be noted that the definition of the θ and ϕ is different in the CST coordinate system in Fig. 3.1 and the coordinate system in Fig. 2.6.

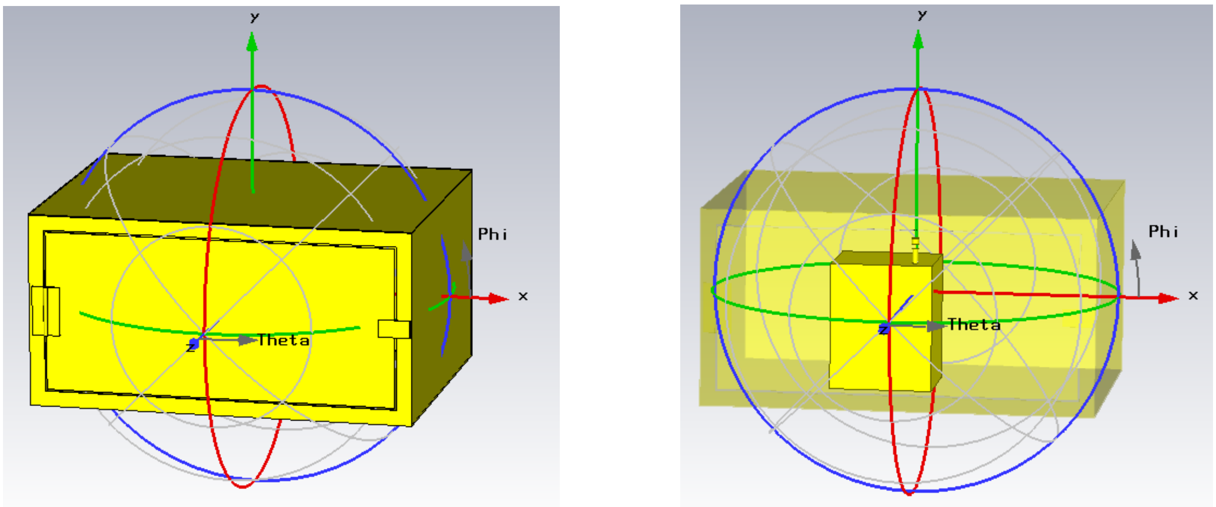

(a) Outside view

(b) Inside view

Figure 3.1: Simulation model of the EUT – a rectangular enclosure with dimensions of 0.4 m × 0.3 m × 0.2 m and interior excitation source, see inside view.

3.1.2 Measurement set-up

To validate the numerical model, the simulated results were compared to measurement results. The measurements were carried out in a SAC, with floor absorbers placed on the ground plane to realize the fully anechoic effect (free space conditions). The measurement set-up was chosen according to the standard CISPR 16-2-3 [CIS10]. It shows the emission test setup in Fig. 3.2, where the receiving antenna is 3 m away from the EUT at a measurement height of 1 m. A small antenna mounted on one side of the comb generator

(RSG 2000, Teseq [Tes14]) with 100 MHz line spacing was used as the exciting source inside the enclosure, as shown in Fig. 3.2a. During the measurements, the EUT was placed in the center of a turntable and rotated in the horizontal direction with 180 steps (with 2° angle resolution) over a complete revolution. The simulation was performed for a planar scan over the horizontal plane to compare the results.

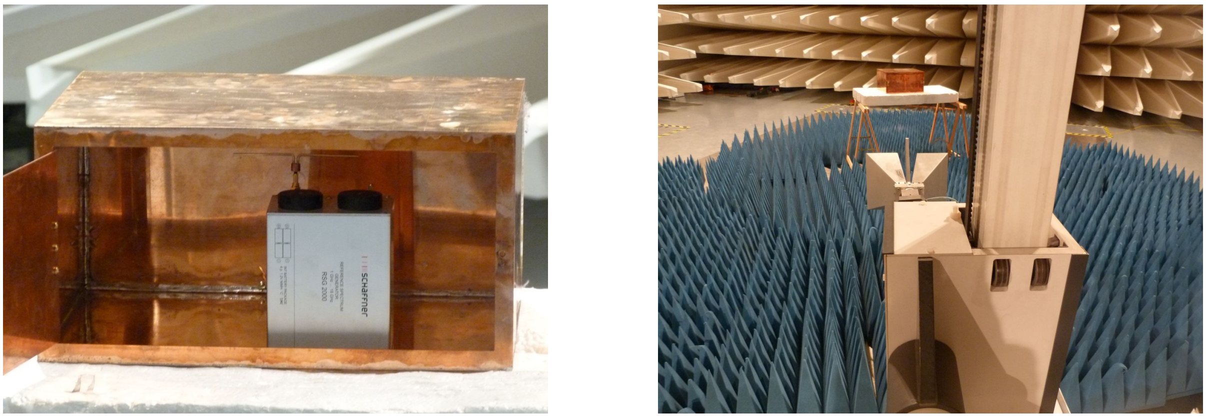

(a) The enclosure with the front plate held by two conducting straps (right strap not shown because of the opened front plate) as the EUT, with a small antenna mounted on the comb generator acting as a source inside the box

(b) SAC with floor absorbers to realize the fully anechoic effect at the Otto von Guericke university in Magdeburg with the receiving antenna at a distance of 3 m from the EUT and at the height of 1 m

Figure 3.2: Measurement of the enclosure in the SAC with floor absorbers to behave as a FAR at the Otto von Guericke university in Magdeburg.

3.1.3 Analysis of radiation patterns

In order to compare the measured and the simulated radiation patterns at an exemplary frequency of 1.5 GHz, the results had to be normalized. The normalization of the field strength was performed according to the output power of the excitation source. The output level of the comb generator during the measurements was 95 dB µV at 50 Ω, e. g. 6.3×10^{-5} W. Nevertheless, for the simulation a power of 1 W was used. For the purpose of obtaining a dimensionless quantity, the square of the electric field strength was normalized to the power. The planar cut result as a function of the azimuth angle ϕ in the horizontal plane is shown in Fig. 3.3.

The two results are quite similar and the main lobe direction and magnitude of the measured and simulated electric field strength matches well with only small deviations. Besides, the minimum emission level shows a relatively large deviation. The simplified simulation model of the EUT may cause this deviation. The simulation model neglected fine details such as screws and junction materials of the EUT. Furthermore, the measurement accuracy was influenced by the positioning accuracy of the large turn table in the SAC, which causes

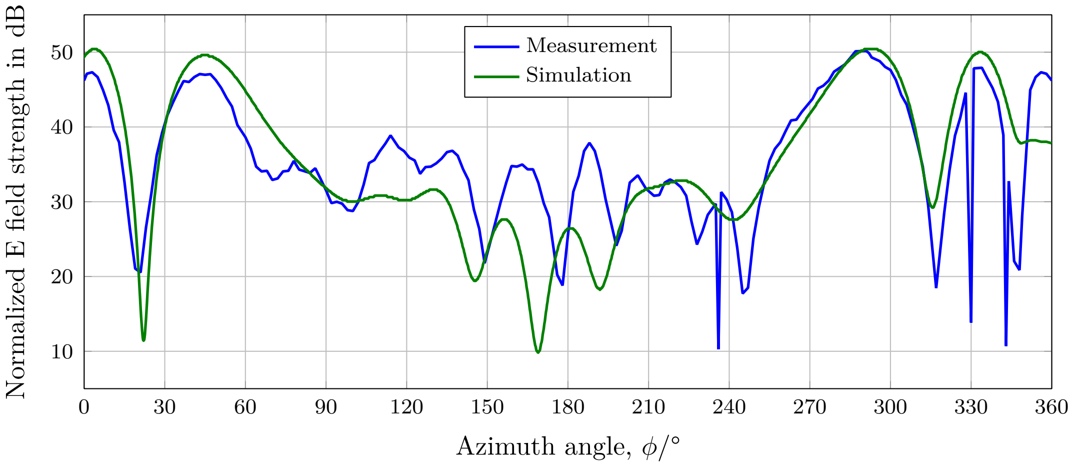

Figure 3.3: Planar cut of the electric field strength of the test object at 1.5 GHz.

deviations of the angle during the horizontal rotation of the EUT. Nevertheless, the results showed that it is feasible to purely simulate the EUT for a statistical analysis.

3.2 Refined EUT model

To increase the accuracy of the simulation results, the EUT was refined. The two straps were removed and a complete through slot was realized on the front plane, as shown in the external view of the experimental set-up in Fig. 3.5a and the simulation model Fig. 3.4a. To make sure that the internal generator excited the internal resonances, a comb generator (RSG 3000, Teseq [Tes11]) with a 10 MHz line spacing was used as the excitation source inside the enclosure. A small monopole antenna was feed by the comb generator, as shown in Fig. 3.4a.

To increase the angle resolution during the measurement, the radiation pattern was measured in the FAR at the University of Technology (TU) Dresden with a 2 m antenna separation, as shown in Fig. 3.5b.

The normalized electric field strength as a function of the azimuth angle on the horizontal plane at 2.1 GHz (as an exemplary frequency) is displayed in Fig. 3.6. It shows that the main lobe matches with small deviations, however, a small angle shift at the angle position of 300° was observed. As described in [MC05], the emission pattern is very sensitive to the detailed construction of the EUT. Numerical modeling techniques are not expected to give the emission pattern accurately. However, so far a good agreement of our EUTs could be achieved. Besides, it can be observed that the main lobe width of the radiation pattern is almost equal. The overall progression of the radiation pattern coincides between the simulations and measurements. The radiation patterns in Fig. 3.6 shows a good agreement. Because the aim of the work is the estimation of the maximum directivity in order to

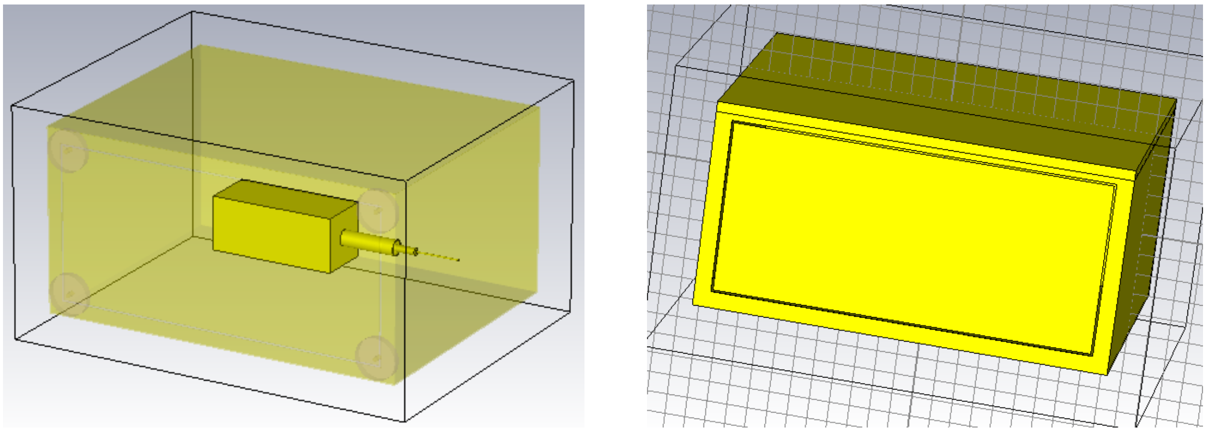
(a) A monopole antenna mounted on the comb generator RSG 3000 inside the enclosure as the excitation source

(b) A complete-through slot on the front plane of the enclosure

Figure 3.4: Simulation model of a slotted enclosure with a complete-through slot on the front plane, a monopole antenna mounted on the comb generator RSG 3000 inside the enclosure as the excitation source.

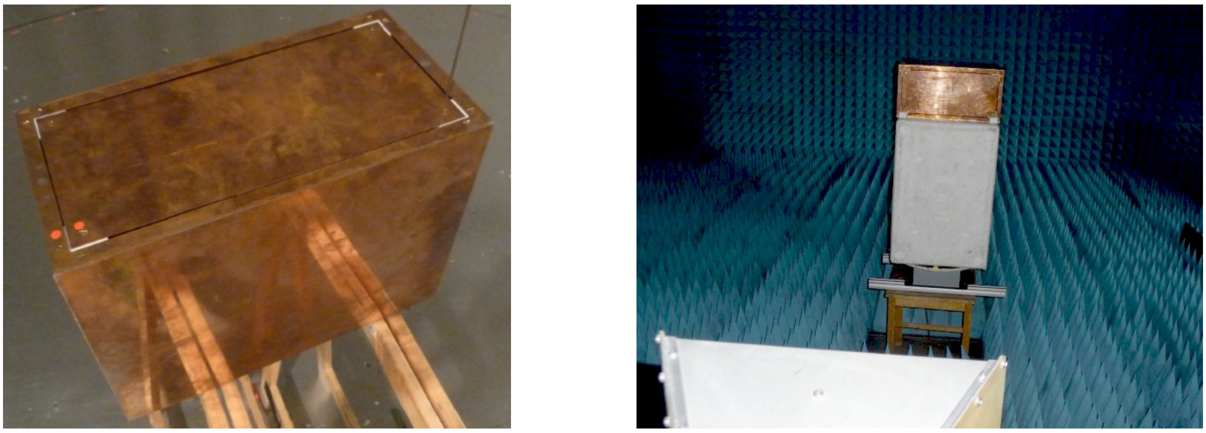
(a) A refined EUT with a complete through slot on the front plane

(b) Measurement in the FAR at the TU Dresden

Figure 3.5: Measurement of the radiation patterns of the refined EUT in the FAR at the TU Dresden (with the measurement distance at 2 m and the antenna height at 1 m).

convert the measured total radiated power to an equivalent E-field strength, the model is sufficient exact for the further investigations. Compared to the SAC measurement with floor absorbers, the FAR measurement seems to provide more detailed information due to a better agreement of the minimum emission level in Fig. 3.6.

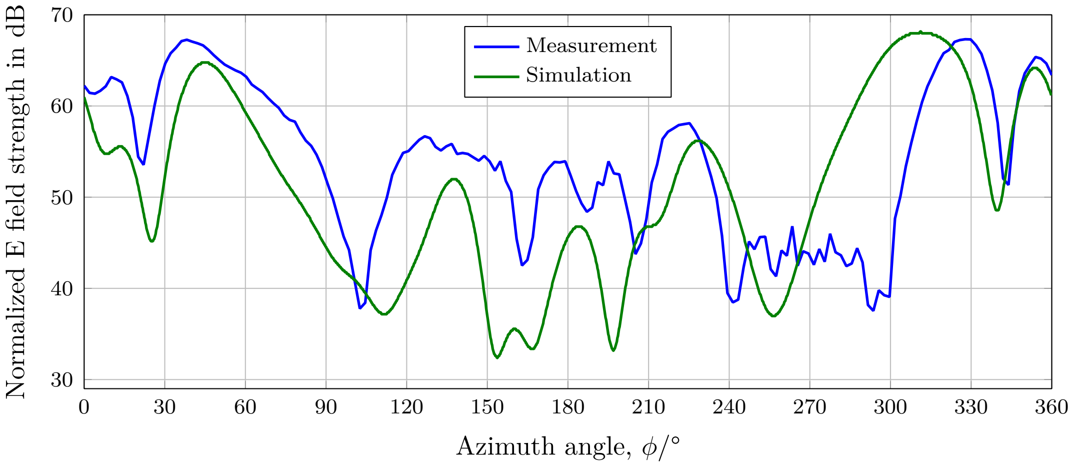

Figure 3.6: Planar cut of the electric field strength at 2.1 GHz.

3.3 Model of EUT with cabling

To get power supply or a communication connection, most electronic equipment is connected by cables to the operation site. The cabling is a well-known source of unintentional radiated emissions and has a massive impact on the radiation behavior of the EUTs. This is due to the wire resonances and a large dimension relative to the enclosure. Therefore, it was considered in this investigation. First, the applicable model of connected cables was analyzed. Then the model was verified by measurements. The basic model of the EUT, e. g. the rectangular enclosure with dimensions of $0.4\,\mathrm{m} \times 0.3\,\mathrm{m} \times 0.2\,\mathrm{m}$ was not changed.

3.3.1 Modeling attached cables

In a first step it was analyzed, how a simple cabling model can be included into the simulation. Standard cables consist of more than one wire and in best case the signal is transfered via symmetrical lines. Due to unsymmetries in the configuration, common mode currents are generated and the radiated emission is increased. To simplify the cabling model, one has to answer the question, if the type of cable does influence the directivity of the equipment or if the cabling can be substituted by just a single wire. Therefore, the impact of different cable configurations on the directivity of an EUT was numerically investigated. Based on the already existing EUT model, four different configurations were considered.

These configurations can be described by:

- a single wire with a length of 0.3 m, placed inside the enclosure with a CM excitation
- a single wire with a length of 1 m, guiding from inside to the outside enclosure with a CM excitation

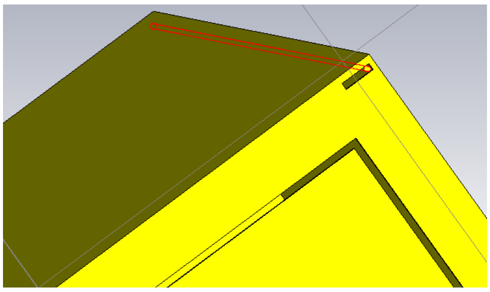

(a) Single wire inside the enclosure

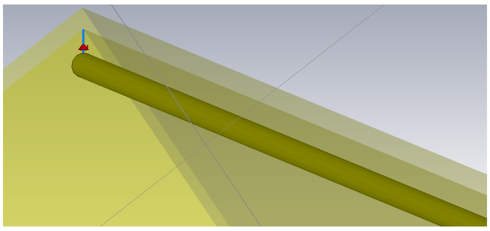

(b) Excitation source between the single wire and the enclosure wall

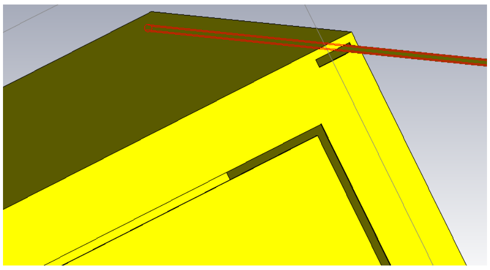

(c) Single wire with the length of 1 m, through a small slot on the top right corner guiding to the outside enclosure

Figure 3.7: Simulation model of different wire configurations attached to a rectangular enclosure with dimensions of 0.4 m × 0.3 m × 0.2 m, located 80 cm above ground.

- two symmetrical wires guiding from inside to outside the enclosure with a DM excitation
- two unsymmetrical wires with a length difference of 1 cm guiding from inside to outside the enclosure with a DM excitation

The wires are placed through a small aperture (with dimensions 2 mm × 9 mm, see Fig. 3.7a) on the top right corner of the enclosure. The aperture is small so that the possible influence on the emission level could be neglected. The wire radius r is identical for all configurations, which is $r = 0.9\,\text{mm}$. The single wire was excited in CM by a source located between the wire and the interior enclosure wall, as it is shown in Fig. 3.7b, as well as in the schematic view in Fig. 3.8.

The two-wire system with a separation of $d_1 = 5\,\text{mm}$ is excited by a DM source between the two wires, as can be seen in Fig. 3.9. When the enclosure is equipped with two wires with identical lengths of 1 m, it is considered to be a symmetrical two-wire configuration. However, when the two wires have a length difference $\Delta l_{12} = 1\,\text{cm}$, the asymmetry causes

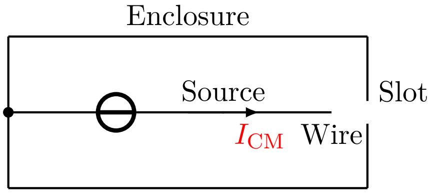

(a) Single wire inside the enclosure

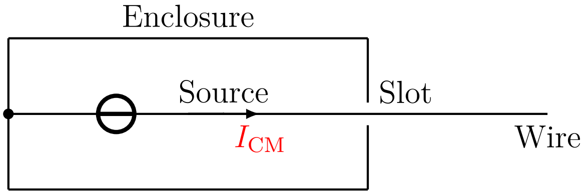

(b) Single wire guiding to the outside of the enclosure

Figure 3.8: Schematic of the single wire system attached to the enclosure, located 80 cm above ground.

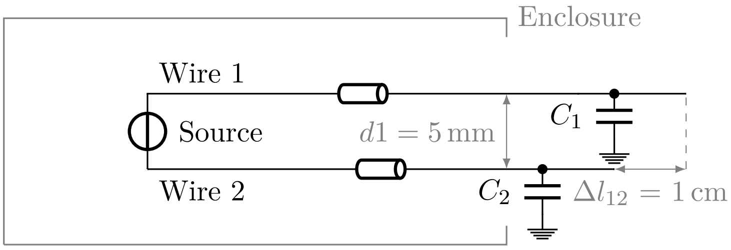

Figure 3.9: Schematic of the system with two unsymmetrical wires located 80 cm above ground, with parasitic capacitances C_1 and C_2 between the wires and ground.

CM currents on the cable. The excitation source keeps a constant power of 1 W for all simulations, which is fed to the attached wire.

The emission level of the simulated EUT is considered to be the summation of the wire radiation and the radiation of the enclosure. It can be predicted that if the wire is located inside the enclosure, it just feeds the cavity and the emission level of the system is dominated by the radiation of the enclosure. When the wire extends from the inside to the outside of the enclosure, both the slot radiation of the enclosure and the wire radiation need to be considered. The magnitude of the CM current I_{CM} for different wire configurations is presented in Fig. 3.10.

Several observations can be made from the simulation results. The current has a larger magnitude inside the enclosure and a smaller magnitude outside the enclosure. This can be caused by the reflection at the feed-through by the small slot and multiple resonances inside the enclosure. As can be seen in Fig. A.4, the modes of the enclosure in the frequency range from 0.6 GHz to 1.8 GHz increases very fast.

For different wire configurations, the current oscillates at multiples of half wavelengths and the peak current occurs almost at the same frequencies. In case of two symmetrical

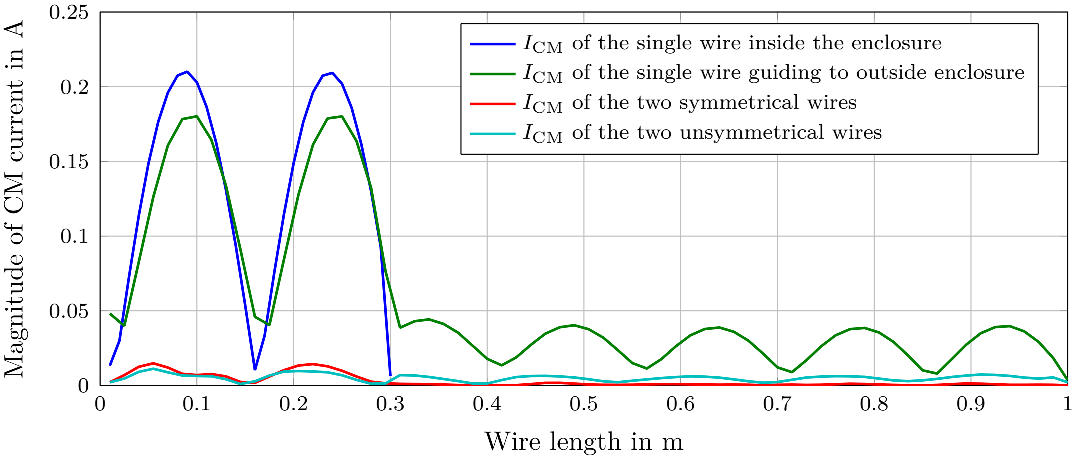

Figure 3.10: Common-mode current I_{CM} for different wire configurations at 1 GHz.

wires, the CM current has very small magnitudes outside the enclosure. Vice versa, the unsymmetrical wire system shows larger magnitude of CM currents. Due to the length difference (1 cm according to Fig. 3.9), the parasitic capacitances C_1 and C_2 between the wires and ground would be different. Therefore, due to this unbalance at the end of the wires, the CM current shows larger magnitudes, compared to the symmetrical two-wire system. It can be also observed that due to the stray capacitance between the wire and the ground, the CM current is not definitely equal to zero at the end of the wire. A similar tendency can be observed for the wire length of 3 m in Fig. B.1.

The configuration with the short wire inside the enclosure was not further considered. The directivity is obtained from simulations with the frequency step of 1 MHz, which consists of altogether 5001 far field monitors in the frequency range from 1 GHz to 6 GHz. The simulation was performed in free space conditions and with the EUT located 80 cm above ground.

The simulated directivity of the EUT placed above ground for the above three configurations as a function of the frequency is shown in Fig. 3.11.

In general, the directivity has similar tendency and only minor differences. At some frequencies, a shift of the resonant frequencies can be observed in Fig. 3.11. The value starts at 12.5 dBi at 1 GHz. After reaching a maximum, it decreases slowly with small oscillations. The maximum value is caused by the ground reflection, which can be seen when the result is compared with the directivity in free space in Fig. 3.12. However, in general the resonances occur almost at the same frequencies for different wire configurations. When the wire length is extended to 3 m, the simulated directivity is shown in Fig. B.2.

It should be noted that the maximum electric field strength at a certain distance will also depend on the wire configurations. As an example, the E-field strength for the slotted enclosure at the distance of 1 m is shown in Fig. 3.13.

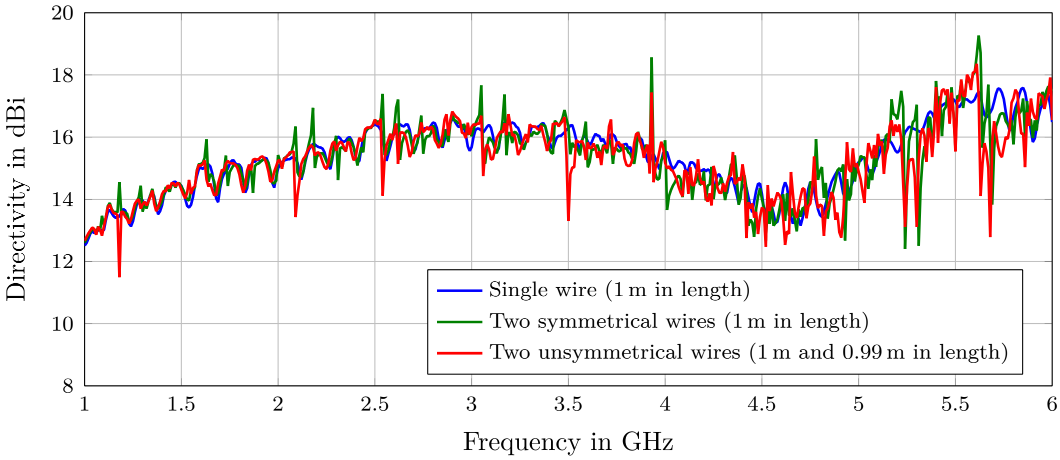

Figure 3.11: Simulated directivity against the frequency for 3 different wire configurations attached to the enclosure, located 80 cm above ground.

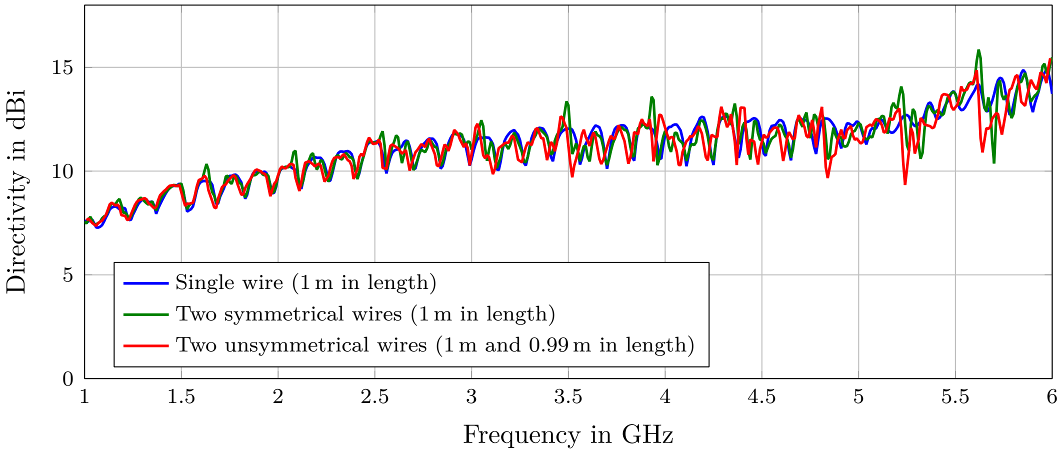

Figure 3.12: Simulated directivity against the frequency for 3 different wire configurations attached to the enclosure, located in free space.

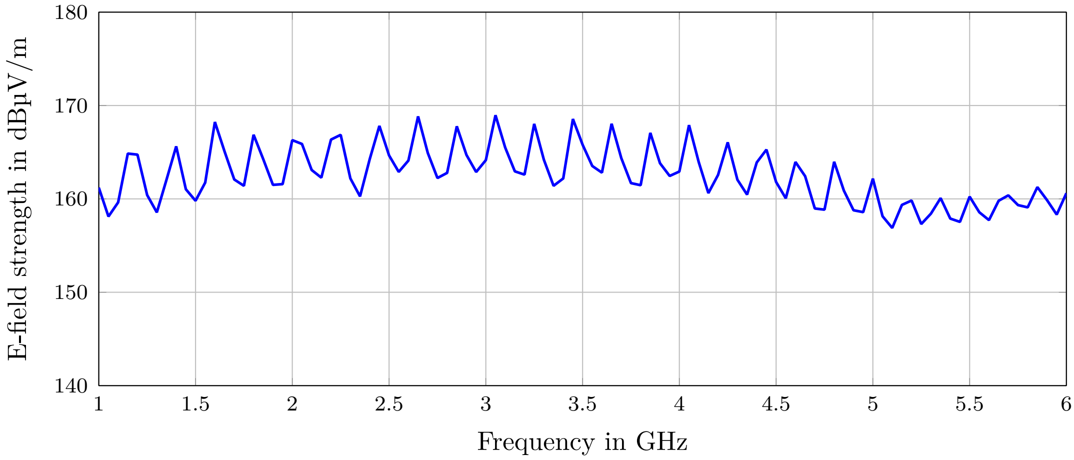

Figure 3.13: Simulated E-field strength for the slotted enclosure at the distance of 1 m, located 80 cm above ground

The amplitude of the field depends on the amplitude of the common mode current on the wire. Therefore, the maximum field will be generated if the wire is directly excited in common mode, which results in large radiated power. A very small field strength will be observed for the symmetrical wires. Although the absolute radiation of one single wire is larger, the directivity is equivalent for all wire configurations. The results indicate that the cable configuration does not have an impact on the directivity. Representing the connected cables of EUTs as a single wire for the simulation models will lead to a good estimate of the directivity of artificial EUTs. Therefore, in this work only the single wire configuration is further analyzed.

3.3.2 Verification of the model

The EUT was extended by the connecting wire with a length of 1 m. In the real test object, it was feed by the comb generator and the wire was placed to the outside enclosure through a small opening, as is shown in the simulation model in Fig. 3.14 and the measurement set-up in Fig. 3.15. The hole had the dimension of 2 mm × 9 mm, therefore the influence on the parasitic capacitance between the wire and the enclosure was neglected. For the simulations, the single wire was excited by a CM source located between the wire and the interior enclosure wall, generating the radiated emission to the outside enclosure. The measurements were carried out in the SAC with floor absorbers with the receiving antenna at a distance of 3 m from the EUT and a height of 1 m. The angle resolution on the horizontal plane of the measurement antenna was 5°.

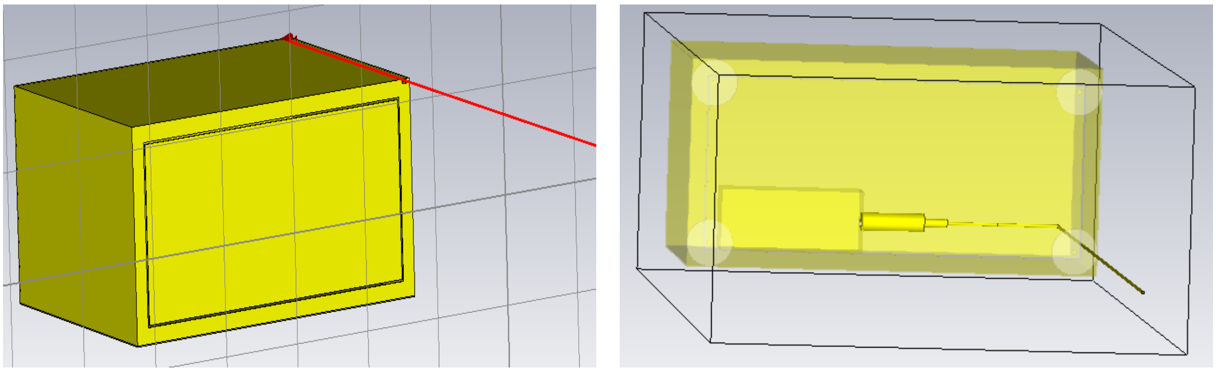

(a) Simulation model of the enclosure with an attached wire traveling through a small hole on the top right corner of the front plane.

(b) The single wire is excited in CM by a source located between the wire and the interior enclosure wall, generating the radiated emission to the outside enclosure.

Figure 3.14: Simulation model of an enclosure with an attached wire.

The radiation pattern of the model containing the enclosure and the attached wire is shown in Fig. 3.16. The measured and simulated radiation pattern at 1.45 GHz (as an exemplary frequency) shows a general similar tendency. Due to the gravity on the wire, the horizontal distance of the wire to ground was not constant during measurements. A constant distance was assumed for the simulation. This may result in small differences

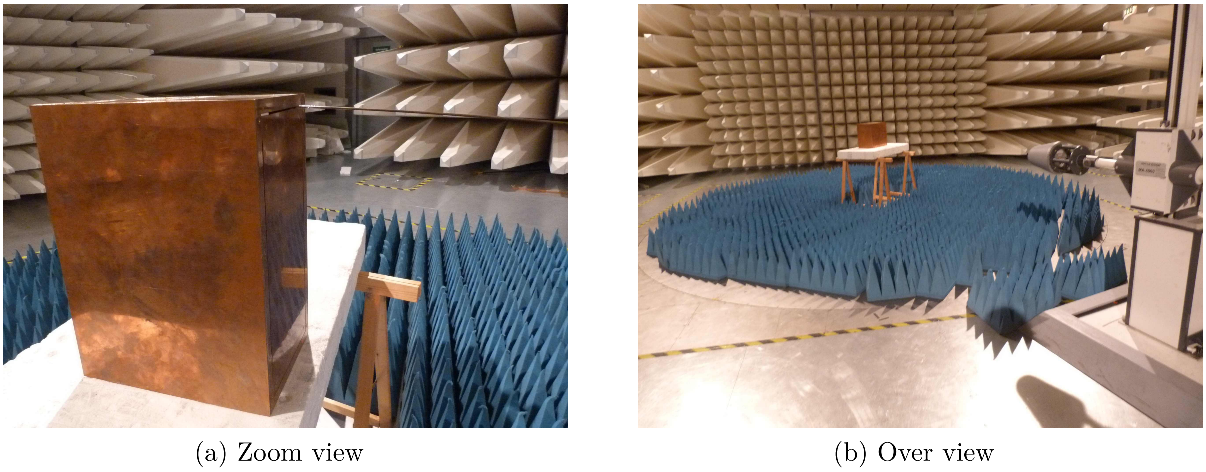
(a) Zoom view (b) Over view

Figure 3.15: Measurement of the radiated E-field strength of the slotted enclosure with an attached wire in the FAR at the Otto von Guericke university in Magdeburg.

between the measured and simulated radiation patterns. Besides, it indicates that the radiation pattern is very sensitive to slight movements of the EUT. Due to a 0.2° angle resolution during the simulation, the simulated results show a smoother curve than the measurement results.

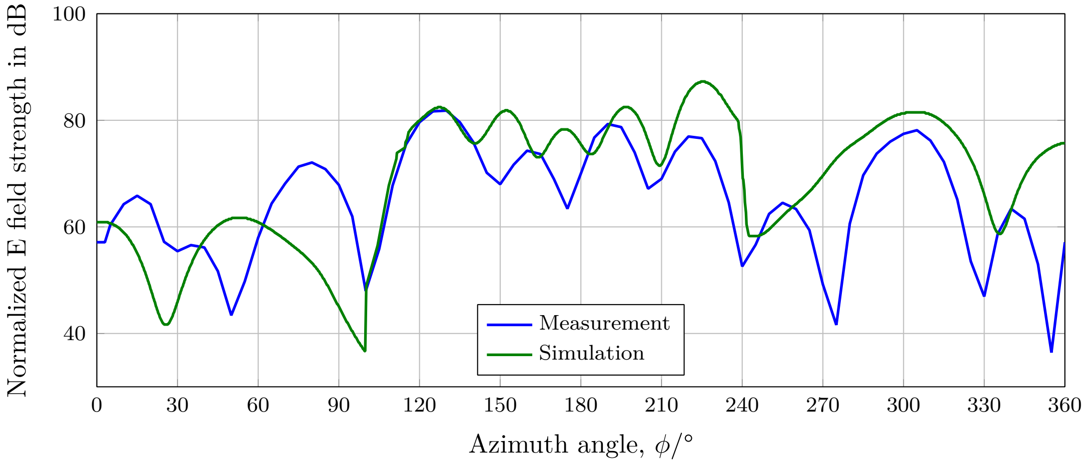

Figure 3.16: Planar cut of the electric field strength at 1.45 GHz for the model consisting of the rectangular enclosure with a connecting wire with a length of 1 m.

3.4 Stochastic modeling of EUTs

The comparison of the measured and simulated radiation patterns of the EUTs showed a sufficient agreement in the aforementioned results, which provides a good validation of the simulation technique. The numerical simulation could be extended to be used with stochastic models. This allows stochastic analysis of EUTs without time-demanding measurement efforts.

3.4.1 Stochastic simulation approach for a slotted enclosure

The previously introduced EUT with dimensions of 0.4 m × 0.3 m × 0.2 m was also used for the stochastic analysis. A linear dipole source with a radius of 1 mm, a length of 100 mm was located inside the box and was excited by an input power of 1 W, as shown in Fig. 3.17. The stochastic analysis was realized by randomly varying the number of slots, the size of the slots, the locations of the slots and the rotation angles of the slots on the enclosure surface, as shown in Fig. 3.18. The details of these parameters are summarized in Table 3.1.

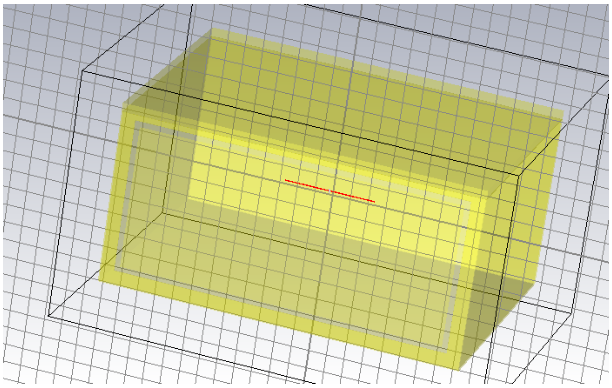

Figure 3.17: Simulated enclosure with a linear dipole antenna ($r = 1\,\mathrm{mm}$, $l = 100\,\mathrm{mm}$) as the excitation source.

Table 3.1: Statistical variations of the slotted enclosure

Parameter	**Statistical variation range**	**Comment**
Number of slots	random number between 1 to 6	always on different planes
Rotation angle	16 angles	22.5° per rotation step
Length	120 mm to 250 mm	
Width	10 mm to 250 mm	
Position	arbitrary on each surface of the enclosure	stochastic, but at least 50 mm distance to the boundary corner

A random number generator was programmed inside the CST software, so that every time the simulated model was randomly changed by considering all these variation factors. The maximum directivity $D_{\max}$ was determined for every stochastic modeled EUT. The evaluation was performed based on 110 samples of EUTs to obtain the statistical properties of the directivity. Figure 3.18 gives two exemplary EUT samples.

To compare the simulation results with the theoretical directivity values of an unintentional emitter, the ratio of ${}^{\langle P_{\mathrm{rec,max}}\rangle}/_{\langle P_{\mathrm{rec}}\rangle}$ (maximum-to-mean received power) over the planar

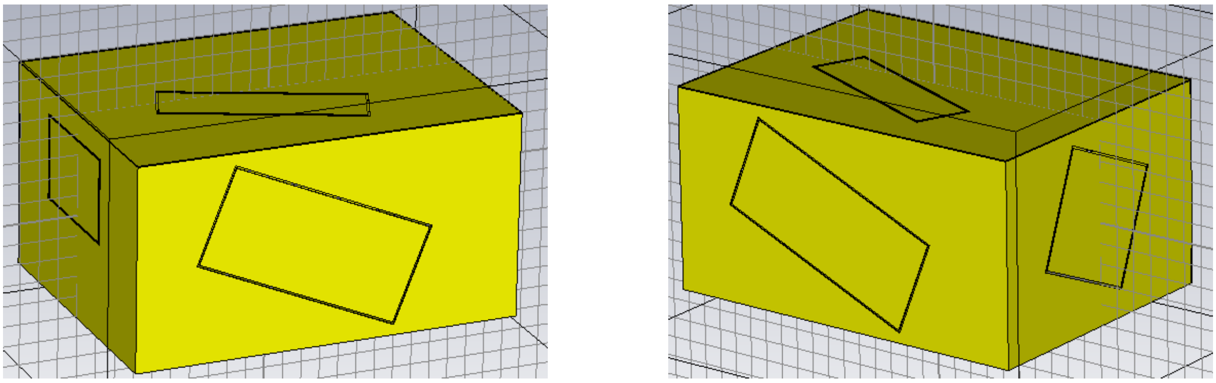

(a) Sample 1

(b) Sample 2

Figure 3.18: Simulation model of EUT – a rectangular enclosure of dimensions 0.4 m × 0.3 m × 0.2 m with randomly arranged slots.

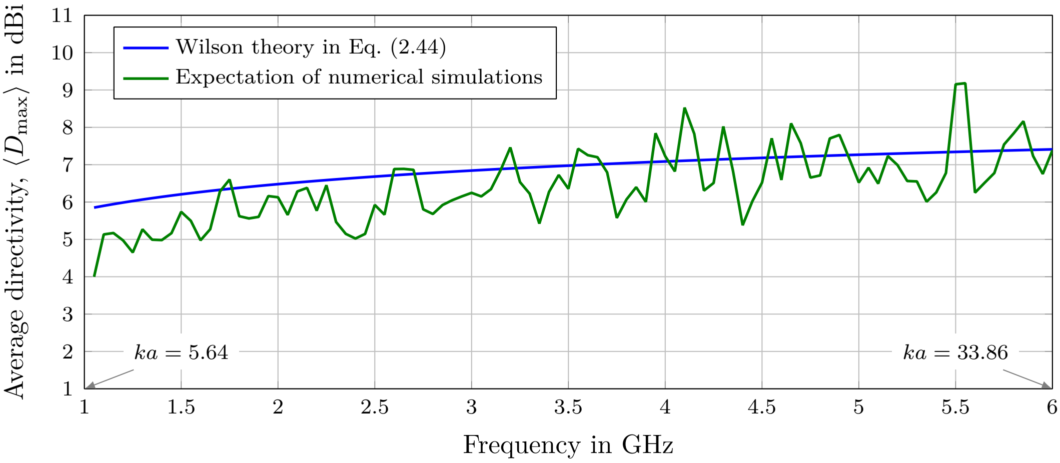

Figure 3.19: Comparison of the expectation values of the maximum directivity D_{max} with 1D sampling based on the numerical simulations and the analytical calculations for the model including the enclosure with randomly located slots

cut was calculated [WHH02]. It is obvious that the ratio of ${}^{\langle P_{\text{rec,max}} \rangle}/_{\langle P_{\text{rec}} \rangle}$ is actually the definition of $\langle D_{\text{max}} \rangle$, which was introduced in Eq. (2.44) in Section 2.7.2.

Here, the effective radius a is assumed to be half-diagonal of the EUT. Based on a large number of sampled models, the expectation value of the maximum directivity over a planar cut was obtained in Fig. 3.19. It can be seen that there is a good agreement between the simulation results and the theoretical values calculated according to Eq. (2.44). The small oscillations of the simulation results are due to the statistical variations. It can be observed that the expectation of the maximum directivity of the EUT is a function of the electrical size ka, which increases slowly with the natural logarithm of ka, see also [WHH02].

The number of sampling points over the whole sphere (spherical method in Section 2.7.2) enclosing the EUT was calculated based on Eq. (2.46). In Fig. 3.20, the green line indicates the numerical simulation results of the expectation value of the maximum directivity and the blue line indicates the analytical results based on Eq. (2.46). It is obvious that for both cases a similar tendency and only minor discrepancy was observed. The small oscillations are resulted by the statistical fluctuations of numerical simulations.

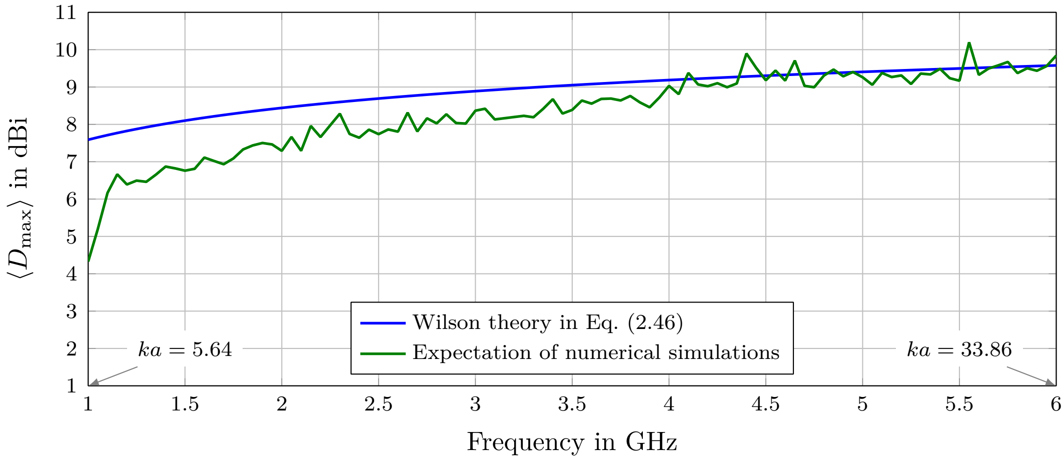

Figure 3.20: Comparison of the expectation values of the maximum directivity $D_{\max}$ with 3D sampling based on the numerical simulations and the analytical calculations for the stochastic model (an enclosure with randomly located slots, located above ground)

One gets a similar tendency for both cases (1D and 3D sampling), which makes it feasible to use the proposed stochastic model for the analysis of the directivity of electric large EUTs. As another prove, the enclosure with stochastic rectangular slots in Fig. A.1 and with parameters in Table A.1 was simulated. The results are shown in Fig. A.2 and Fig. A.3.

3.4.2 Stochastic models of an EUT with an attached wire

An analysis of the directivity can be done using a single, common mode excited wire instead of modeling the complex cabling of EUTs, as it was shown in Section 3.3. A stochastic analysis of the directivity in the frequency range of 1 GHz to 6 GHz (see Fig. 3.21) was done using CST Microwave Studio. The connecting wire first runs in the interior of the housing and is guided through a small opening to the outside enclosure. The novel statistical analysis considers a random changing length of the connecting wire and a random width of the enclosure along the wire direction.

It shows in Fig. 3.21 the model of the rectangular slotted enclosure with a connecting wire. The maximum 3D directivity was calculated, which is the maximum of the D_φ component in the azimuth direction and the D_θ component in the vertical direction. The wire was excited in each case by a common mode source between the wire and the inner housing wall, feeding a power of 1 W. The statistical properties of the directivity were obtained in an exemplary manner by randomly changing the width of the housing from 2 cm to 28 cm and length of the wire was randomly changed from 30 cm to 80 cm, as

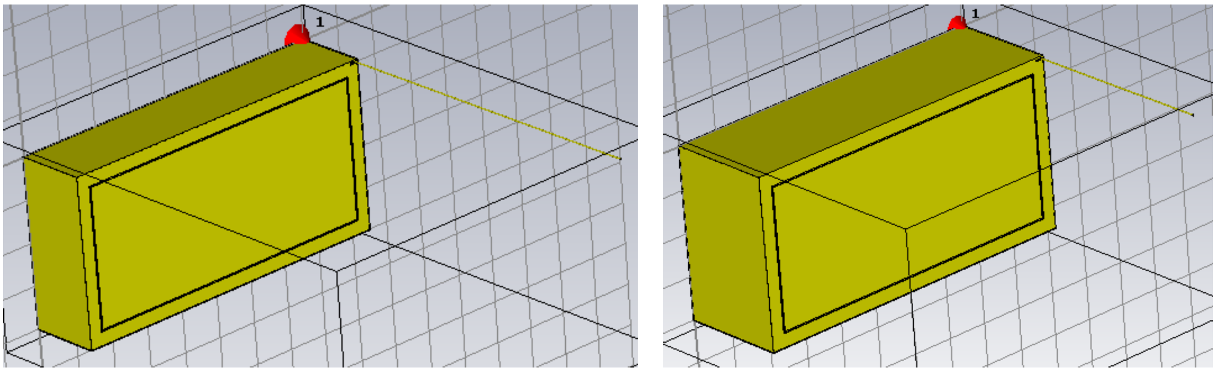

(a) Sample 1 (b) Sample 2

Figure 3.21: A slotted rectangular enclosure with an attached wire linked to the inside through a small slot on the top right corner of the front plane, with statistical variations of parameters in the frequency range from 1 GHz to 6 GHz

summarized in Table 3.2. The length of the housing was always 40 cm and the height was fixed to 20 cm. The calculation was repeated with varying parameters many times and the results were statistically evaluated. The maximum directivity of an unintentional radiator with 3D sampling can be described by the Eq. (2.43) in Chapter 2. The average value of the maximum directivity $\langle D_{\max} \rangle$ based on many numerical simulations was compared with the analytical results according to Eq. (2.46) in [WHH02]. The result is shown in Fig. 3.22. It can be seen that the comparison of the simulation results and the theoretical values shows a good agreement with minor variations. The rectangular slotted enclosure with a connecting wire acts rather as an intentional radiator, resulting in a higher directivity, compared with the analytical results of the directivity for unintentional radiators.

Table 3.2: Statistical variations of the parameters regarding the model consisting of a slotted enclosure with an attached wire

Parameter	**Statistical variation range**
Width of the enclosure	random number between 2 cm to 28 cm
Length of the wire	random number between 30 cm to 80 cm

The different quantiles of the directivity distribution are also calculated and shown in Fig. 3.23, where the boundary of the minimum and maximum directivity locates between 5 dBi to 12 dBi.

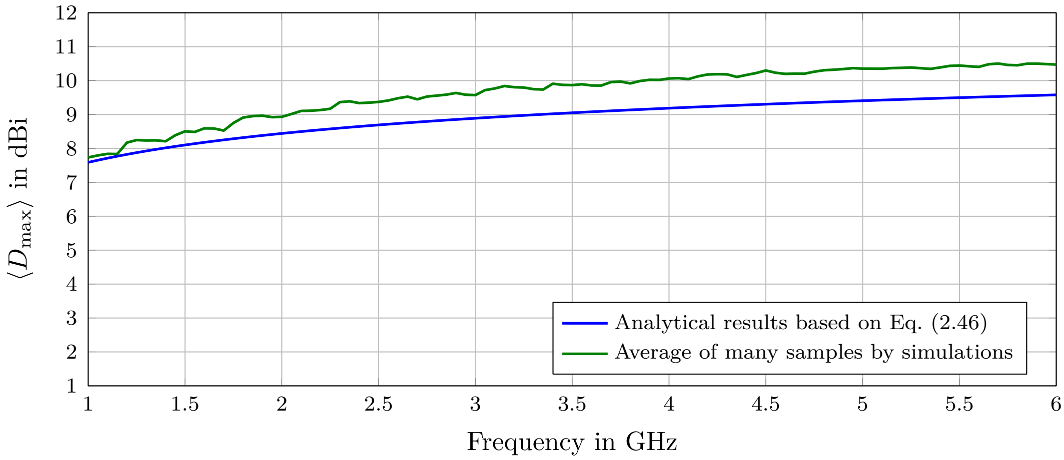

Figure 3.22: Comparison between the simulation and analytical result of the expectation value of the maximum directivity $D_{\max}$ for the stochastic model of the slotted enclosure with a connecting wire

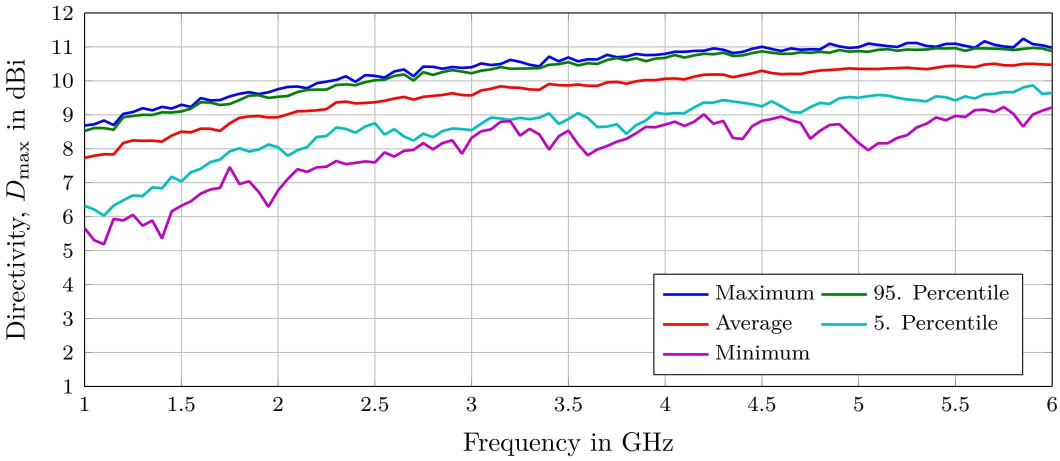

Figure 3.23: Statistical distribution of the maximum 3D directivity for the stochastic model of the slotted enclosure with a connecting wire

3.5 Analytical approximation of directivity based on the current distribution

To generalize the expression of the directivity, it is possible to combine the numerical simulation and the analytical approximation. Through numerical simulations, the current along the wire can be obtained as shown in Fig. 3.24. Due to the superposition of the forward and reflected current waves along the wire, the current oscillates in a resonate state.

The electric field strength of the ELEUT can be obtained based on the current distribution

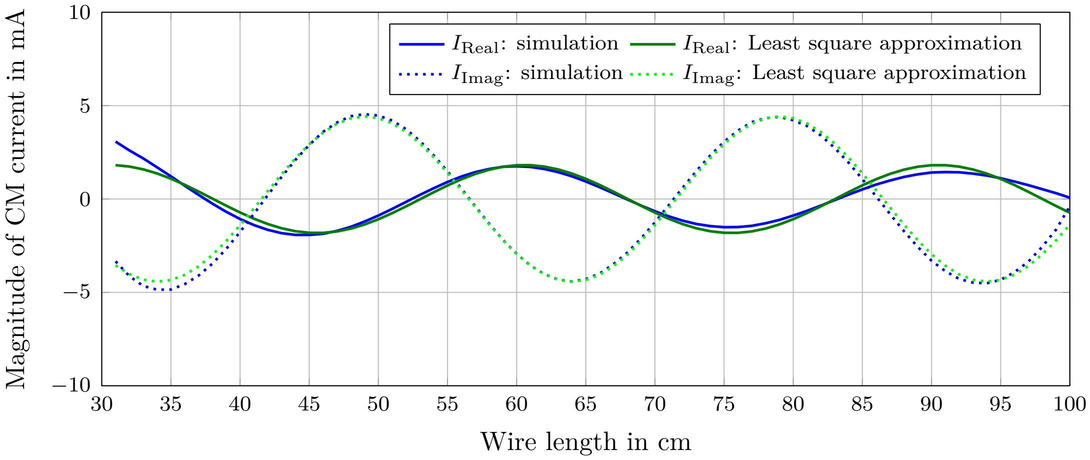

Figure 3.24: Real and imaginary part of the common mode current I_{CM} along the wire outside the enclosure at 1 GHz for the model of the slotted enclosure with an attached wire with a length of 1 m by simulations and a least square approximation.

through the following equation:

$$E_\theta(r) = \frac{\mathrm{j}k\eta}{4\pi r}\,\mathrm{e}^{-\mathrm{j}kr}\sin\theta\int\limits_{z_1}^{z_2} I(z)\,\mathrm{e}^{\mathrm{j}kz\cos\theta}\,\mathrm{d}z \tag{3.1}$$

where $E_\theta(r)$ is the E-field strength in the θ direction at the observation distance r. The corresponding coordinate system to represent the geometry is shown in Appendix Fig. F.1. The wave impedance is represented by η and $I(z)$ is the current along z direction, as shown in Fig. 3.24. According to the least square method, the current along the wire could be expressed by: $I(z) = C_1\cos(kz) + C_2\sin(kz)$, where the C_1 and C_2 are the complex coefficients for triangular functions of the currents. The current consists of real and imaginary parts, which can be also written as: $I(z) = \Re\{I(z)\} + \Im\{I(z)\}$, with $\Re\{I(z)\} = C_1^1\cos kz + C_2^1\sin kz$ and $\Im\{I(z)\} = C_1^2\cos kz + C_2^2\sin kz$. The corresponding coefficients are displayed in Table F.1.

Let $F(\theta) = \int\limits_{z_1}^{z_2} I(z)\,\mathrm{e}^{\mathrm{j}kz\cos\theta}$, which is equivalent to:

$$F(\theta) = C_1\int\limits_{z_1}^{z_2}\cos(kz)\,\mathrm{e}^{\mathrm{j}kz\cos\theta}\,\mathrm{d}z + C_2\int\limits_{z_1}^{z_2}\sin(kz)\,\mathrm{e}^{\mathrm{j}kz\cos\theta}\,\mathrm{d}z = F_1(\theta) + F_2(\theta) \tag{3.2}$$

The first part $F_1(\theta)$ can be obtained by integrating the cos–part:

$$F_1(\theta) = \frac{C_1}{2}\left[\int\limits_{z_1}^{z_2}\left(\mathrm{e}^{\mathrm{j}k(1+\cos\theta)}\right)^z\,\mathrm{d}z + \int\limits_{z_1}^{z_2}\left(\mathrm{e}^{-\mathrm{j}k(1-\cos\theta)}\right)^z\,\mathrm{d}z\right] \tag{3.3}$$

$$= \frac{-\mathrm{j}C_1}{2k}\left(\frac{1}{A}\,\mathrm{e}^{\mathrm{j}kAz_2} - \frac{1}{A}\,\mathrm{e}^{\mathrm{j}kAz_1} - \frac{1}{B}\,\mathrm{e}^{-\mathrm{j}kBz_2} + \frac{1}{B}\,\mathrm{e}^{-\mathrm{j}kBz_1}\right) \tag{3.4}$$

The second part $F_2(\theta)$ can be obtained by integrating the sin–part:

$$F_2(\theta) = \frac{C_2}{2\mathrm{j}} \left[\int_{z_1}^{z_2} \left(\mathrm{e}^{\mathrm{j}k(1+\cos\theta)} \right)^z \,\mathrm{d}z - \int_{z_1}^{z_2} \left(\mathrm{e}^{-\mathrm{j}k(1-\cos\theta)} \right)^z \,\mathrm{d}z \right] \tag{3.5}$$

$$= \frac{-C_2}{2k} \left(\frac{1}{A}\,\mathrm{e}^{\mathrm{j}kAz_2} - \frac{1}{A}\,\mathrm{e}^{\mathrm{j}kAz_1} + \frac{1}{B}\,\mathrm{e}^{-\mathrm{j}kBz_2} - \frac{1}{B}\,\mathrm{e}^{-\mathrm{j}kBz_1} \right), \tag{3.6}$$

with $A = 1 + \cos\theta$, $B = 1 - \cos\theta$, $F(\theta)$ can be obtained by summing up both parts:

$$F(\theta) = F_1(\theta) + F_2(\theta) \tag{3.7}$$

$$= \frac{1}{2k} \left[\frac{C_2 + \mathrm{j}C_1}{A} \left(\mathrm{e}^{\mathrm{j}kAz_1} - \mathrm{e}^{\mathrm{j}kAz_2} \right) + \frac{C_2 - \mathrm{j}C_1}{B} \left(\mathrm{e}^{-\mathrm{j}kBz_1} - \mathrm{e}^{-\mathrm{j}kBz_2} \right) \right] \tag{3.8}$$

According to Eq.(F.3), the solution of the electric field strength can be written as:

$$E_\theta(r) = \frac{\mathrm{j}\eta}{8\pi r}\,\mathrm{e}^{-\mathrm{j}kr} \sin\theta \left[\frac{C_2 + \mathrm{j}C_1}{A} \left(\mathrm{e}^{\mathrm{j}kAz_1} - \mathrm{e}^{\mathrm{j}kAz_2} \right) + \frac{C_2 - \mathrm{j}C_1}{B} \left(\mathrm{e}^{-\mathrm{j}kBz_1} - \mathrm{e}^{-\mathrm{j}kBz_2} \right) \right] \tag{3.9}$$

Based on the above derivations, the electric field strength can be expressed by the complex coefficients of triangular functions. In the next part, the radiated power can be calculated.

The radiated power per unit solid angle can be expressed by [Smi97]:

$$\frac{\mathrm{d}\left\langle P_{\mathrm{rad}} \right\rangle}{\mathrm{d}\Omega} = \frac{1}{2\eta} \left| rE \right|^2 \tag{3.10}$$

Combined with Eq. (3.9), the following expression can be obtained:

$$\left| rE_\theta \right|^2 = \frac{\eta^2}{64\pi^2} \sin^2\theta \left| \frac{C_2 + \mathrm{j}C_1}{A} \left(\mathrm{e}^{\mathrm{j}kAz_1} - \mathrm{e}^{\mathrm{j}kAz_2} \right) + \frac{C_2 - \mathrm{j}C_1}{B} \left(\mathrm{e}^{-\mathrm{j}kBz_1} - \mathrm{e}^{-\mathrm{j}kBz_2} \right) \right|^2 \tag{3.11}$$

As a result, the radiated power per unit solid angle can be written as:

$$\frac{\mathrm{d}\left\langle P_{\mathrm{rad}} \right\rangle}{\mathrm{d}\Omega} = \frac{\eta}{128\pi^2} \sin^2\theta \left| \frac{C_2 + \mathrm{j}C_1}{A} \left(\mathrm{e}^{\mathrm{j}kAz_1} - \mathrm{e}^{\mathrm{j}kAz_2} \right) + \frac{C_2 - \mathrm{j}C_1}{B} \left(\mathrm{e}^{-\mathrm{j}kBz_1} - \mathrm{e}^{-\mathrm{j}kBz_2} \right) \right|^2 \tag{3.12}$$

The total radiated power is determined by integrating over the whole solid angle [Smi97]:

$$\left\langle P_{\mathrm{rad}} \right\rangle = \int_0^{2\pi} \int_0^{\pi} \frac{\mathrm{d}\left\langle P_{\mathrm{rad}} \right\rangle}{\mathrm{d}\Omega} \sin\theta \,\mathrm{d}\theta \,\mathrm{d}\phi \tag{3.13}$$

Combined with Eq. (3.12), the total power equals:

$$\begin{aligned}\langle P_{\mathrm{rad}} \rangle = \frac{\eta}{64\pi} \int_0^{\pi} \sin^3\theta \, \Bigg| \frac{C_2 + \mathrm{j}C_1}{A} \left(\mathrm{e}^{\mathrm{j}kAz_1} - \mathrm{e}^{\mathrm{j}kAz_2} \right) & \\ + \frac{C_2 - \mathrm{j}C_1}{B} \left(\mathrm{e}^{-\mathrm{j}kBz_1} - \mathrm{e}^{-\mathrm{j}kBz_2} \right) \Bigg|^2 \, \mathrm{d}\theta, & \quad (3.14)\end{aligned}$$

The last step is to calculate the directivity by taking the ratio of the power in a certain direction over the average power [Smi97]:

$$D(\phi) = \frac{4\pi}{\langle P_{\mathrm{rad}} \rangle} \left(\frac{\mathrm{d} \langle P_{\mathrm{rad}}(\phi) \rangle}{\mathrm{d}\Omega} \right) \tag{3.15}$$

With the power in ϕ direction and the total radiated power, the directivity $D(\phi)$ can be calculated and the result is shown in Fig. 3.25. Likewise, the maximum directivity is obtained by taking the ratio of the maximum power and the average power over all solid angles.

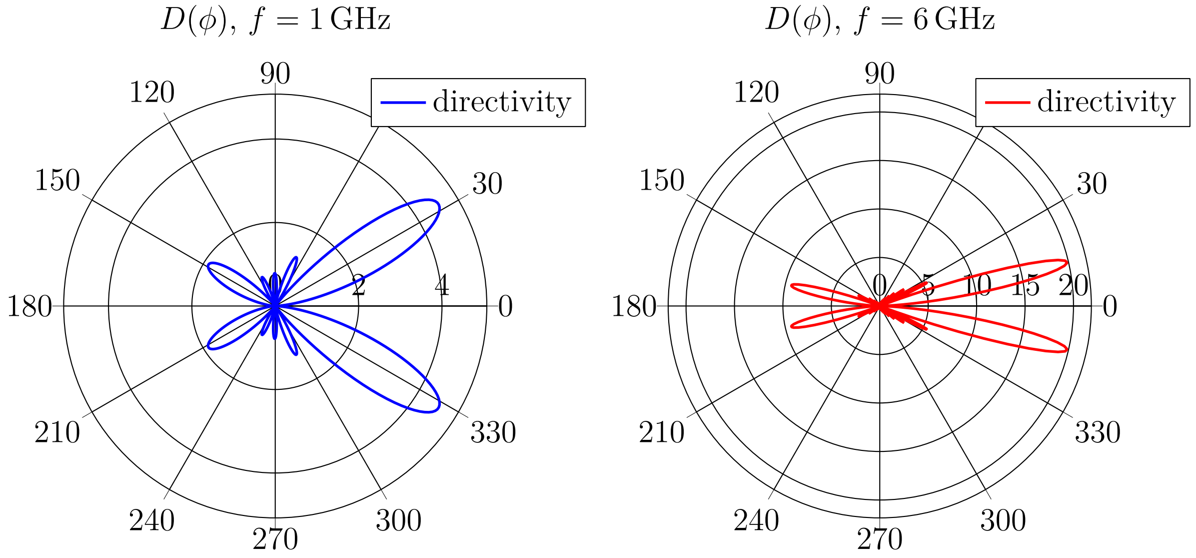

Figure 3.25: Directivity $D(\phi)$ in dBi as a function of the azimuth angle ϕ from 0° to 360°, at 1 GHz and 6 GHz respectively, based on the current distribution obtained from numerical simulations

The directivity pattern as a function of the azimuth angle ϕ from 0° to 360° is compared at 1 GHz and 6 GHz. It is pointed out that a larger magnitude of the directivity is observed at 6 GHz, with more narrower lobes. The directivity at every frequency point is determined by taking the maximum directivity along the whole azimuth angle in the range from 0° to 360°, which corresponds to the direction of the maximum emission level. Furthermore, the directivity can be analytically approximated. The derived directivity as function of the frequency is displayed together with the linear, 2nd order and exponential approximation

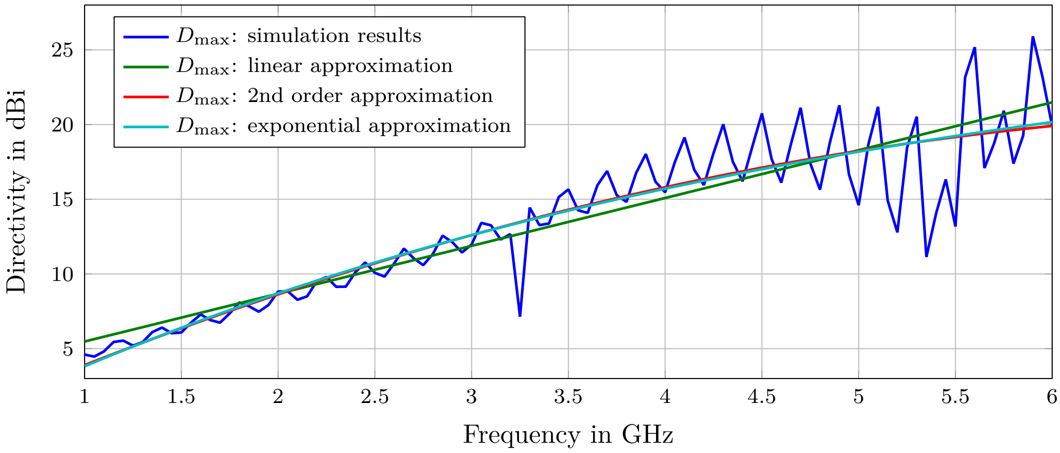

Figure 3.26: Maximum directivity $D_{\max}$ by simulations and three approximation methods for the model of a slotted enclosure with a single connecting wire with a length of 1 m, located 80 cm above ground

through curve fitting in Fig. 3.26. Therefore, by combining numerical simulations and analytical approximations, the directivity could be obtained in a straightforward manner.

3.6 Chapter conclusion

The possibility to analyze the radiation characteristic of real electronic devices by numerical simulations was investigated in this chapter. In a first step, a simple enclosure with slots, representing a PC sized equipment, was analyzed. The cabling was neglected. It could be shown that the numerical calculated maximum directivity fits to measured data, even if the total radiation pattern is very sensitive to details of the real test object. As an improvement, the possibility to include the cabling into the model was investigated. It could be shown that the cables connected to an EUT can be represented by common mode excited single wires, without impacting the directivity of the object. Again the model was validated by measurement results. Finally, these models were used for statistical analysis. This was done by changing the slots, the size of the EUT or the length of the wire in a random way. The simulated directivity agrees well with the theoretical results based on Chapter 2. Therefore, numerical simulation models can be used to perform statistical analysis on the directivity of electronic devices rather than performing time consuming round robin tests with a large number of tests. Furthermore, an analytical method to determine the directivity of EUTs with cables based on the simulated current distribution was suggested.

4 Directivity of EUTs

In Chapter 3, different simulation models have been analyzed and verified by corresponding measurements. These models together with analytical methods are used to give a reasonable statement about the expected directivity for arbitrary EUTs in this chapter. First, the influencing factors on the directivity evaluation of EUTs are analyzed, especially the influence of the cabling [WV16]. The results are used to investigate the different analytical and numerical methods to estimate the directivity. Finally, a statistical analysis of the directivity based on different wire lengths attached to an electrically large EUT with randomly placed slots will be carried out. The results are critically assessed and the most appropriate method to determine the directivity for converting results for alternative test methods is suggested for further use.

4.1 Influencing factors on the maximum directivity of EUTs

This part investigates the possible influencing factors on the directivity estimates for EUTs. Recent investigations on similar topics have been reported in [ZHGG11, GB08, ZHG10]. In [GB08], an electrical large EUT with connected cables was investigated up to 1 GHz. In this work, an ELEUT consisting of a slotted metallic enclosure with an attached cable was investigated and the considered frequency range is extended to 6 GHz. As shown in Section 3.3, it is appropriate to substitute the cabling connected to an EUT by a single wire fed by a common mode current in order to calculate the directivity of EUTs. The applied simulation model containing the enclosure and the attached wire was shown in Fig. 3.8b. The rectangular enclosure has dimensions of $0.4\,\text{m} \times 0.3\,\text{m} \times 0.2\,\text{m}$, located 80 cm above a PEC ground or alternatively in free space. The common mode excitation source for the wire is located between the wire and the interior enclosure wall. The influence of the length and the orientation of the wire on D_{max} was investigated by numerical simulations. The wire was divided into horizontal and vertical segments and the ratio of the segments was changed. Furthermore, the model was simulated in different EMC environments.

4.1.1 Influence of the enclosure

Firstly, the influence of the enclosure was investigated by comparing the directivity of a single wire feed by a point source and the directivity of the enclosure with a connected wire fed by a common mode source. Both cases were simulated above a perfect conducting ground. The simulated maximum directivity D_{max} for the slotted enclosure with a wire and a single wire without box is shown in Fig. 4.1 for the cases of of 1 m and 3 m long wire separately.

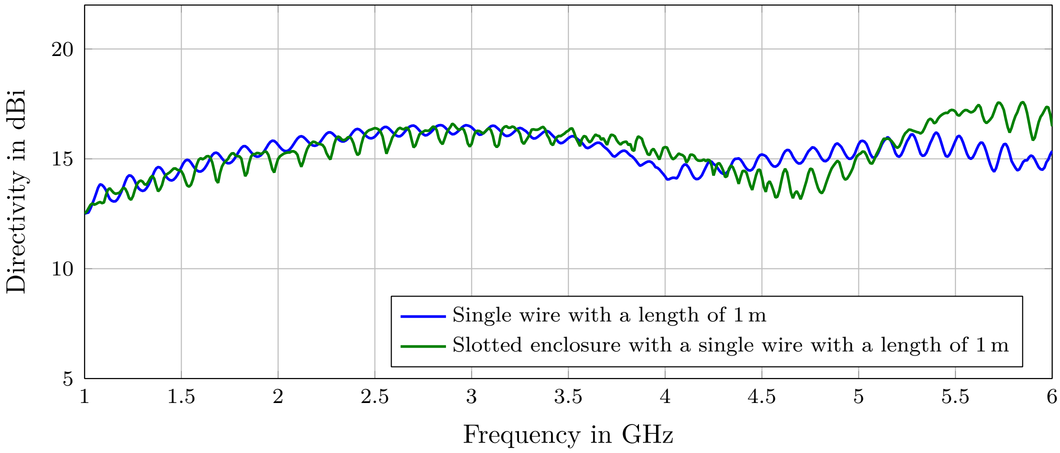

(a) for the wire with a length of 1 m

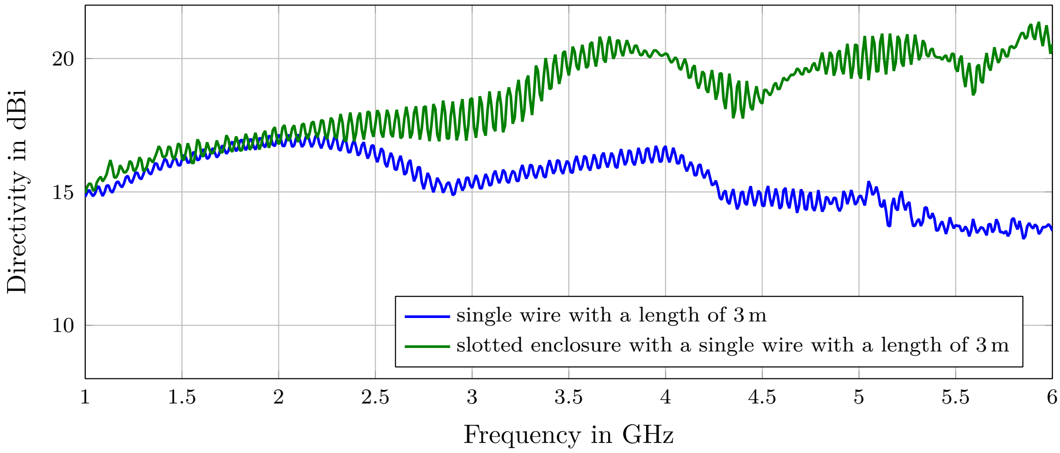

(b) for the wire with a length of 3 m

Figure 4.1: Maximum directivity D_{max} as a function of the frequency for the model of only a single wire (with a length of 1 m and 3 m respectively) and the same wire attached to a slotted enclosure, with the location 80 cm above ground

As can be seen in Fig. 4.1a, D_{max} of only a single 1 m long wire (in the same height as that of the slotted enclosure, located 80 cm above a PEC ground) and D_{max} of the same wire attached to the slotted enclosure shows comparable magnitudes up to 5 GHz, which indicates that the wire radiation dominates, compared to the radiation from the enclosure. The wire resonances can be observed as well. Only the minimum is slightly shifted by

0.75 GHz. Above 5 GHz the curve for the slotted enclosure with a wire reaches higher values.

Extending the wire length for the same structure to 3 m, the simulated $D_{\max}$ in Fig. 4.1b shows larger values than in the case of a 1 m long wire in Fig. 4.1a. This is caused by the longer wire which increases the maximum directivity as well [Col85]. It can be also observed that the longer the wire is, the smaller the resonance frequency is. Therefore, more dense resonance frequency points can be observed for the longer wire. It is interesting to point out that the directivity above 2 GHz is higher for the enclosure with a wire, compared to the directivity of only a single wire. This was observed for the 1 m long wire in Fig. 4.1a at higher frequencies as well, e. g. the deviation of the directivity values between both cases increases with longer wires.

The simulations for the same cases in free space are shown Fig. 4.2. The same tendency can be observed. The directivity is higher if the wire is connected to an enclosure, e. g. an EUT with cabling, compared to the directivity of a single wire. Not only the wire radiation but also the enclosure radiation have to be considered when a longer wire is attached.

4.1.2 Influence of wire length

The influence of the cable length of EUTs on the maximum directivity was further investigated using the model of the slotted enclosure with an attached wire. The wire, acting as antenna, was varied in length in a range of 1 m to 3 m with a step of 0.5 m. It is summarized in Fig. 4.3 that the maximum directivity $D_{\max}$ is changing with the wire length. In general, $D_{\max}$ increases with increasing the wire length, which also provides a good validation of the results in Fig. 4.1.

The simulation were repeated with the model in free space and a similar tendency can be observed as shown in Fig. 4.4.

4.1.3 Influence of the wire segmentation and orientation

The cables connected to EUTs are orientated in different directions in real applications. The test setup for table-top equipment in a FAR below 1 GHz normally includes a power supply cable that runs inside the test volume with a length of 80 cm in horizontal and 80 cm in vertical direction. Even if this requirement changes for frequencies above 1 GHz, the influence of vertical and horizontal segments must be considered for the determination of the maximum directivity. Therefore, a simple segmentation in horizontal-vertical and a more complex segmentation in horizontal-vertical-horizontal was investigated.

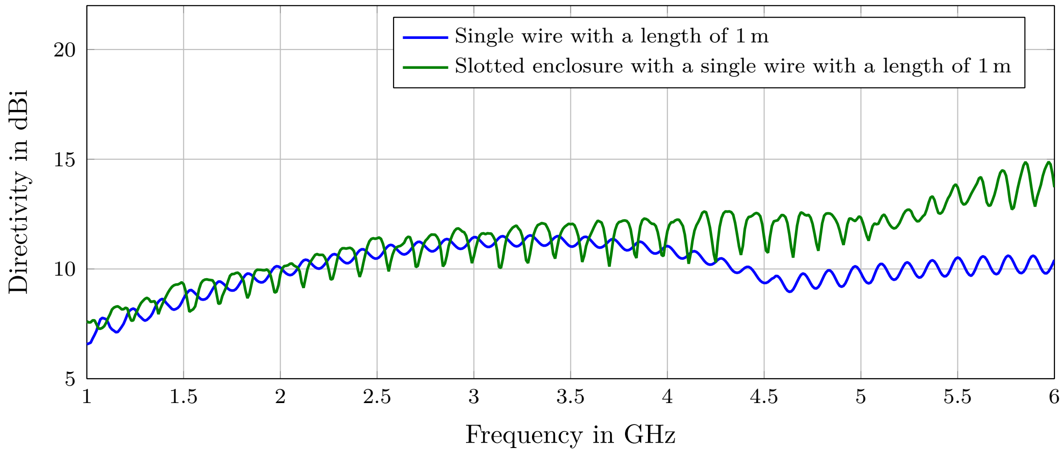

,

(a) for the wire with a length of 1 m

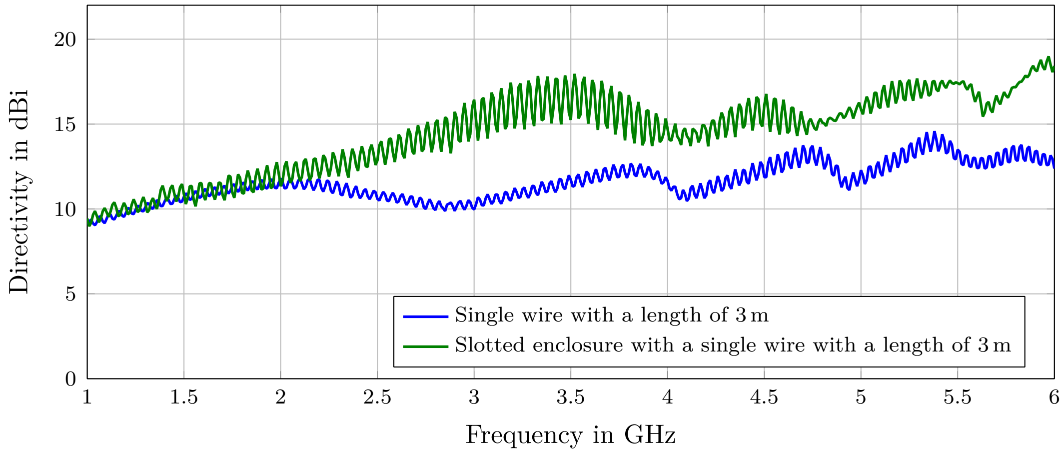

(b) for the wire with a length of 3 m

Figure 4.2: Maximum directivity D_{max} as a function of the frequency for the model of only a single wire (with a length of 1 m and 3 m respectively) and the same wire attached to a slotted enclosure, within location in free space

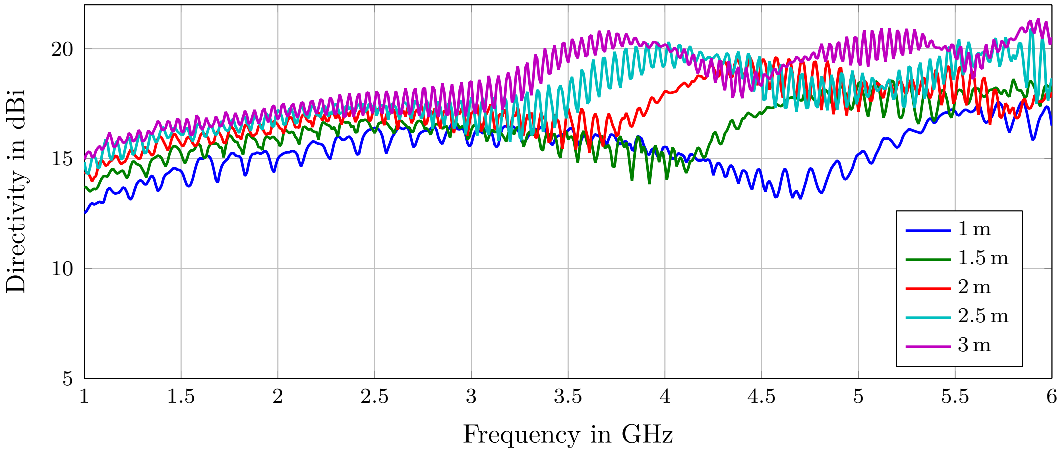

Figure 4.3: Maximum directivity D_{max} as a function of the frequency for the model of a single wire (with different wire lengths) attached to a slotted enclosure, located 80 cm above ground

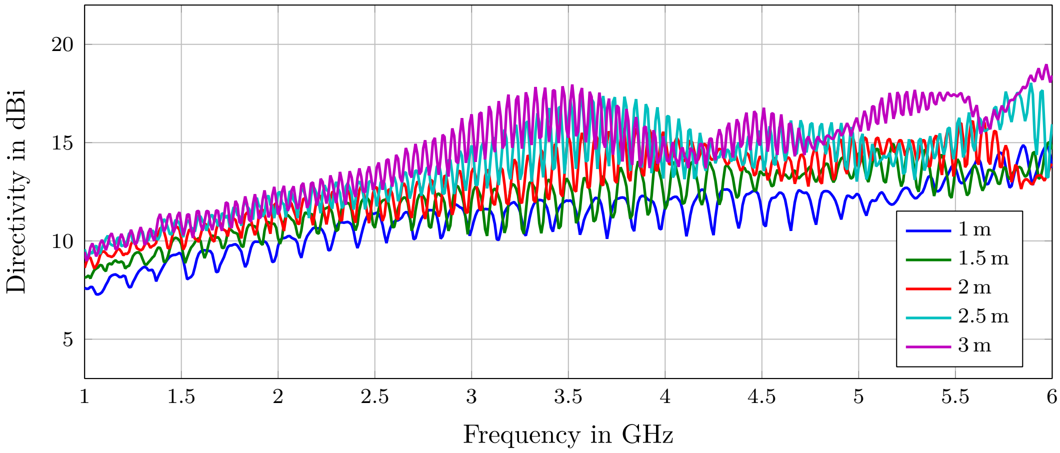

Figure 4.4: Maximum directivity $D_{\max}$ as a function of the frequency for the model of a single wire (with different wire lengths) attached to a slotted enclosure, located in free space

4.1.3.1 Horizontal and vertical wire segments

The same previously introduced EUT with dimensions of 0.4 m × 0.3 m × 0.2 m as shown in Fig. 4.5 was investigated. The wire is excited by a voltage source and placed in the middle of the enclosure. The connected wire has horizontal and vertical segments. The total length of the wire was chosen to be 1 m constant. Only the ratio between the horizontal and vertical segments was changed.

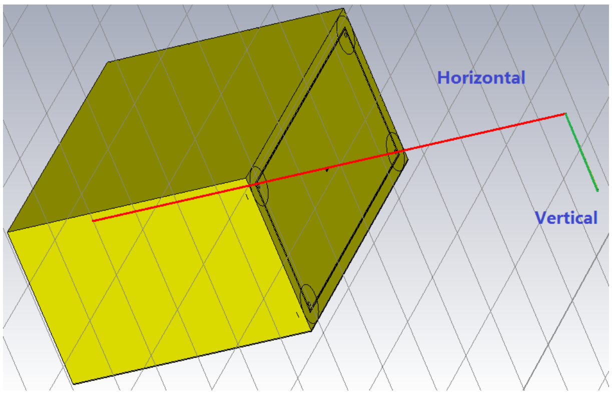

Figure 4.5: Simulation model of the EUT– a rectangular slotted enclosure of 0.4 m × 0.3 m × 0.2 m with two different wire orientations – horizontal and vertical.

The schematic view of the box with the wire and its excitation source is shown in Fig. 4.6.

The maximum directivity was investigated based on the length ratio r_{hv} of the horizontal to the vertical segment. It can be defined as the length of the horizontal segment l_{hor} divided by the length of the vertical segment l_{ver}, which is $r_{\text{hv}} = {}^{l_{\text{hor}}}/_{l_{\text{ver}}}$. It is varied in five steps: 1:1, 5:2, 2:5, 1:6 and 6:1, while keeping the total wire length of 1 m unchanged. The ratios are chosen manually.

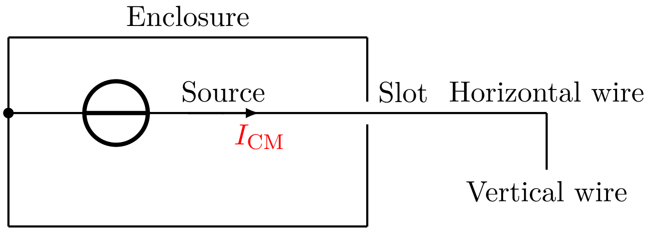

Figure 4.6: Schematic illustration of the enclosure and the outwardly guided wire with two different wire orientations – horizontal and vertical.

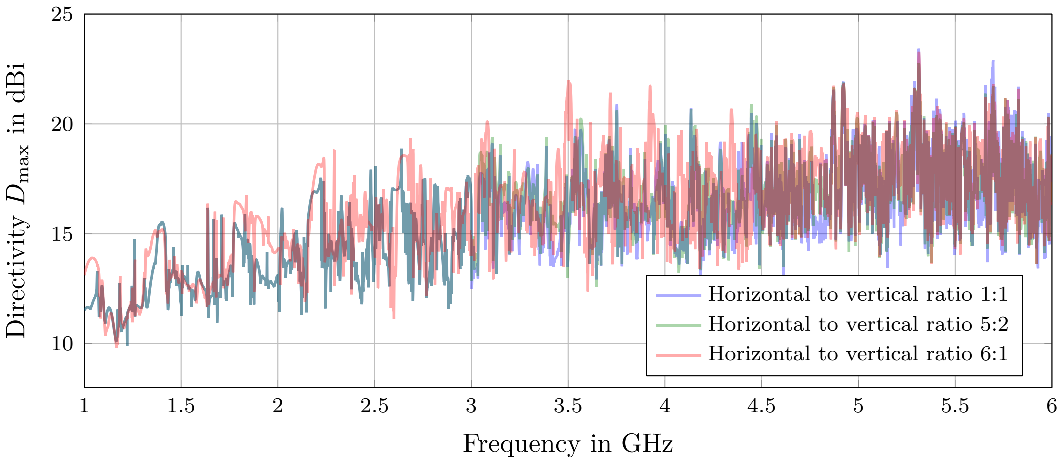

(a) horizontal to vertical ratio a

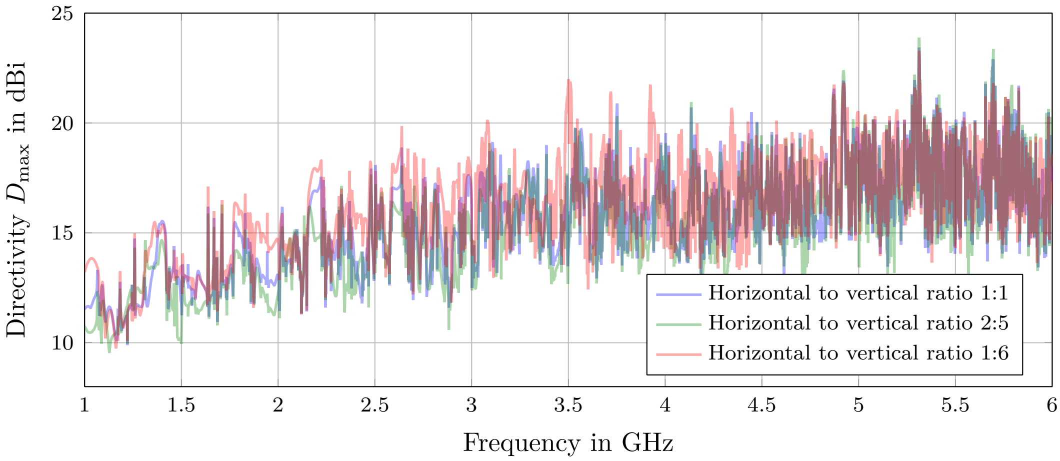

(b) horizontal to vertical ratio b

Figure 4.7: Maximum directivity D_{max} as a function of the frequency for different ratios of horizontal to vertical dimensions

A comparison of r_{hv} with r_{vh} in Fig. 4.7 implies that D_{max} mainly depends on the total wire length, not significantly influenced by the ratio r_{hv} or r_{vh}. The total wire length is the crucial influencing factor on D_{max}.

4.1.3.2 Wire with three segments

In order to illustrate the influence of different wire orientations, an EUT with a wire consisting of three parts including two horizontal segments and a vertical segment was analyzed, as it is schematically displayed in Fig. 4.8. The total wire length of 1 m kept unchanged.

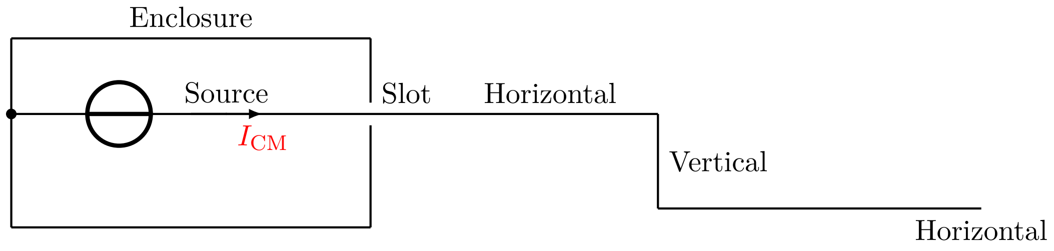

Figure 4.8: Schematic illustration of the enclosure and the outwardly guided wire with two horizontal segments and a vertical segment.

Three cases when the wire with a horizontal segment and a vertical segment with different length ratios, and the wire with two horizontal segments and a vertical segment are shown in Fig. 4.9.

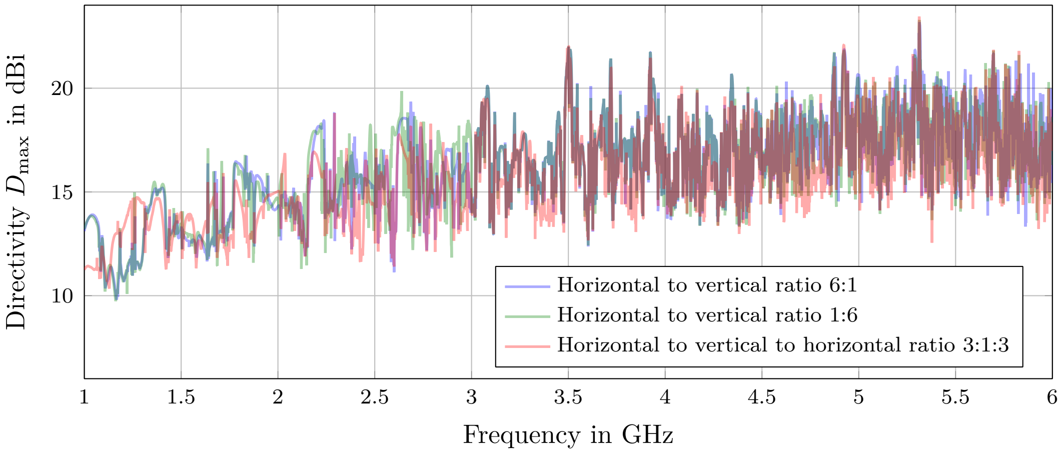

Figure 4.9: Maximum directivity D_{max} as a function of the frequency for different wire orientations, while keeping the total wire length of 1 m unchanged

It can be seen that D_{max} does not depend on the wire orientations, as long as the total wire length is identical. Even for the connecting wire with 3 wire segments in the ratio of 3:1:3 for the horizontal to vertical to horizontal segments, D_{max} does not change significantly. The amplitude of the maximum directivity D_{max} for the three cases is almost identical and the effect due to the wire orientations can be neglected. The conclusion can be drawn that the wire orientations have no influence on D_{max}, only the total wire length influences D_{max}. Therefore, it seems possible to simplify the model of an EUT with a connected cable by representing the cable by only a single straight wire. This makes the use of analytical models simple and feasible.

4.1.3.3 Horizontal and vertical segments with variation of the enclosure size

The variation of the enclosure size on the influence of $D_{\max}$ is investigated by changing the box width (parallel to the wire direction) in 3 steps: 0.4 m, 0.3 m and 0.2 m, while keeping the other two dimensions – length and height – unchanged. The connecting wire kept unchanged with a horizontal segment of 0.7 m and a vertical segment of 0.3 m, as shown in Fig. 4.6.

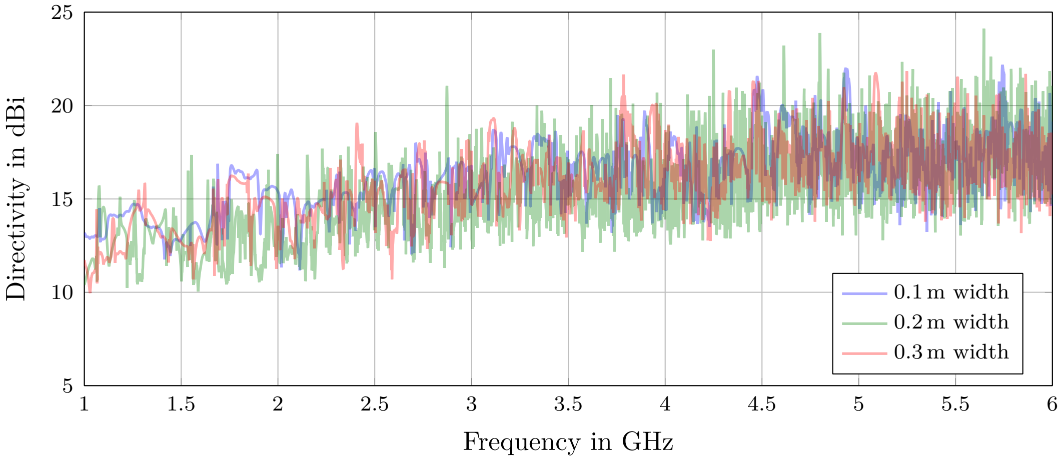

Figure 4.10: Maximum directivity $D_{\max}$ as a function of frequency by changing the box width in three steps: 0.4 m, 0.3 m and 0.2 m, while keeping the length of the horizontal segment with 0.7 m and the vertical wire segment with 0.3 m

The diagrams in Fig. 4.10 clearly show a similar tendency of directivity progression. No obvious frequency shifts were observed. The finding suggests that the dimension of the enclosure along the wire direction is not a dominant factor to the directivity estimation as long as the wall with the attached wire is large enough. Even if it is very thin, it can still act as an image plane to realize an equivalent dipole antenna structure. The thickness of the enclosure is insignificant in this case. It was suggested that as long as the box size along the wire direction is larger than $\lambda/10$ at the frequency of interest, the result gives a reasonable prediction [WFS01].

4.1.4 Influence of the ground plane

Physically, it is assumed that in an ideal situation, a ground plane doubles the maximum electric field through constructive interference due to the reflected path. The ground interference effect occurs by the combination of the direct radiation from the EUT and the reflected radiation from the ground. The reflected radiation undergoes a propagation phase delay, which assumes to be equivalent to the image of the EUT. Based on the image theory, when the EUT is horizontally oriented above the ground plane, a second equivalent antenna has to be considered.

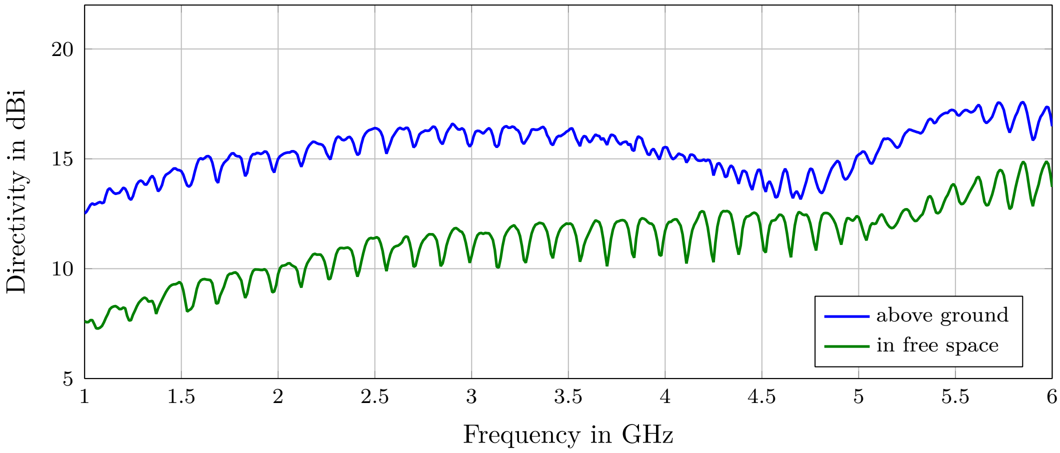

Figure 4.11: Maximum directivity $D_{\max}$ as a function of the frequency for the model of a single wire (with a length of 1 m) attached to a slotted enclosure, located in free space and 80 cm above ground

The comparison of $D_{\max}$ in free space and above ground is shown in Fig. 4.11. The simulation results show that approximately 6 dB difference of the directivity values could be taken into account due to the ground plane reflection effect, compared to the $D_{\max}$ in free space. If the ground plane is not infinitely large in area, the phenomena of diffraction occurs, which results in the bending of the EM waves when the waves encounter obstacles and the ground plane does not sufficiently doubles the electric field. However, in the simulation the ground plane is assumed to be infinitely large in area and the diffraction effect could be neglected.

4.1.5 Influence of a slot

When an equipment enclosure is electrically large ($ka > 1$), the field inside the enclosure presents rapid spatial variations due to the internal modes. For ventilation or other purposes, a single or multiple slots on the enclosure wall are necessary, which results in a more complex system. Therefore, the influence of a slot in the enclosure on the resulting directivity was investigated using the same model, consisting of the enclosure and an attached wire with the length of 1 m. The EUT was placed 80 cm above a PEC ground, represented by the boundary condition of 'electric field' in the simulation by CST Microwave Studio. The rectangular enclosure had again the dimensions of 0.4 m × 0.3 m × 0.2 m. The wire was fed by a common mode voltage source with a 50 Ω series resistance and a Gaussian pulse as the excitation signal, which is shown by the red arrow in Fig. 4.12. To investigate the influence of the slot on the front plane of the enclosure two models with and without a slot were investigated, as shown in Fig. 4.12a and Fig. 4.12b respectively.

The CM radiation from cables attached to the enclosure will be greatest at or near the resonance of the cables. The open-ended wire causes standing waves due to the reflection

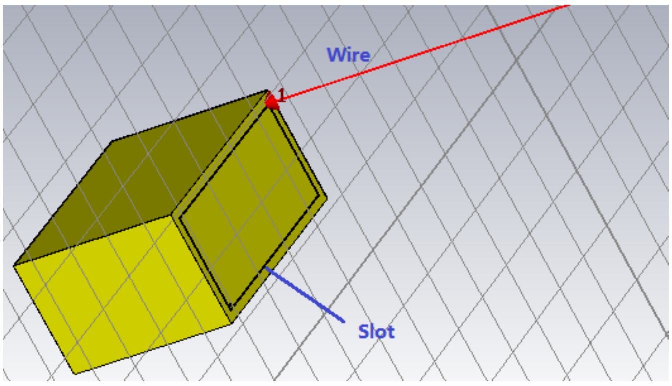

(a) A rectangular enclosure with a slot on the front plane

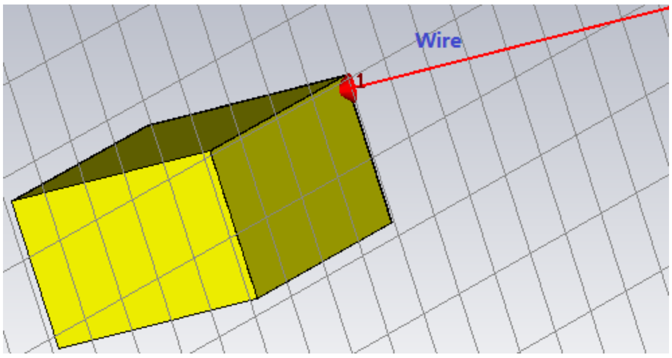

(b) A rectangular enclosure without a slot

Figure 4.12: Simulation model of a single wire attached to the rectangular enclosure with dimensions of 0.4 m × 0.3 m × 0.2 m with a plate thickness of 1 mm and the excitation source located between the wire and the enclosure, located 80 cm above ground.

of current waves at the end. The resulting CM current distribution is shown in Fig. 4.13, which is consistent with the assumption that the wire could be approximated by a standing wave antenna with a sinusoidal current distribution [Kar14]. The CM current contributes significantly to the radiated electromagnetic fields [Mar01], where the radiation can be considered to be proportional to the CM current. The simulated CM current I_{CM} along the wire at 1 GHz for the two models is compared in Fig. 4.13, where the only difference between these two models is the existence of the slot on the enclosure front plane. In general, the magnitude of the CM current has only a slight difference. The emission of the slotted enclosure is slightly larger than that for the model without slots, which may be due to the radiation of slot resonances. The maximum directivity of these two models was numerically obtained and is compared in Fig. 4.14. The results show that a similar tendency and only a minor difference are observed. This indicates that the slot on the front plane of the rectangular enclosure has in this case no significant influence on the directivity. This seems plausible due to the type of excitation, which was a direct CM excitation between the enclosure and the wire. Therefore, the cavity's internal resonances have only a small influence on the emission level.

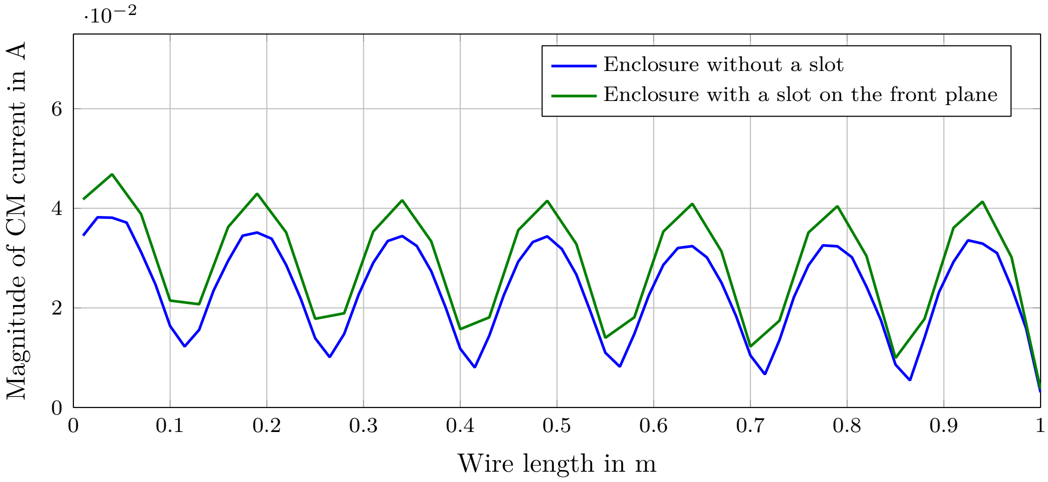

Figure 4.13: Common mode current I_{CM} at 1 GHz along the single wire with a length of 1 m attached to the enclosure, located 80 cm above ground.

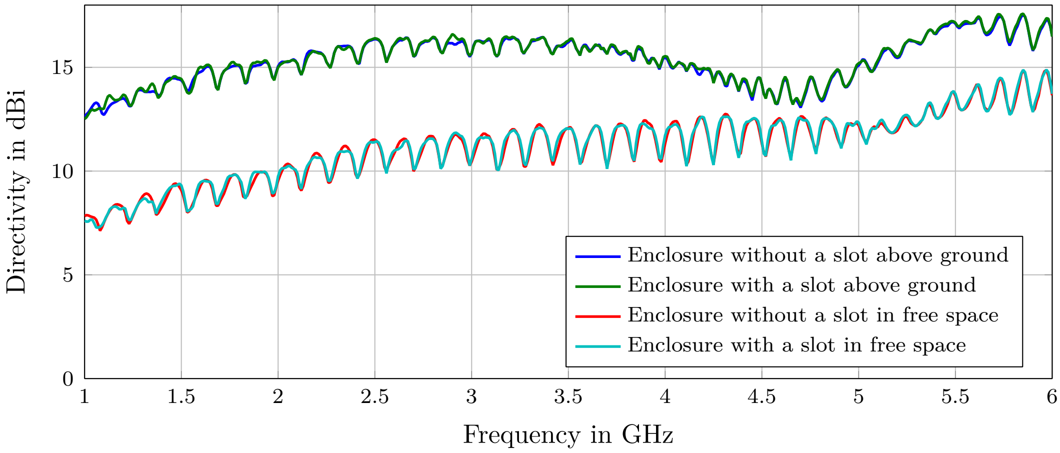

Figure 4.14: Simulated directivity of the rectangular enclosure with an attached wire, with and without a slot on its front plane, located 80 cm above ground and in free space.

4.1.6 Difference between the spherical and planar sampling

In order to find out how large the deviation of the planar sampling and the spherical sampling, the directivity was numerically obtained for both cases. A rectangular enclosure of dimensions $0.4\,\mathrm{m} \times 0.3\,\mathrm{m} \times 0.2\,\mathrm{m}$ with randomly arranged slots in Fig. 3.18 was analyzed. A linear dipole was the excitation source, as shown in Fig. 3.17. The simulation approach was described in details in Section 3.4.1.

The maximum directivity with planar sampling (Ring method in Section 2.7.3.2) considers only the D_ϕ component in the azimuth direction that could be determined by Eq. (2.44). In comparison with the spherical sampling in Fig. 3.20, the directivity in Fig. 3.19 is on average 3 dB smaller. This effect can be observed in [Wil04] as well. The discrepancy between the averaged directivity values with spherical and planar scan on the EUT is shown in Fig. 4.15. The difference varies between 0.03 and 6.32 for the numerical simulation results and varies between 1.98 and 3.57 for the theoretical results based on the Wilson theory. Table 4.1 shows the expectation and standard deviation of the directivity difference over all considered frequency points.

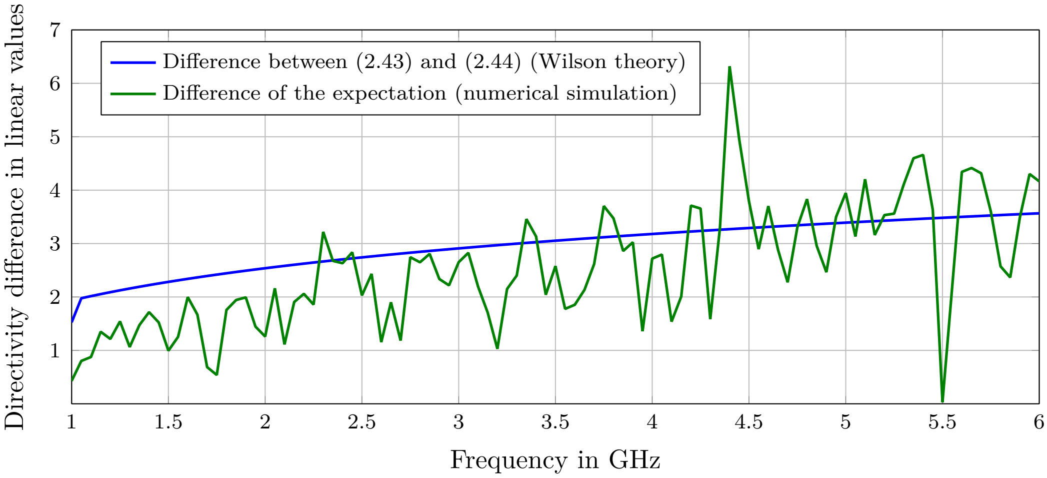

Figure 4.15: Difference of the directivity for planar and spherical sampling

Table 4.1: Statistical properties of the directivity difference between planar and spherical sampling

Parameter	**Simulation**	**Wilson Theory**
Expectation	2.56 (4.08 dB)	2.97 (4.73 dB)
Standard deviation	1.13	0.44

The standard deviation (with a value of 1.13) of the numerical simulation results is larger than the standard deviation (with a value of 0.44) based on the Wilson theory, which gives the explanation of a larger statistical oscillation in the simulation results. The relatively larger standard deviation is caused by the variation of the simulated EUT samples. It is stated in [Wil04] that the theoretical difference between the planar cut and spherical result is bounded by 3 dB. However, it shows in Fig. 4.15, for both cases, the average deviations were greater than 3 dB. It could be expected that the average deviation becomes smaller and closer to 3 dB when more sampling points are selected.

4.1.7 Summary of the factor influencing the directivity

The simulation procedure for the rectangular slotted enclosure with a connecting wire was carried out to obtain the directivity values. An analysis of the effect of different influencing factors on the maximum directivity was presented. The following conclusions can be drawn from the above studies: An ideal ground plane doubles the maximum electric field strength because of a constructive interference and therefore approximately 6 dB directivity difference was predicted, compared to the directivity in free space. It is also shown that the maximum directivity D_{max} increases along with the wire length. For the considered model, the total emission level is the summation of the wire radiation and the enclosure radiation.

Furthermore, for the configuration of the connecting wire consisting of a horizontal segment and a vertical segment attached to the slotted enclosure, it was shown that with the ratio r_{hv} or r_{vh} increasing, D_{max} exhibits no significant differences, as long as the total wire length keeps unchanged. Also the variation of the enclosure size along the wire direction has no significant influence on D_{max}.

4.2 Analytical estimation of the directivity

In this section, the analytical methods to determine the directivity of EUTs and cables introduced in Chapter 2 will be analyzed and compared to numerical results. The assessment of the methods will be done for cordless EUTs and EUTs with cables separately, keeping in mind that a suitable method needs to be applicable in both cases. Finally, it will be decided, if one of the method could be used to determine the reliable value of the directivity of arbitrary EUTs.

4.2.1 Directivity of cordless EUTs

As it was already shown in Section 3.4.1, the spherical wave theory as described in Section 2.7.2 can be used to estimate the directivity of unintentional radiators without attached cables. On the other hand, the TWA and SWA are used to determine the radiation of cables. However, these theories are not straightforward applicable. Nevertheless, both methods are shortly assessed in respect to the results and usability for the case of cordless equipment.

4.2.1.1 Directivity of cordless EUTs based on the spherical wave theory

In [Kra07a], the expectancy value of the maximum directivity $\langle D_{\mathrm{max}} \rangle$ based on many statistical samples was calculated, according to Eq. (2.43).

In Fig. 4.16, the maximum directivity based on the upper boundary $\uparrow D_{\mathrm{max}} \uparrow$ [Han88, WHH02] and the expectation value $\langle D_{\mathrm{max}} \rangle$ [Kra07a] is compared. As the electrical size ka (see also Section 2.4) increases, the expectancy value of the maximum directivity increases very slowly. Especially for large values of ka the expectancy value might underestimate the

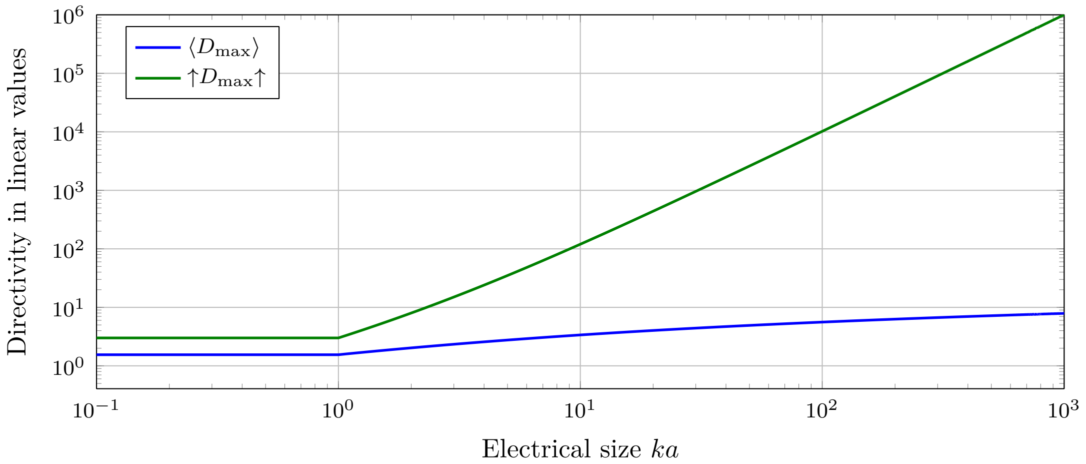

Figure 4.16: Comparison of the upper boundary $\uparrow D_{\max} \uparrow$ [Han88, WHH02] and the expectation value $\langle D_{\max} \rangle$ [Kra07a] of the maximum directivity

actual directivity of the EUT, which is theoretically bounded by the maximum directivity $\uparrow D_{\max} \uparrow$.

On the other hand, the results in Fig. 3.19 and Fig. 3.20 show a good agreement of the expectation values of the maximum directivity based on 1D sampling and 3D sampling between numerical and analytical results according to the spherical wave theory. Including the statistical approaches to guarantee the EMC performance, one can conclude that the spherical wave theory would give appropriate directivity values for cordless equipment and could be used for the conversion of measurement results between different test environments.

4.2.1.2 Directivity using SWA theory

The previously introduced cordless EUT with dimensions of $0.4\,\mathrm{m} \times 0.3\,\mathrm{m} \times 0.2\,\mathrm{m}$ was used in Section 3.4.1 for the calculation of the directivity. Correctly, the SWA and TWA are not applicable due to the missing cable. Nevertheless, it can be checked, if usable results are achievable. The directivity of a wire above ground acting as a standing wave antenna can be calculated according to Eq. (2.30). In order to use this formula, one would need the proper value for the antenna length. The effective radius of the EUT is half of the diagonal dimension of the enclosure, which is $\sqrt{20\,\mathrm{cm}^2 + 30\,\mathrm{cm}^2 + 40\,\mathrm{cm}^2}/2 = 26.9\,\mathrm{cm}$. Using this effective radius as the antenna length of the SWA, one can obtain the directivity values.

The result is compared with the numerical values in Fig. 4.17. One can see that the directivity would be overestimated by the analytical results. As assumed, the SWA is not applicable for cordless equipments.

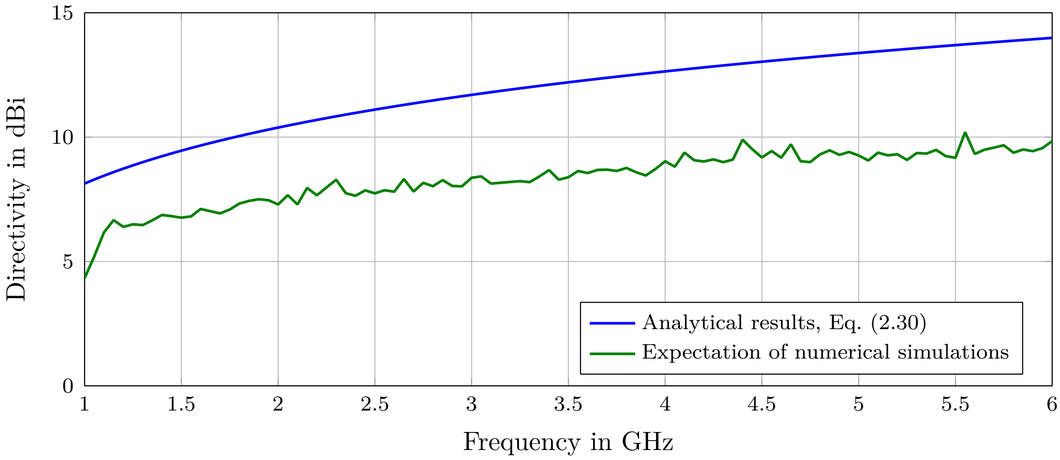

Figure 4.17: Comparison of the maximum directivity $D_{\max}$ for the model of a rectangular enclosure above ground using SWA theory and simulations

4.2.2 Directivity of EUTs with attached cables

Real EUTs do have often external power supply or data connections to the environment which is normally realized via cabling. It has to be analyzed, if the spherical wave theory and the analytical expressions for cables are also valid for the case of an EUT with attached cables. Furthermore, the influencing factors on the directivity need to be assessed.

4.2.2.1 Directivity of EUTs with cables based on the spherical wave theory

The application of the spherical wave theory needs the use of the effective radius of spheres enclosing the EUT. For a cordless EUT, it is just the radius of the enclosing sphere and the match to the simulation results is good. This concept is not straightforward applicable for EUTs with attached cables and would need some modifications. Referring to Fig. 2.4, one could define the effective radius by a way, that the sphere completely includes the enclosure and the cables.

In [Han88, WHH02], the upper boundary of $D_{\max}$ of an unintentional radiator is estimated by Eq. (2.34). Based on this equation, the resulting effective radius a could be determined through a reverse calculation, when using the simulated maximum directivity $D_{\max}$. The resulting effective radius for the EUT with an attached wire of 1 m length is depicted in Fig. 4.18.

Compared to the total wire length of 1 m and the geometrical size of the enclosure, the calculated effective radius is too small. Obviously, Eq. (2.34) overestimates the actual directivity of the EUT. As is shown before, the value of the upper bound of the directivity are overestimating the reality. This phenomena can be observed when the wire length is extended to 3 m in Fig. B.3.

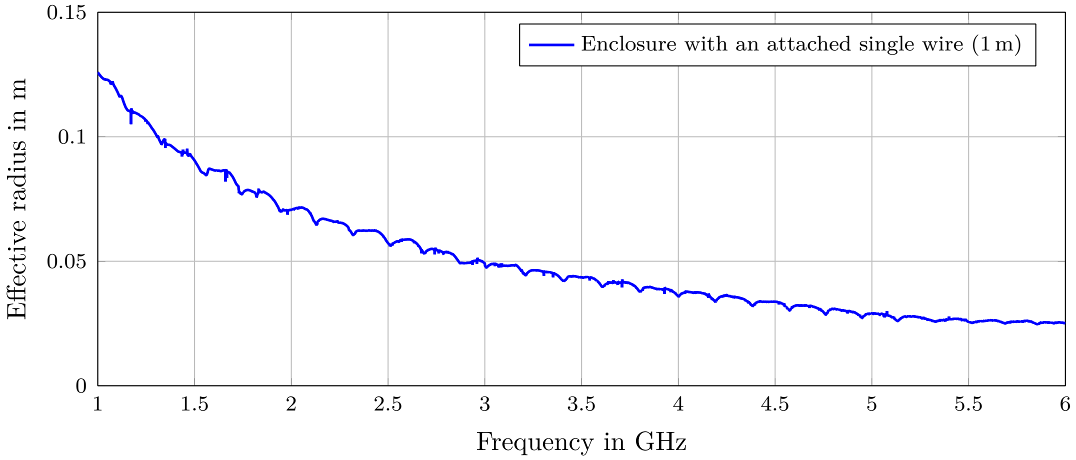

Figure 4.18: Effective radius for the enclosure with an attached single wire (with a length of 1 m), based on the upper boundary of the maximum directivity [Han88, WHH02].

On the other hand, it was shown in Fig. 3.22, the expectation value of the maximum directivity $\langle D_{\max} \rangle$ using the spherical wave theory shows similar tendency to the simulation results. The numerical results seem to be higher than the analytical results due to the influence of the wire.

More calculations were done using the model of the enclosure with different wire lengths as already used in Section 4.1.2 to check if the spherical wave theory is valid. The maximum directivity $D_{\max}$ for the model of a single wire (with different wire lengths) attached to a slotted enclosure (located in free space) is shown in Fig. 4.4. The numerical simulation results are compared to the analytical results based on the Wilson theory shown in Fig. 4.19. As can be seen, the application of the SW theory results in too small directivity values

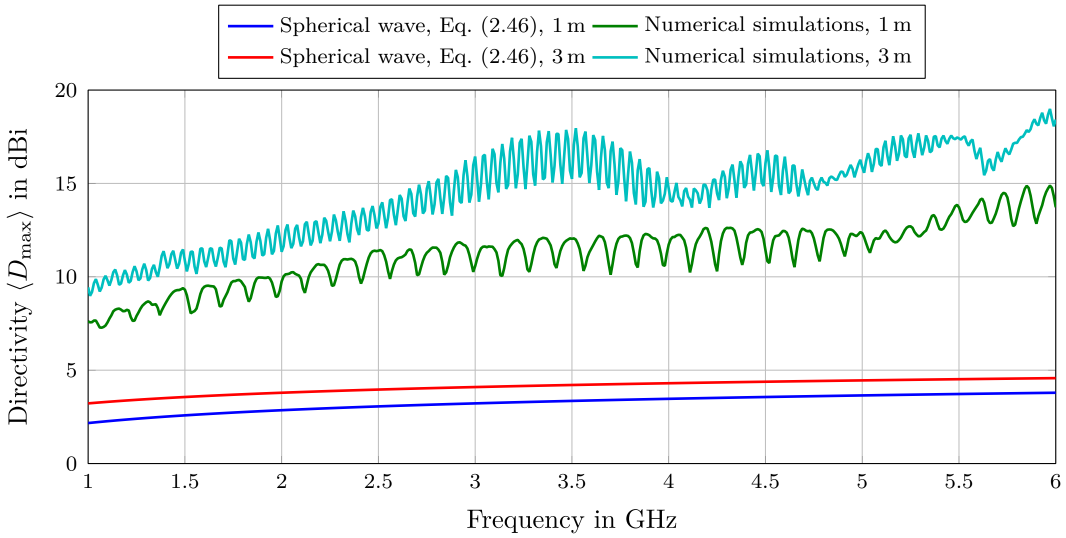

Figure 4.19: Comparison of the expectation value of the maximum directivity $\langle D_{\max} \rangle$ for the model including a rectangular enclosure attached by a wire with the length of 1 m and 3 m, using spherical wave theory and numerical simulation

and it is not really applicable .

4.2.2.2 Directivity of EUTs with cables based on the SWA theory

Generally, it is complicated to describe the maximum directivity $D_{\max}$ of an EUT with attached cables using analytical methods. As mentioned before, the maximum directivity $D_{\max}$ based on the upper boundary overestimates the actual directivity of the EUT. The expected value for the maximum directivity $\langle D_{\max} \rangle$ underestimates the actual directivity. However, the estimated directivity values according to the TWA and SWA theory locates between these two extremes [Stu81, ZHGG11].

In [ZHGG11], a model of an electrically large cable dominated desktop system was investigated. The cable termination with 150 Ω connected to the ground plane ensures that a traveling wave propagates along the wire and correspondingly the TWA theory can be applied to this model.

For comparison, the model in this work considers the connected wires open at the end, which generates a standing wave propagating on the wire. It can be considered to be as a SWA [WFS01], which consists of two TWAs in opposite directions. The aim here is to find an analytical approximation of $D_{\max}$ when the emission level is dominated by the wire radiation. The maximum directivity of the system can be analytically described by the SWA theory [Bal97, WFS01]. In [WV15b] it was shown that this theory reasonably estimate $D_{\max}$ of the antenna system consisting of a slotted enclosure with different wire routings. As is described in Section 2.6.1, Equation (2.30) can be used to estimate the directivity of a long wire antenna above ground [Kar14]. Actually, this equation can be linked to Chapter C Eq. (C.15). Here, it is assumed that the whole system including the enclosure and the wire was considered to be an antenna system and l_{TWA} is equal to the effective radius a of the sphere enclosing the system. The simulation results of the EUT with the 1 m long attached wire and the analytical results according Eq. (2.30) are shown in Fig. 4.20.

The simulation results show the wire resonances, which are missing for the analytical result. Furthermore, there is a slight resonance effect at 4.95 GHz caused by the ground reflection, which is consistent to the influence of the ground plane depicted in Fig. 4.11.The analytical results are consistent with the simulation results with a sufficient accuracy, see also [WHV16].

As mentioned before, bends on the cables are not affecting the directivity in large scale and the entire length of the cable determines the directivity. The analytical results and the simulation results for a bended wire are compared in Fig. 4.21. Here, the equivalent length of the SWA l_{SWA} is taken as 1 m, which is the total length of the horizontal and the vertical segment. In spite of the reflections at the bending between the horizontal and vertical segments, one gets still a good agreement between both cases. However, based

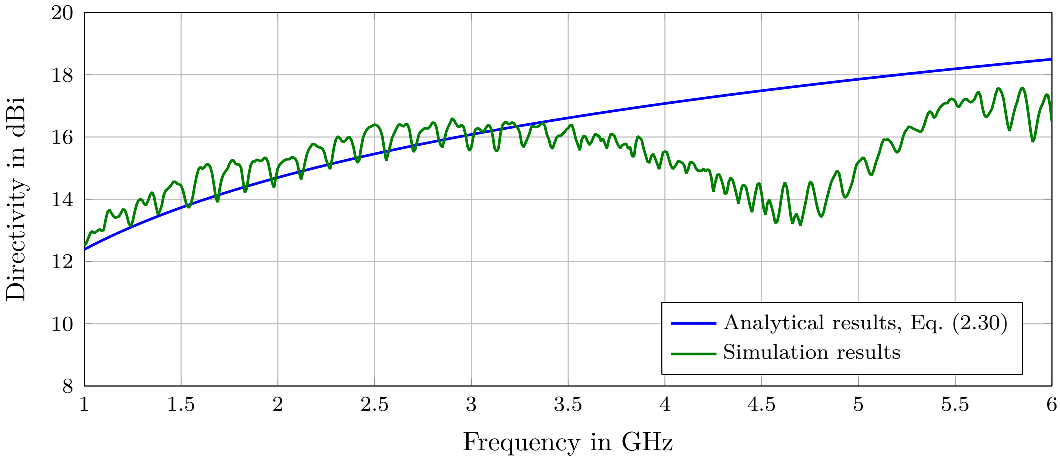

Figure 4.20: Comparison of the simulated and analytically approximated maximum directivity $D_{\max}$ for the model including a rectangular enclosure with a connecting wire with a length of 1 m, located 80 cm above ground

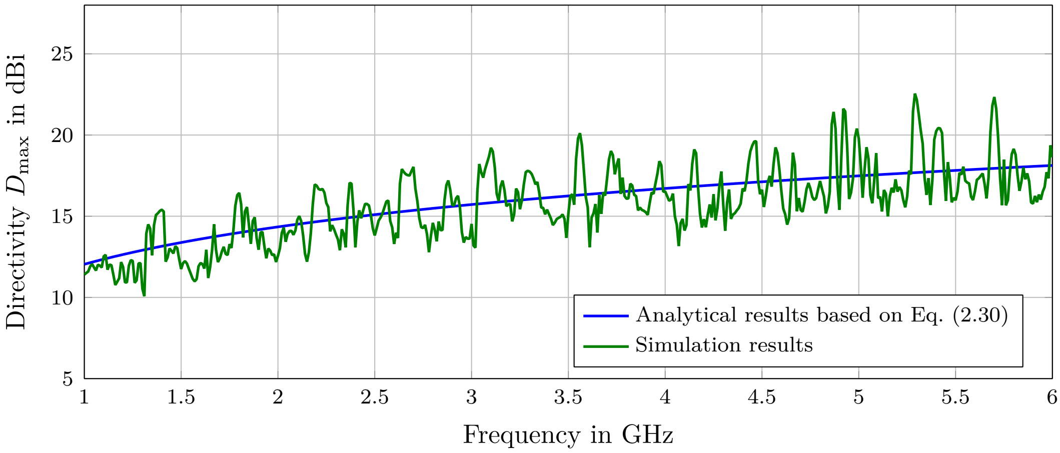

Figure 4.21: Maximum directivity $D_{\max}$ for the model of a slotted enclosure with a single connecting wire including a horizontal segment with a length of 0.7 m and a vertical segment with a length of 0.3 m, located 80 cm above ground

on the above discussions, Eq. (2.30) for the SWA theory should be only applied in the frequency range from 1 GHz to 6 GHz, if the wire length is equivalent to or less than 1 m. The results in Fig. 4.17 shows the great discrepancy between the SWA results and simulation results in case of missing cables. So the SWA is not really applicable for EUTs with short wires. On the other hand, for the model of long wires attached to the enclosure, the directivity could be described by the SWA theory only in a limited range.

4.2.2.3 Combination of numerical and analytical solution

In Section 3.5, it was shown that the combination of the numerical simulation and analytical approximation can be used to find a general expression for the directivity. If the current distribution along the wire is known as in Fig. 3.24, then the directivity can be analytically calculated, as it is shown in Fig. 3.26. In a similar manner, the directivity of the enclosure with an attached wire with different lengths can be obtained by the combination of numerical simulations and analytical solutions.

4.2.3 Summary of the applicable analytical methods

As a short summary, the spherical wave theory could be used to estimate the directivity for cordless devices but not for devices with cables. On the other hand, the SWA theory could not be used to estimate the directivity of cordless devices and delivers usable results for devices with attached wires only in a limited range. However, the combination of numerical and analytical methods provides a general solution.

4.3 Numerical Estimation of the Directivity

In order to obtain an emission limit for MSC measurements, it is necessary to investigate the directivity for arbitrary EUTs. As shown in the previous section, the analytical methods are not usable in general. Therefore, the numerical method is used in this section. The EUT shown in Fig. 4.22 with different wire lengths l outside the enclosure is analyzed. The stochastic slots are randomly distributed on the EUT surface and the following situations are investigated:

- stochastic EUT with an electrically small wire with a length of $l = 1\,\mathrm{cm}$;
- stochastic EUT with an electrically large wire with a length of $l = 1\,\mathrm{m}$;
- stochastic EUT with an electrically large wire with a length of $l = 3\,\mathrm{m}$;
- stochastic EUT with a stochastic wire length in the range from $l = 1\,\mathrm{cm}$ to $1\,\mathrm{m}$, which includes both electrically smallness and electrically largeness
- stochastic EUT with a stochastic length in the range of $l = 0.2\,\mathrm{m}$ to $1.8\,\mathrm{m}$.

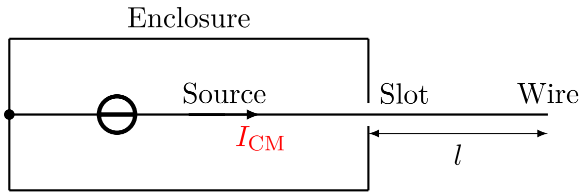

Figure 4.22: Schematic of the enclosure with an attached wire with different wire lengths, located in free space.

A sampled simulation model is shown in Fig. 4.23, where the excitation source is located between the wire and inner wall of the enclosure.

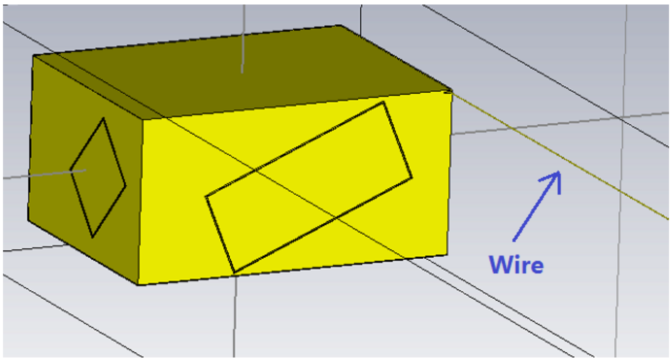

Figure 4.23: Simulation model of a single wire in different lengths attached to the rectangular enclosure with dimensions of 0.4 m × 0.3 m × 0.2 m with stochastically slots distributed on the enclosure surface, located in free space.

4.3.1 Directivity for the stochastic EUT with an electrically small wire

This part investigates the stochastic model of an ELEUT with an electrically small wire. The investigated frequency range is 1 GHz to 6 GHz so that the length of the wire outside the enclosure chosen to be 1 cm to make sure that the attached wire is electrically small.

The statistical results of the directivity are obtained based on the stochastic model of the electrically large EUT, which is realized by randomly changing the slotted area on the surface. The length of the attached wire is kept constant, which is 1 cm. Based on 110 sampled EUTs, the statistical distribution of the maximum directivity is shown in Fig. 4.24.

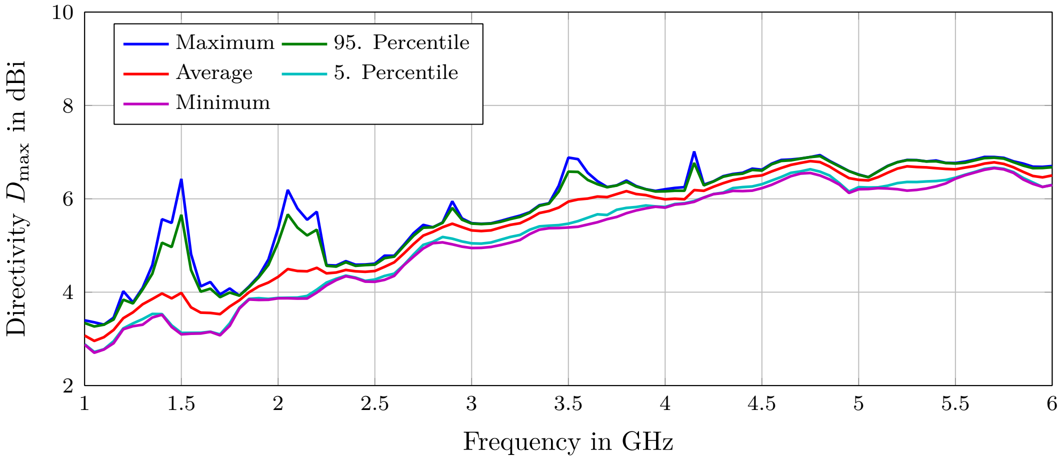

Figure 4.24: Statistical distribution of the maximum 3D directivity for the model of the enclosure with stochastic slots and an electrically small wire with a length of 1 cm, located in free space

The resonance point at 1.5 GHz corresponds to a wavelength of 0.2 m, which is almost equivalent to the dimension of the enclosure. In a similar manner, the resonance points at 2.1 GHz, 2.8 GHz, 3.8 GHz and 4.2 GHz are also due to the box resonances.

4.3.2 Directivity for the stochastic EUT with an electrically large wire with a length of 1 m

Similar procedures for the stochastic EUT with an electrically large wire with a length of 1 m were carried out. In the frequency range from 1 GHz to 6 GHz, it can be ensured that the wire satisfies the condition of electrical largeness in Eq. (2.13). The results are shown in Fig. 4.25, which illustrates a generally larger magnitude of the directivity than the model of the EUT with an electrically small wire as shown in Fig. 4.24.

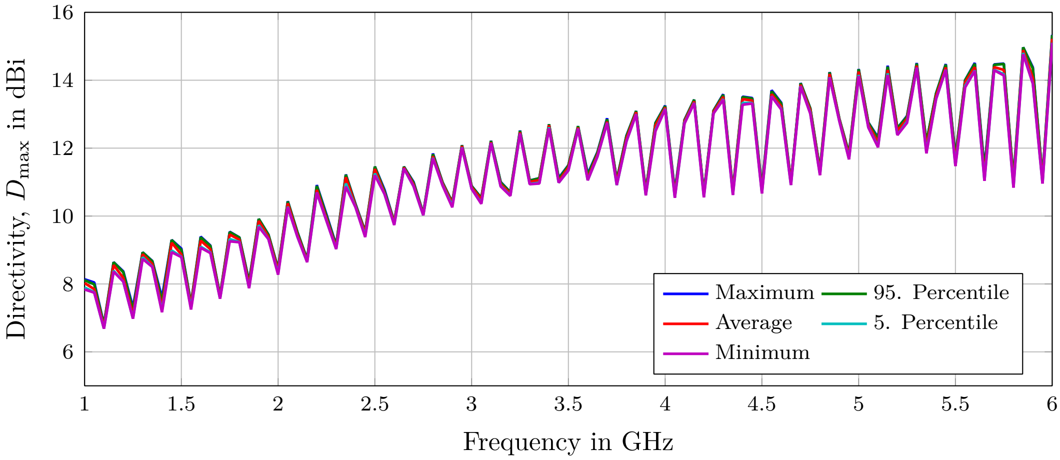

Figure 4.25: Statistical distribution of the maximum 3D directivity for the model of slotted enclosure with an electrically large wire with a length of 1 m, located in free space

Compared to Fig. 4.24, it shows in Fig. 4.25 that with stochastically changing the box dimension, the directivity distribution does not change significantly. This proves that the wire radiation is dominating. Because the wire length is kept constant, only the box dimension is changed, but the directivity has almost no variation. In comparison, for 1 cm wire length (electrically small) in the above section, the directivity is changed because of changing box dimensions therefore in this situation, the box radiation is dominating compared to the wire radiation.

4.3.3 Directivity for the stochastic EUT with an electrically large wire with a length of 3 m

This part focuses on the directivity derivation when the length of the attached wire is extended to 3 m. The slots are randomly distributed on the surface of the enclosure. The average value and other quantiles of the simulated directivity over 110 sampled EUT models is shown in Fig. 4.26.

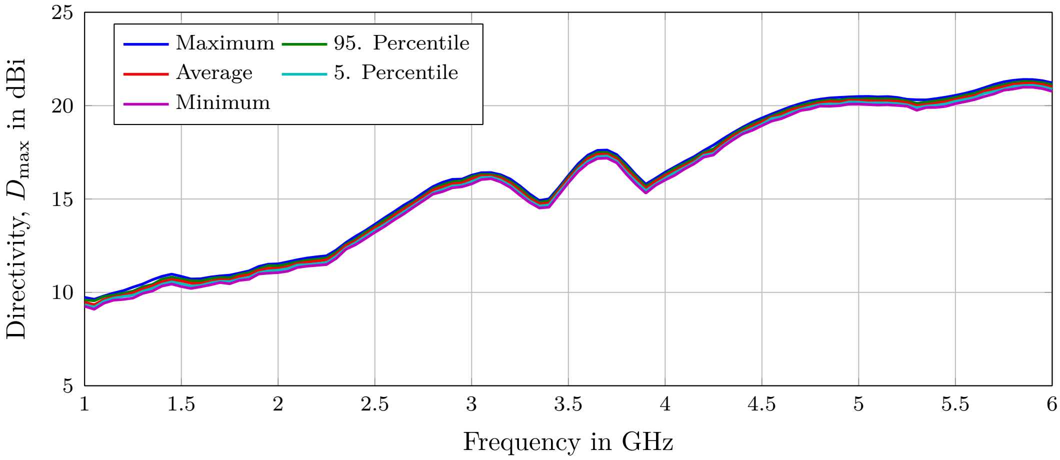

Figure 4.26: Statistical distribution of the maximum 3D directivity for the model of slotted enclosure with an electrically large wire with a length of 3 m, located in free space

4.3.4 Directivity for stochastic EUT and stochastic wire length

The model is extended to the slots randomly distributed on the surface of the enclosure and at the same time the wire length is randomly varied in the range of 0.01 m to 1 m. This situation includes the range of both electrically smallness and electrically largeness of the wire. The distribution of the obtained directivity is shown in Fig. 4.27.

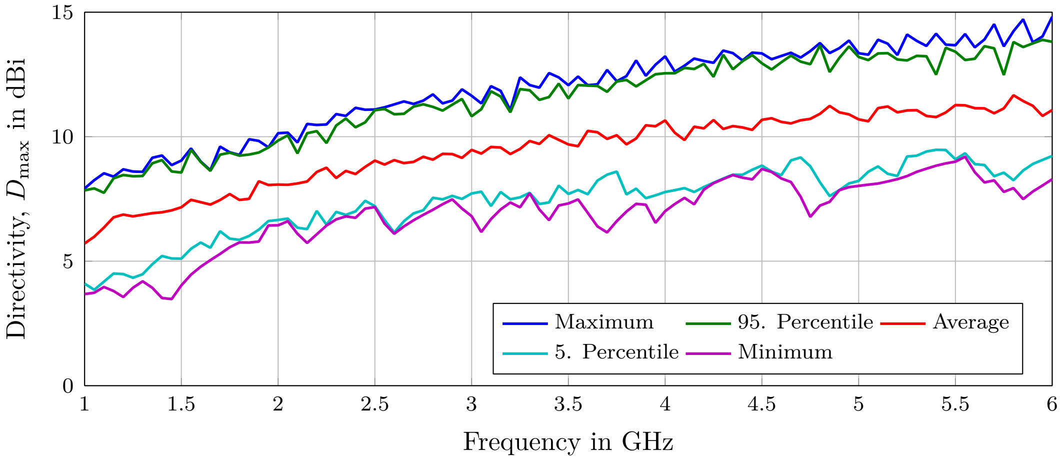

Figure 4.27: Statistical distribution of the maximum 3D directivity for the model of slotted enclosure with an attached wire with a stochastic length in the range from 0.01 m to 1 m, located in free space

The length of the cable in a real test setup might be longer than 1 m. Therefore, the directivity for the random EUTs with a stochastic wire length from 0.2 m to 1.8 m was simulated and is shown in Fig. 4.28. It shows a general larger magnitude than the shorter wire in Fig. 4.27.

The comparison of the statistical distribution for different number of samples is shown in Fig. 4.29. The results show a very similar tendency of the statistical results with 110

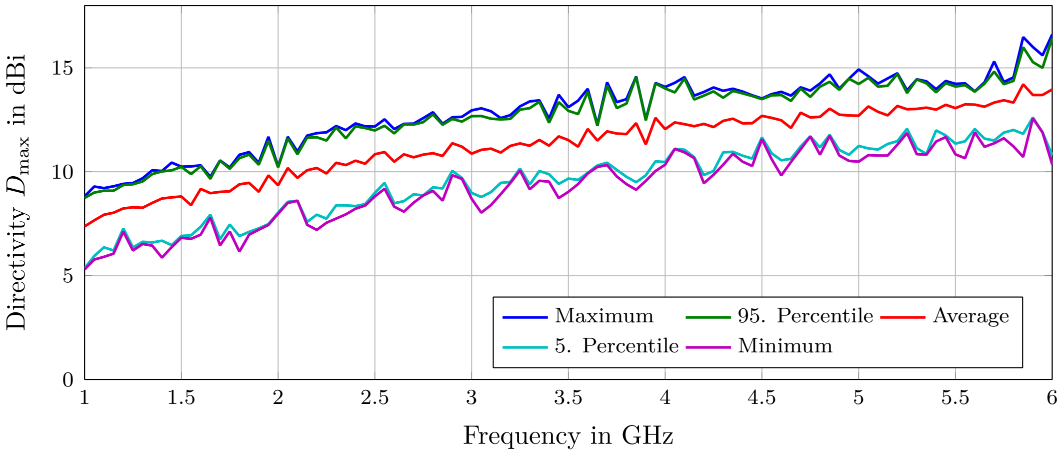

Figure 4.28: Statistical distribution of the maximum 3D directivity for the model of slotted enclosure with an attached wire with a stochastic length in the range from 0.2 m to 1.8 m, located in free space

and 150 samples. The same phenomena can be observed for other statistical investigations. Therefore, the further statistical results are based on 110 samples.

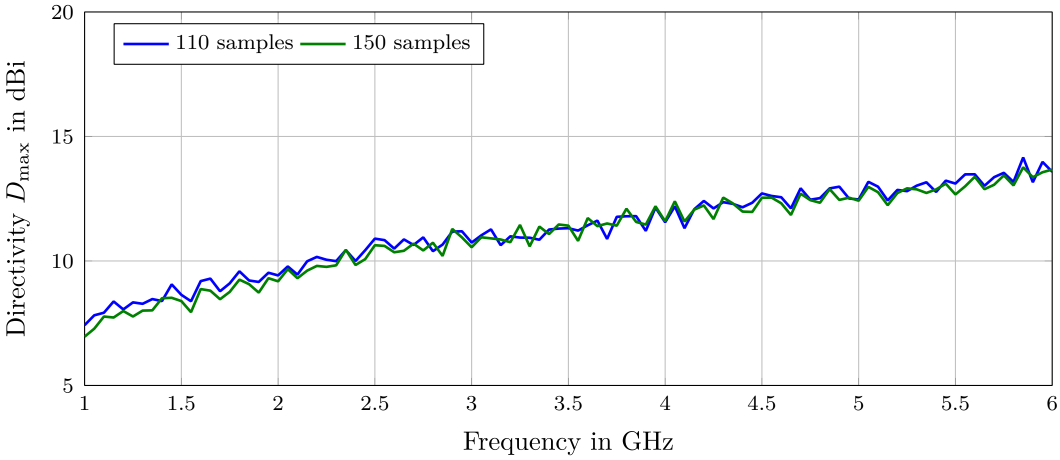

Figure 4.29: Statistical distribution of the maximum 3D directivity (with different sample numbers) for the model of slotted enclosure with an electrically large wire with a stochastic length of 0.2 m to 1.8 m, located in free space

4.3.5 Summary of the applicable numerical method

Based on the above discussions, the average value of the maximum 3D directivity is compared between different stochastic models, which can be seen from Fig. 4.30.

When the wire length increases, the directivity shows also larger values. The wire radiation is dominating compared to the radiation from the slotted enclosure. This can be also observed in the comparison of the maximum 3D directivity, as is shown in Fig. 4.30b. In the standard [CIS06a], the measurement set-up of the EUT with connecting wires in the

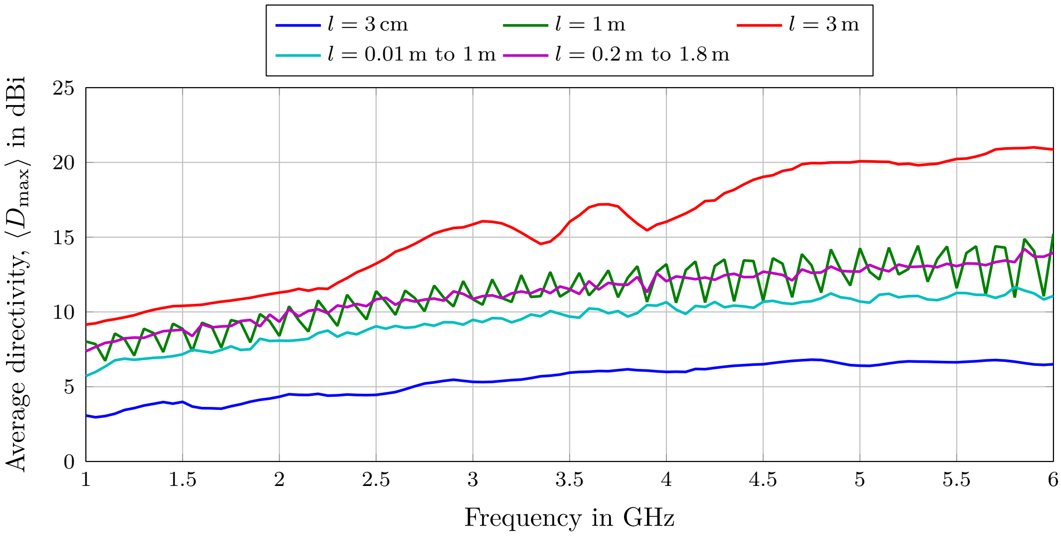

(a) average value of the maximum 3D directivity

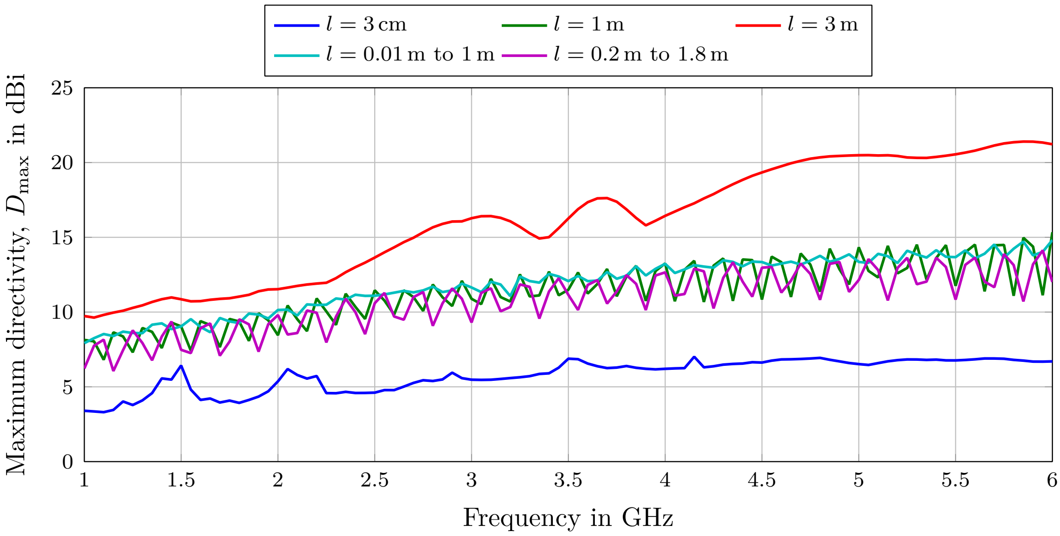

(b) maximum 3D directivity

Figure 4.30: Comparison of the average value and the maximum of 3D directivity for the model of the enclosure with different wire lengths, located in free space

FAR is regulated. The EUT with connecting wires should be placed on a non-conductive table and the EUT cabling should have a length of 0.8 m in horizontal and 0.8 m in vertical direction. The total wire length is taken as the summation of the horizontal and vertical lengths, which is 1.6 m. As a worst case, the results of the wire length from 0.2 m to 1.8 m in Fig. 4.30b can be applied to obtain a new emission limit in the next chapter.

4.4 Chapter conclusion

An analysis of different influencing factors on the maximum directivity D_{max} was presented. It was shown that D_{max} increases along with the wire length. The total emission level is the summation of the wire and the enclosure radiation. If the connected wire consisting of a horizontal segment and a vertical segment, only the total wire length influences the maximum directivity.

The determination of the directivity by analytical and numerical methods was investigated. The upper boundary of the directivity according to the spherical wave theory overestimates the actual directivity. The expectation value of the maximum directivity underestimates the actual directivity. The directivity values according to the standing wave antenna theory locate between these two extremes, which match very well with the simulation results. However, this theory is not applicable for cordless equipments and all cable lengths. At higher frequencies, the wire radiation is dominating, compared to the enclosure radiation. However, the enclosure radiation cannot be neglected. Both the wire and the enclosure radiation have to be taken into account.

In order to include all these situations, it is necessary to use numerical simulation techniques. Based on a number of sampled EUTs, the different quantiles of the directivity could be calculated. In Section 4.3, the directivity of different long wires attached to an ELEUT with randomly placed slots was determined. The maximum directivity based on statistical analysis in Fig. 4.30 provides the results, which could be applied for the conversion algorithm in the next chapter. Taking into account the measurement set-up of the EUT with cables in the FAR according to standard [CIS06a], the total wire length is taken as the summation of horizontal and vertical length, which is 1.6 m. Therefore, the results of the wire length from 0.2 m to 1.8 m in Fig. 4.30b will be used further on to suggest a power limit in the MSC.

5 Application to Measurement Procedures

The radiated power of EUTs measured within the Mode Stirred Chamber is up to now not directly comparable to a limiting value of applicable standards. Applying the CISPR 16-4-5 includes the complicated calculation of conversion factors. The comparison of different physical quantities according to the standard procedure is questionable and relies on round robin tests of multiple EUTs. A direct conversion of the measured power using an approved directivity value for certain EUTs would make the use of alternative method more easier, but still not straightforward. A direct application would acquire a limit of the radiated power. The different application methods are summarized in Fig. 5.1.

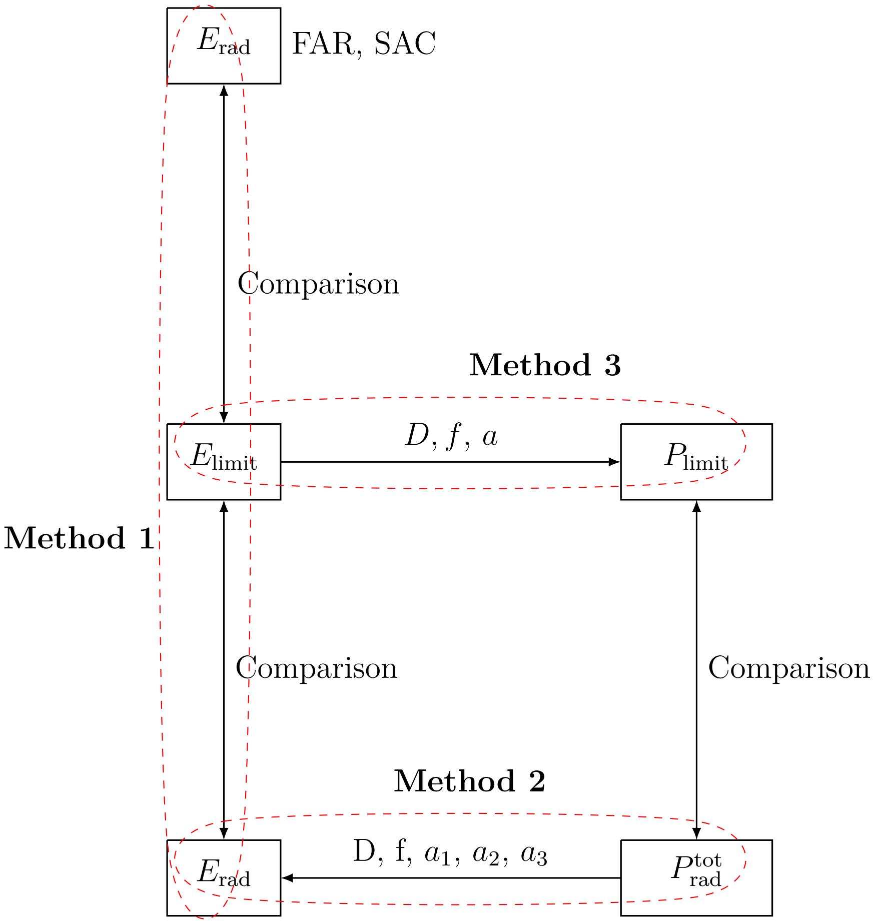

Figure 5.1: Different procedures to convert measurement results

The advantages and comparison of these three methods are discussed as followed.

1. Method: Applying CISPR 16-4-5

   The conversion method according to standard CISPR 16-4-5 was already described in Section 2.9.1 and can be applied for measurements in different facilities like FAR, SAC and MSC. However, this method is not really practicable, because different physical quantities are compared and the results based on CISPR 16-4-5 depend on the number of samples. In Section 5.1, the method will be applied to measurements in the MSC based on the simulation and measurement results.

2. Method: Calculation of the E_{rad}

   The estimated directivity values of EUTs can be used to calculate the corresponding radiated electric field strength E_{rad} at the applicable measurement distance. This calculated field strength E_{rad} can be directly compared to the limiting values of the appropriate standard. However, this method would still depend on the establishment of the expected directivity value for different EUT classes and the conversion of the measured radiated power in the MSC to an electric field strength.

3. Method: Power limit

   A proposal for a radiated power limit for MSC measurements can be derived based on established E-field limits and the expected directivity of EUTs as described in Section 5.3. The test objects can be classified according to the predictable electrical size, e. g., 0.03 m, 0.1 m, 0.5 m, 0.75 m, 2.5 m and 3 m. This method proves to be very practicable, because a directly measurable radiated power can be compared with this power limit.

5.1 Method 1: CISPR 16-4-5

The conversion of the radiated emissions of EUTs in different measurement environments based on CISPR 16-4-5 can be applied to an ATM. In this work, the MSC is introduced as the ATM and the FAR is used as the ETM. As mentioned before, the measurement of the total radiated power P_{rad} of the EUT in the MSC provides a beneficial alternative approach to the conventional direct measurements of the electric field strength. Here, the conversion algorithm based on CISPR 16-4-5 is analyzed by numerical simulation technique. The advantage to perform simulation procedures is the relative swift simulation speed and an avoidance of the complicated measurement set-up. The calculated E-field strength in the simulations takes into consideration all polarizations as in the real-world measurements. The model of the EUT with a horizontal connecting wire with a length of 1 m and with stochastic slots distributed on the surface as shown in Fig. 4.23 was used for the simulations. Here, 10 stochastic variations of EUTs are considered. As described in

Chapter 3, for CST simulations, the structure was internally excited by a discrete port between the wire and the enclosure (with an input power 1 W, driven by a Gaussian signal).

The maximum electric field strength on a sphere of a radius of $r = 3\,\mathrm{m}$ around the EUT was chosen as reference quantity E_{ref} and the values are shown in Fig. 5.2.

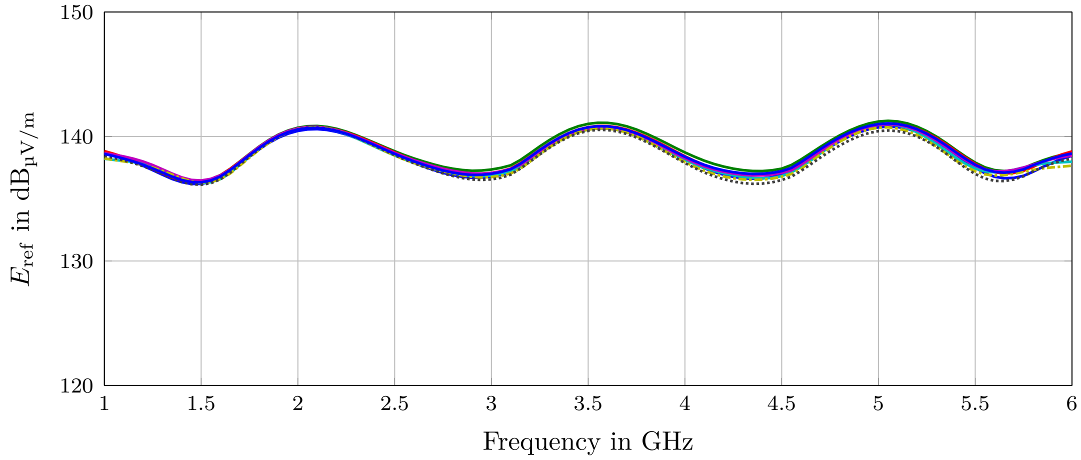

Figure 5.2: Reference quantity E_{ref} for 10 variations of the stochastic model of the slotted enclosure with the attached wire with 1 m length

The measurand of the established test method is the measured electric field strength in the FAR as described before in Fig. 2.17. The simulated maximum E-field strength was taken from 72 sampled values by a planar sampling with 5° resolution. For each EUT, the maximum E-field strength on the Ring at the height of 1 m was obtained. These values for a stochastic EUT as an example are observed in Chapter G. The measurand $E_{\mathrm{FAR,3m}}$ in the FAR are shown in Fig. 5.3.

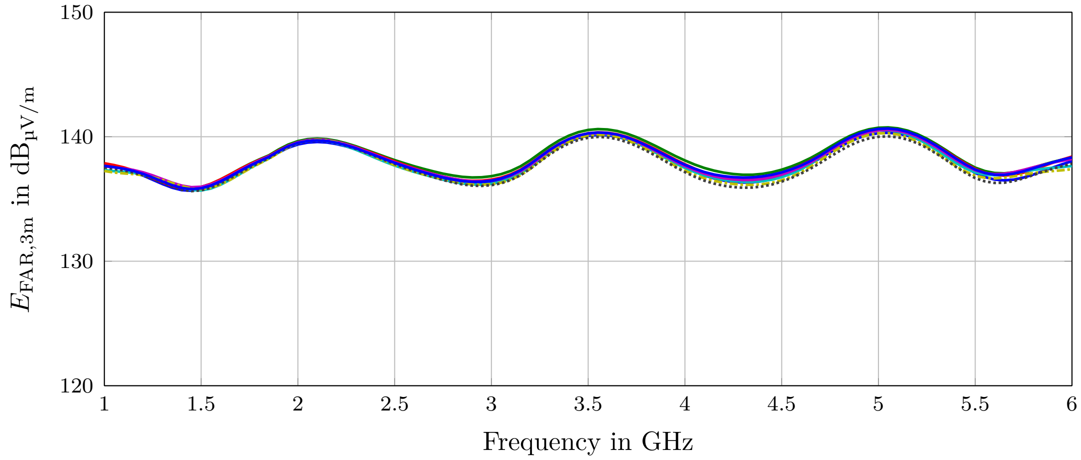

Figure 5.3: E-field strength in the FAR for 10 variations of the stochastic model of the slotted enclosure with the attached wire with 1 m length

The measurand of the alternative test method (MSC) is the total radiated power. The simulated radiated power of different stochastic EUTs is shown in Fig. 5.4. The procedure of CISPR 16-4-5 was applied using these input data.

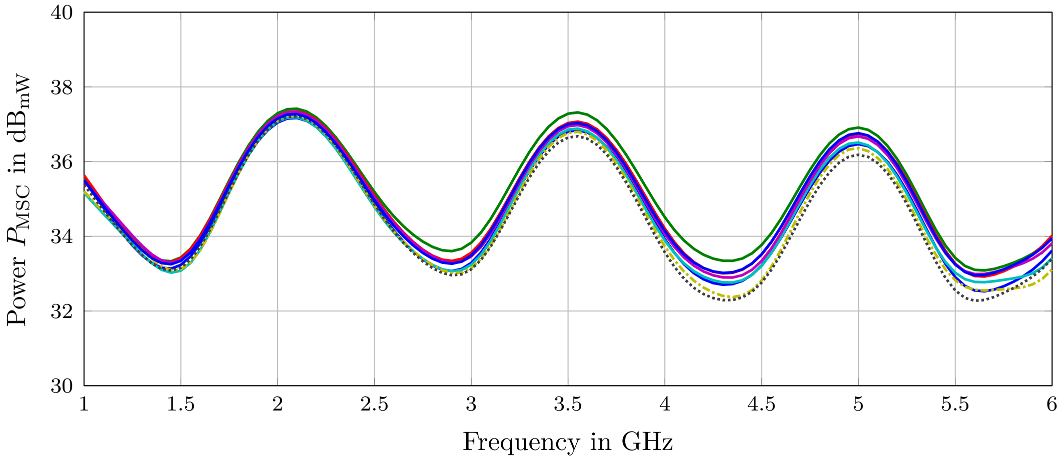

Figure 5.4: The radiated power based on the MSC method for 10 variations of the stochastic model of the slotted enclosure with the attached wire with 1 m length

5.1.1 Determination of the deviation

The deviation from the reference quantity is determined by subtracting the measured quantity from the reference quantity E_{ref}. The deviation has to be calculated separately for each variation of EUTs in the FAR and MSC.

The deviation D_{MSC} for the MSC is calculated in dB scale according to:

$$D_{\mathrm{MSC}} = E_{\mathrm{ref}} - P_{\mathrm{MSC}} \tag{5.1}$$

where P_{MSC} is the measured power in the MSC, as is shown in Fig. 5.4 and E_{ref} is the reference quantity as shown in Fig. 5.2.

Analogously, the deviation between the measured E-field strength in the FAR at 3 m measurement distance $E_{\mathrm{FAR,3m}}$ and the reference quantity E_{ref} is calculated in dB scale according to:

$$D_{\mathrm{FAR,3m}} = E_{\mathrm{ref}} - E_{\mathrm{FAR,3m}} \tag{5.2}$$

where $D_{\mathrm{FAR,3m}}$ is the deviation of the FAR and $E_{\mathrm{FAR,3m}}$ is shown in Fig. 5.3.

In the next step, the mean values of the deviation are computed according to Eq. (2.53) for the alternative and Eq. (2.54) for the established test method. Therefore the corresponding deviation $\overline{D}_{\mathrm{MSC}}$ is shown in Fig. 5.5 and the deviation $\overline{D}_{\mathrm{FAR}}$ is depicted in Fig. 5.6.

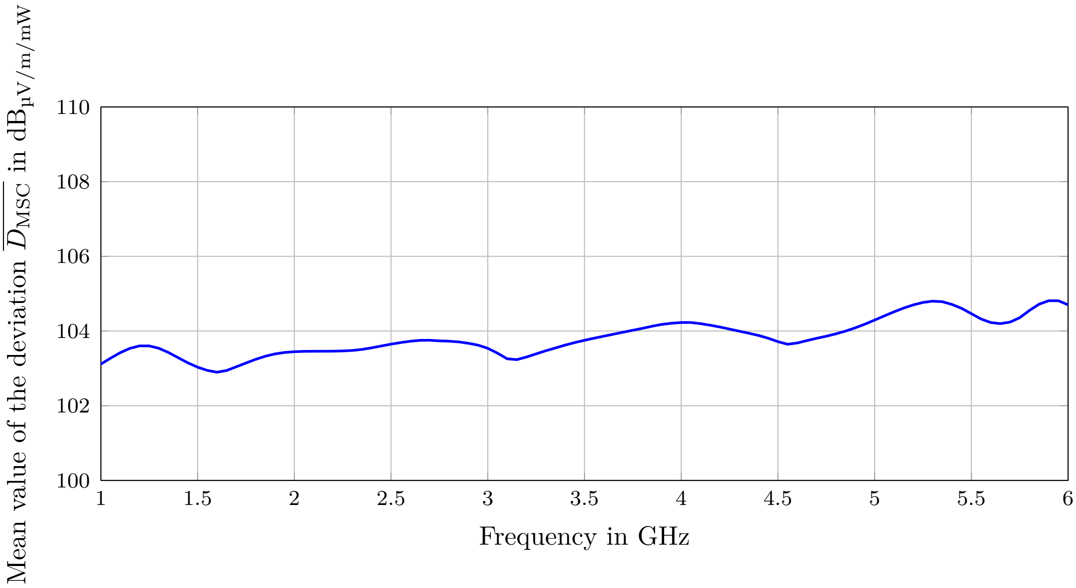

Figure 5.5: Mean value of the deviation $\overline{D}_{\mathrm{MSC}}$ from the reference quantity based on the MSC method for the stochastic model of the slotted enclosure with the attached wire with the length of 1 m

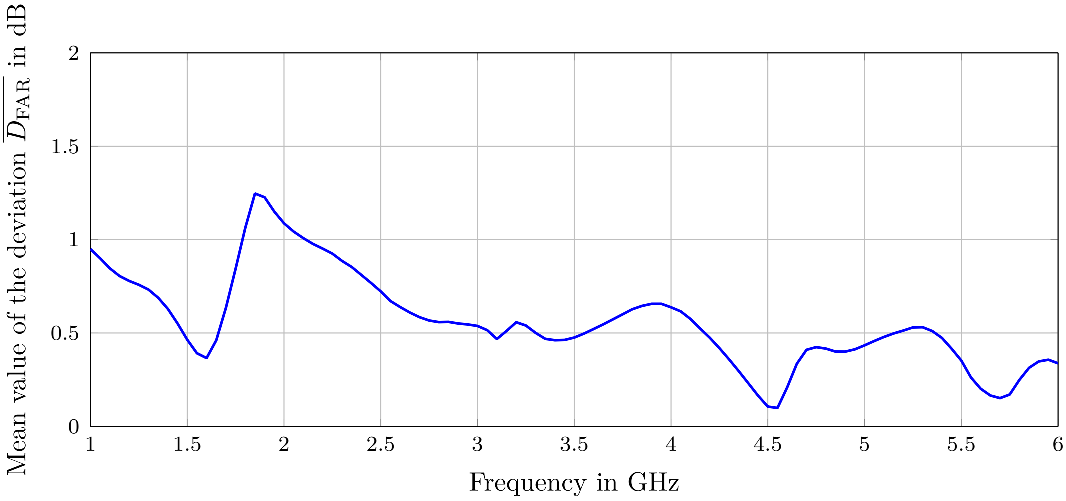

Figure 5.6: Mean value of the deviation $\overline{D}_{\mathrm{FAR}}$ from the reference quantity based on the FAR method for the stochastic model of the slotted enclosure with the attached wire with the length of 1 m

5.1.2 Determination of uncertainty

The inherent uncertainty ($u_{\mathrm{ATM,inherent}}$ and $u_{\mathrm{ETM,inherent}}$) are calculated according to Eq. (2.57) and Eq. (2.58). The inherent uncertainty of the FAR measurement is mostly influenced by the use of the ring sampling instead of a complete spherical sampling. Using a coverage factor $\kappa = 1.96$, the resulting expanded uncertainty of the established measurement method (FAR) is shown in Fig. 5.7. Similarly, the uncertainty of the MSC method can be calculated and shown in Fig. 5.8.

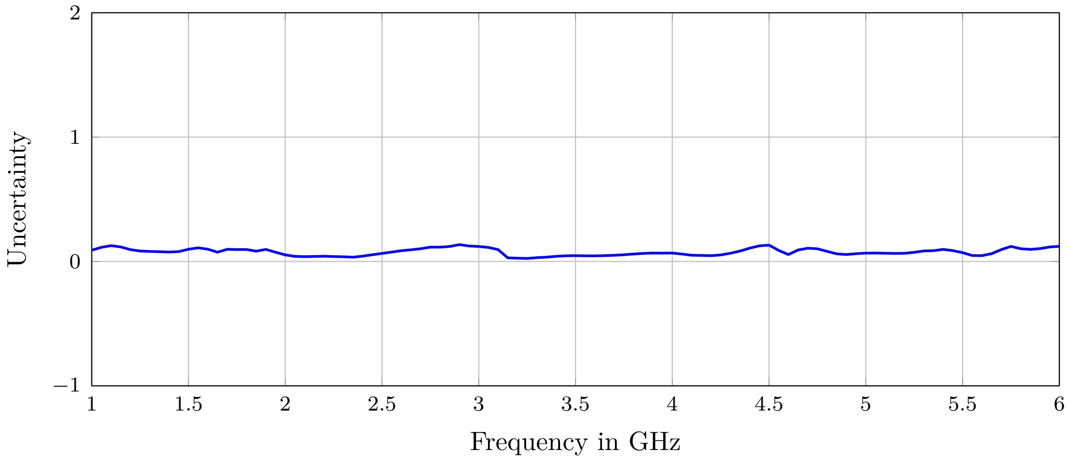

Figure 5.7: Uncertainty for the 3 m FAR results for the stochastic model of the slotted enclosure with the attached wire with the length of 1 m

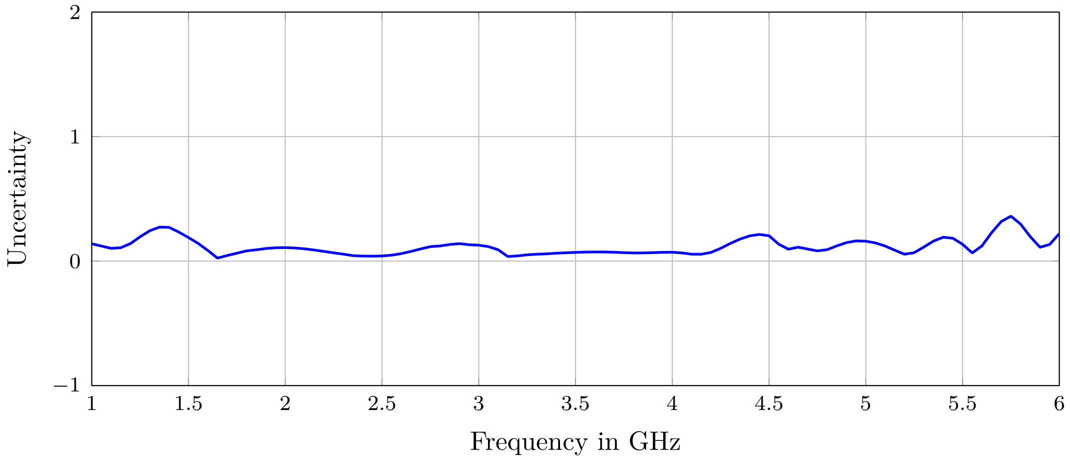

Figure 5.8: Uncertainty for the MSC results for the stochastic model of the slotted enclosure with the attached wire with 1 m length

5.1.3 Determination of the conversion factor

The average conversion factor $\overline{K}_{\mathrm{MSC}}$ is the difference of two mean deviations in logarithmic scales:

$$\overline{K}_{\mathrm{MSC}} = \overline{D}_{\mathrm{MSC}} - \overline{D}_{\mathrm{FAR,3m}} \tag{5.3}$$

which is the same equation as Eq. (2.61) in Chapter 2. The resulting conversion factor is shown in Fig. 5.9.

According to Eq. (5.3) and [Mag17], it is obvious that the reference quantity does not affect the conversion factor, which means the choice of the reference quantity is not really useful in the conversion procedures. The conversion factor builds a relation between the measured E-field strength in the FAR and the radiated power in the MSC. This method is

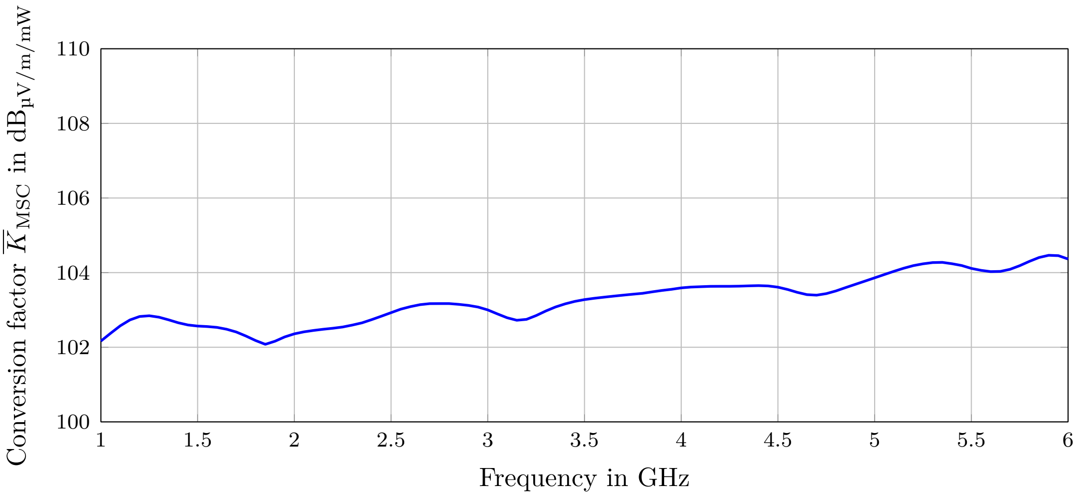

Figure 5.9: Conversion factor $\overline{K}_{\mathrm{MSC}}$ towards 3 m FAR results for the stochastic model of the slotted enclosure with the attached wire with 1 m length

in some sense, not so practical, because for each EUT, one would have to use the conversion factor to obtain the limit value.

5.1.4 Determination of the limit for the alternative method

The limit for the electric field strength $L_{\mathrm{FAR}}(f)$ according to [CIS15] is shown in Fig. 5.10, which has the value of 70 dBµV/m over the frequency range of 1 GHz to 6 GHz.

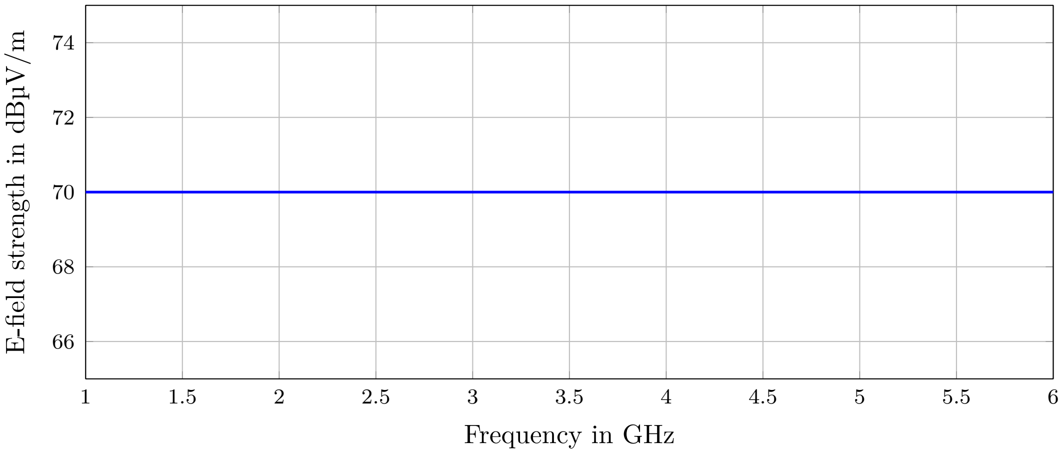

Figure 5.10: Existing CISPR class B limit L_{FAR} [CIS15]

According to Eq. (2.64), the limit for the alternative test methods can be calculated by $L_{\mathrm{MSC}}(f) = L_{\mathrm{FAR}}(f) - \overline{K}_{\mathrm{MSC}}(f)$, which is shown in Fig. 5.11.

Besides, the difference of the uncertainty of the test methods has to be taken into account by the condition in Eq. (2.66). As is shown in [Mag17], if the total radiated power in the MSC results in a smaller inherent uncertainty than the E-field strength in the FAR method, the limit of the MSC is not necessary to be corrected. However, if the uncertainty of the MSC method is larger than the FAR method, Eq. (2.64) should be used and the emission limit has to be corrected. The resulting limit is shown in Fig. 5.12, which was obtained by taking the mean value of the calculated limit in Fig. 5.11 over the frequency.

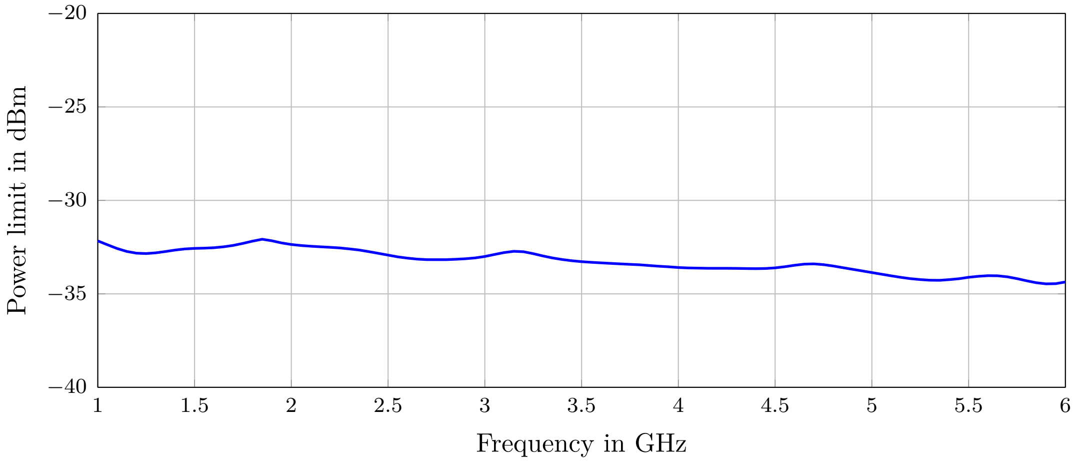

Figure 5.11: Calculated power limit for measurements in the MSC for stochastic EUTs with 1 m cable

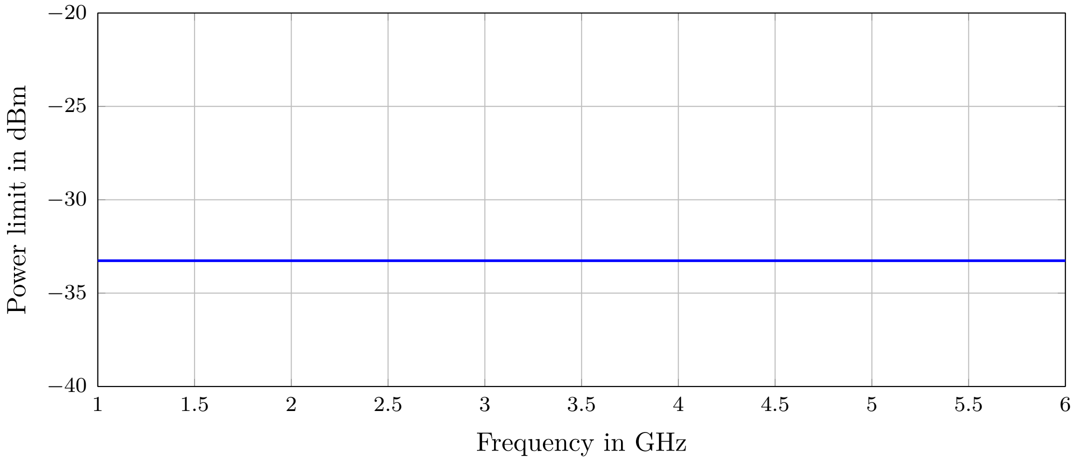

Figure 5.12: Proposed limit for measurement in the MSC for stochastic EUTs with 1 m cable

In [Mag17], it is pointed out that when the uncertainty of both alternative and established methods is comparable, it is possible to choose the reference quantity in a manner that the uncertainty of alternative method is smaller than the established method. In this case, it's not necessary to correct the emission limit. Therefore, the reference quantity has no influence on the conversation method. This whole procedure seems to be futile.

In fact, the conversion method described in CISPR 16-4-5 is based on the actual measurements of EUTs and is therefore limited usable, only for a certain class of EUTs. For a general solution, the Method 3 described in Fig. 5.1 - the new derived power limit based on the electrical size is recommended.

5.2 Method 2: E-field limit

The electric field strength can be directly calculated from the measured total radiated power in a MSC by Eq. (2.14). Rearranging the formula and using dB units gives Eq. (5.4).

$$\frac{E}{\mathrm{dB(V/m)}} = 10\log_{10}\left(\frac{\frac{D\eta}{4\pi r^2}}{(\mathrm{V/Am^2})}\right) + \frac{P_{\mathrm{rad}}^{\mathrm{tot}}}{\mathrm{dB(W)}} \tag{5.4}$$

The first term on the right side is the conversion factor. To use the formula, the directivity of the EUT must be known. In general, this condition is not fulfilled. To overcome this disadvantage, numerical calculated values could be used. The use of the directivity leads more or less to a conversion factor. This conversion factor does not include uncertainties of the FAR-measurements and in case that the directivity is well estimated, the results are reliable. Correspondingly, the resulting value of the conversion factor is shown in Fig. 5.13. A quadratic interpolation was applied to obtain this smooth curve, which is displayed in blue color.

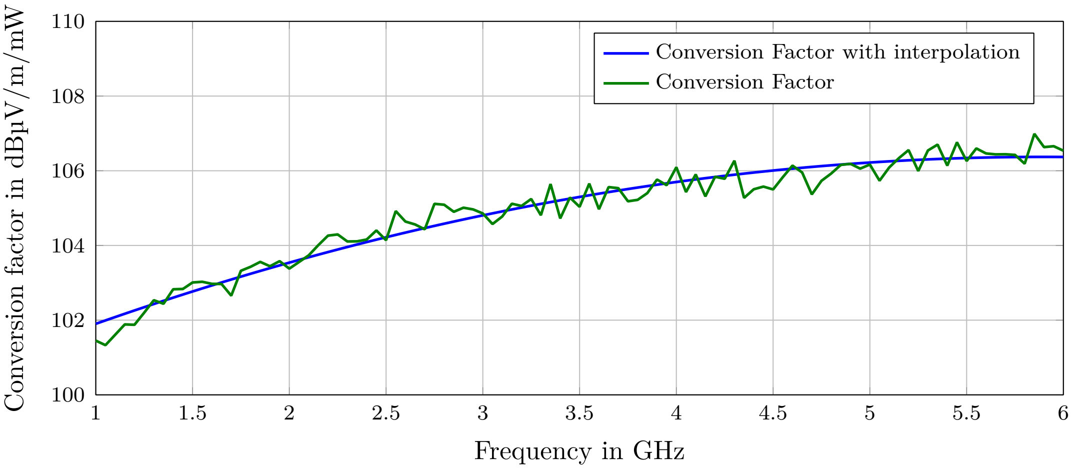

Figure 5.13: Conversion factor of the stochastic EUT with a cable length in the range 0.2 m to 1.8 m to convert the measured radiated power to an E-field strength

5.3 Method 3: Power limit based on the electrical size

The previous methods include always a conversion of the measured value to an electrical field strength and cannot be directly applied when performing standardized EMC tests. The conversion procedure described in CISPR 16-4-5 is limited to certain EUTs, which is expensive and time-consuming. Therefore, the conversion procedure is not efficient and not very practical.

It would be useful to directly compare the measured total radiated power in an MSC with a limiting value, e. g. a power limit. By rearranging Eq. (2.14), the appropriate power limit could be calculated according to Eq. (5.5):

$$P_{\text{rad}}^{\text{Limit}} = \frac{E_{\text{Limit}}^{2} 4\pi r_{\text{meas}}^{2}}{D\eta} \tag{5.5}$$

In this equation, E_{Limit} is the limiting value of the electric field strength at the measurement distance r_{meas} from the EUT, D is the directivity of the EUT and η is the free space wave impedance.

Due to the influence of the electrical size of the EUT on its directivity and therefore on the conversion factor, the test objects could be classified according to different electrical sizes and different limits would be derived. Limits of the EUT with different long attached cables could be calculated, based on the numerical results of the directivity described in Section 4.3.

In fact, these limits are not practically usable. A partly stable limit line needs to be adopted and the use of different limits for different EUTs does not seem to be an approach for international standards. The stable line can be obtained by averaging the calculated data and clustering it into frequency ranges.

In Fig. 5.14, the resulting limit for the different EUTs is shown, whereby the directivity was obtained above in Section 4.3.5 as shown in Fig. 4.30. Considering the test setup for field measurements, the size of the equipment and the cable length, one could use a proper chosen size of EUTs to calculate a power limit.

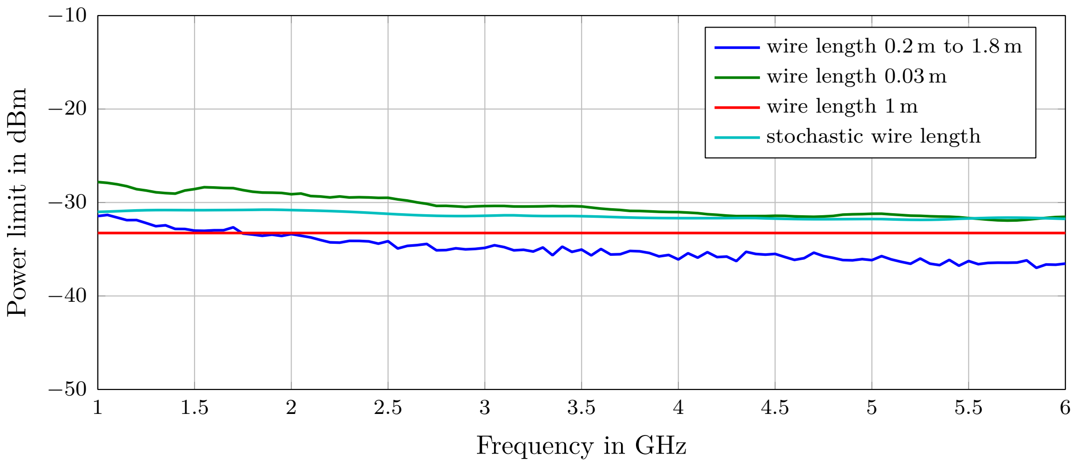

Figure 5.14: Calculated limit for MSC method based on statistical investigations for the slotted enclosure with different wire lengths

The proposed limit for the EUT with a wire length from 0.2 m to 1.8 m is shown in Fig. 5.15, which was calculated using the numerical results of the directivity described in Section 4.3.

This proposed limit was chosen as an appropriate stable line, which is the mean value of the limits in Fig. 5.14 for different wire lengths attached to the slotted enclosure.

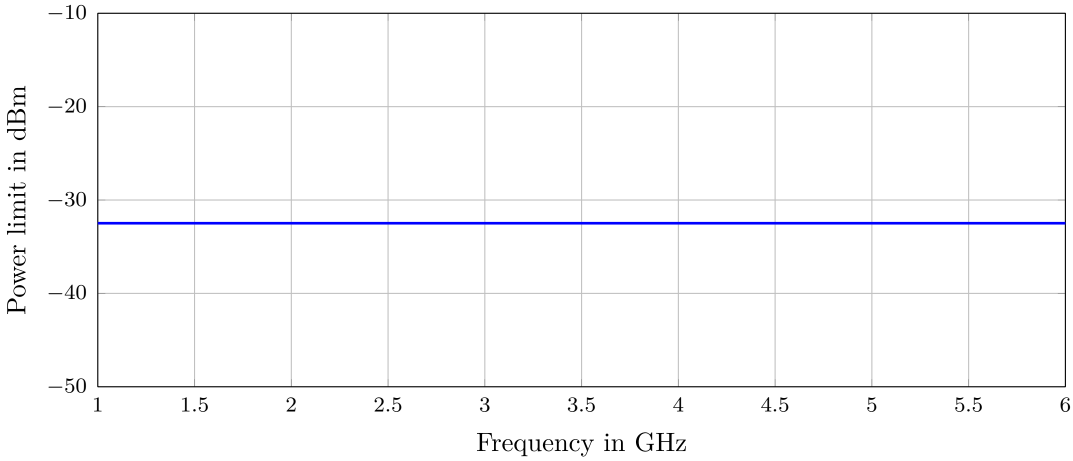

Figure 5.15: Proposed limit for MSC method based on statistical investigations for the slotted enclosure with a wire length in the range from 0.2 m to 1.8 m

5.4 Experimental investigation

Procedures to apply the MSC as ATM for the radiated emission measurements were analyzed based on numerical simulations in the previous chapters. The application of this procedure was experimentally investigated with the same EUT as it was used for the simulations. The results are shown and discussed in this section.

5.4.1 Measurements of the EUTs

5.4.1.1 Measurements in the MSC

MSCs have been used primarily for radiated immunity measurements. However, MSCs are reciprocal devices, and they can also be used for radiated emission measurements [Hil98]. In a radiated emission measurement, the radiated power of the EUT feeds the MSC and this radiated power is measured by a receive antenna and an EMI receiver. The measurements in a MSC are thorough and robust because the results are insensitive to the EUT placement in the chamber and independent of EUT radiation patterns.

The total radiated power can be measured in a simple manner. According to IEC 61000-4-21, the emission measurement procedures was performed with the EUT calibration and the EUT measurement. First of all, the radiated power of the comb generator was recorded using a spectrum analyzer directly, which is shown in Fig. 5.16a and Fig. 5.17a. The measurement was carried out in average mode, by setting the spectrum analyzer to the

RBW of 1 MHz and the VBW of 1 MHz. A continuous tuner rotation was applied in the MSC.

Then, the comb generator is connected with the reference source and measured in the MSC. Here, a horn antenna was selected as the reference antenna, which can be seen in Fig. E.1. Due to the reflection at the port, only a part of the power from the source is radiated by the horn antenna. The well-established method introduced in [Int11, Kra07b] determines the radiated power of the EUT $P_{\text{rad,EUT}}$ by performing a measurement of a reference source with a known power, while keeping the chamber conditions the same, which can be seen in Fig. 5.16b and Fig. 5.17b. Under the condition that the radiated power $P_{\text{rad,ref}}$ and the received power $P_{\text{rec,ref}}$ of the reference source is known, the coefficient of the insertion loss IL can be determined straightforward:

$$\mathrm{IL} = \frac{P_{\text{rec,ref}}}{P_{\text{rad,ref}}} \tag{5.6}$$

This ratio – insertion loss is the same for both the reference antenna and the EUT, therefore the following expression can be obtained:

$$\frac{P_{\text{rec,EUT}}}{P_{\text{rad}}} = \frac{P_{\text{rec,ref}}}{P_{\text{rad,ref}}} \tag{5.7}$$

Rearranging the equation Eq. (5.7), the expression to calculate the total radiated power of the EUT can be obtained:

$$P_{\text{rad}} = \frac{P_{\text{rad,ref}}}{P_{\text{rec,ref}}} \cdot P_{\text{rec,EUT}} \tag{5.8}$$

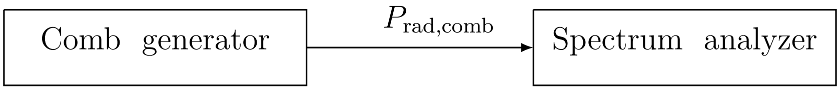

(a) the output power of the comb generator

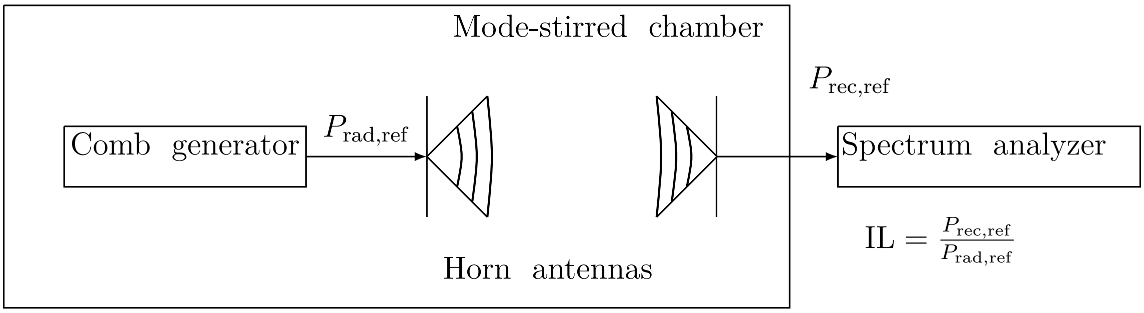

(b) measurement of the received power of the horn antenna

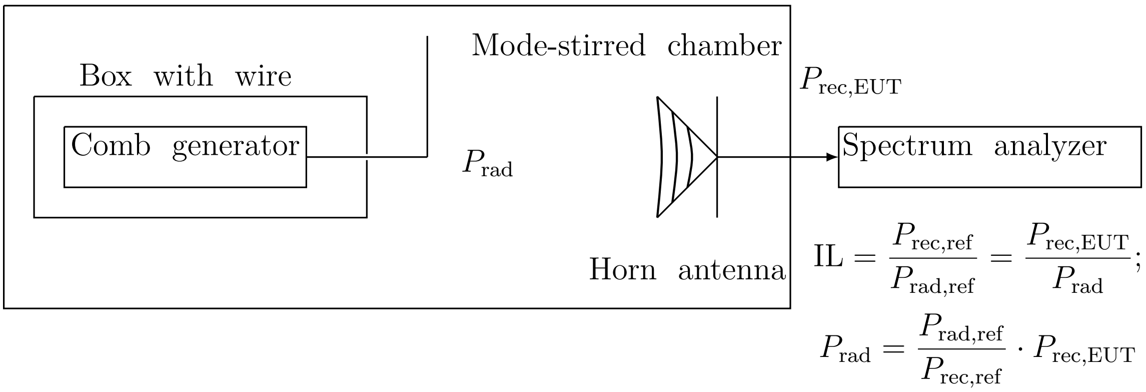

(c) measurement of the radiated power of the EUT in the MSC

Figure 5.16: Schematic of the measurement set-up in the MSC

The quantity $P_{\mathrm{rec,EUT}}$ is the received power of the EUT, which was read directly from the spectrum analyzer. This method is advantageous because of canceling the efficiency and the impedance mismatch effects of the receiving antenna under the condition that the same receiving antenna is used for both the EUT and the reference antenna measurement. Here, a monopole mounted on a comb generator as the excitation source inside the EUT was used. The measurement set-up is shown in Fig. 5.16c and Fig. 5.17c.

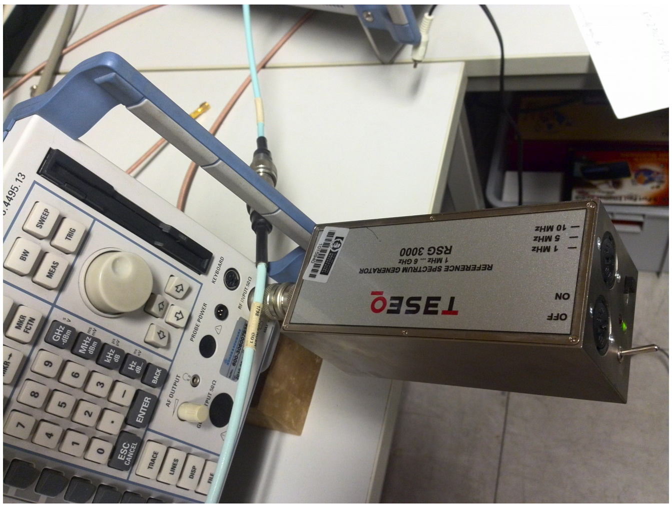

(a) measurement of the output power of the comb generator

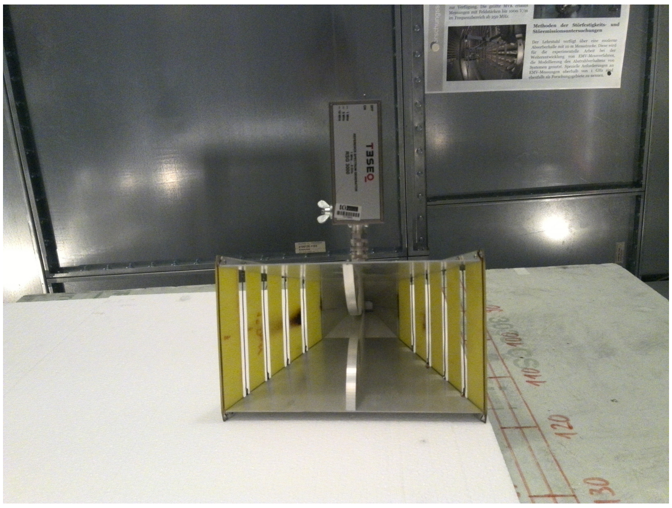

(b) measurement of the received power of the horn antenna

(c) measurement of the radiated power of the EUT in the MSC

Figure 5.17: Measurement of the EUT in the MSC at the Otto von Guericke University in Magdeburg.

Here, two EUTs are considered, the slotted enclosure and the slotted enclosure with an attached wire with 1 m length. The blue curve in Fig. 5.18 shows the total radiated power of the comb generator $P_{\mathrm{rad,comb}}$ and the green curve displays the received power of the reference source $P_{\mathrm{rec,ref}}$. The measured total radiated power for the slotted enclosure according to Eq. (5.8) is shown in Fig. 5.19. Similarly, the total radiated power of the slotted enclosure with an attached wire is displayed in Fig. 5.20. These measured radiated power can be compared with the power limit in the further analysis.

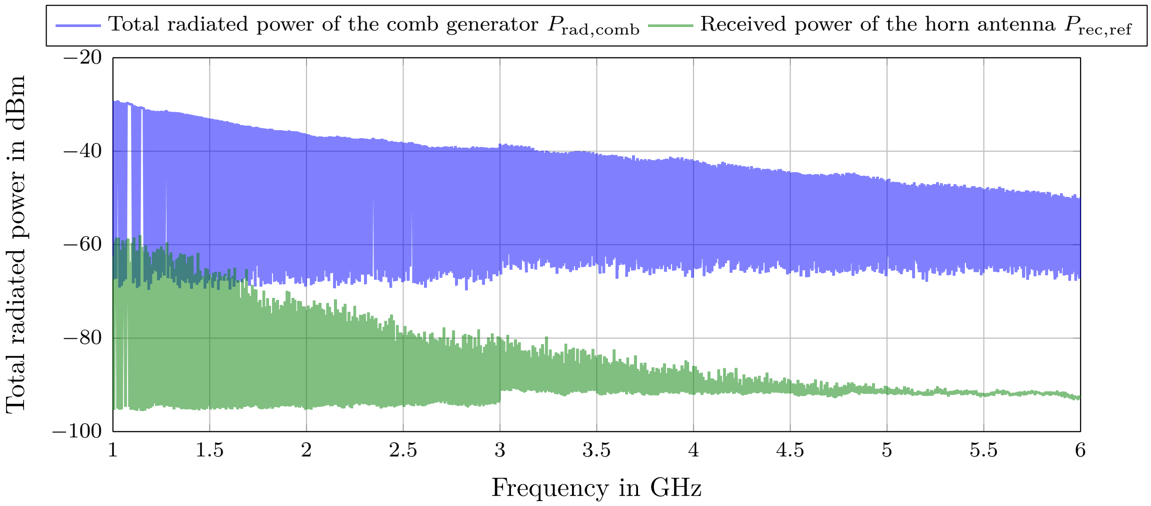

Figure 5.18: Total radiated power of the comb generator and the received power of the horn antenna

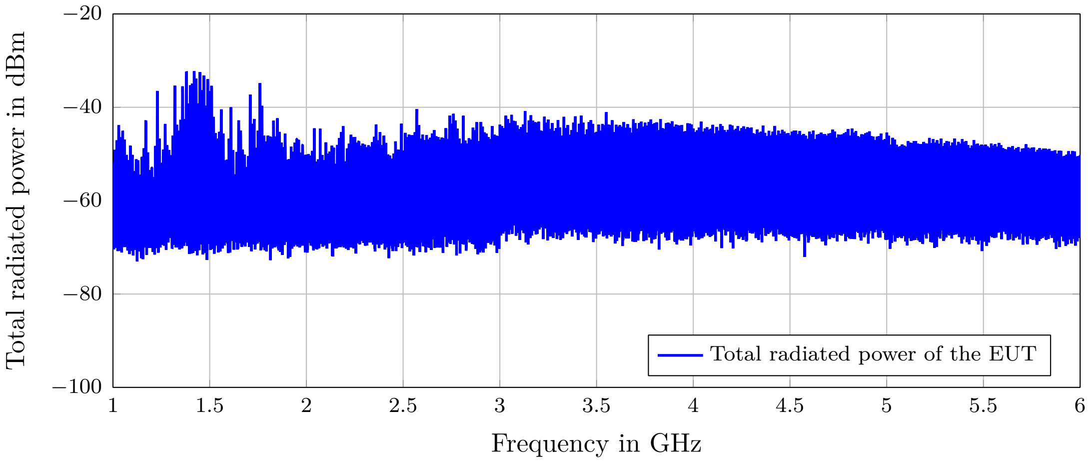

Figure 5.19: Total radiated power of the slotted enclosure excited inside by a monopole mounted on a comb generator

5.4.1.2 FAR Measurements

The FAR is a shielded structure with absorbing materials on the walls, ceiling and floors. In an ideal situation, only the direct radiation from the EUT could be measured by the

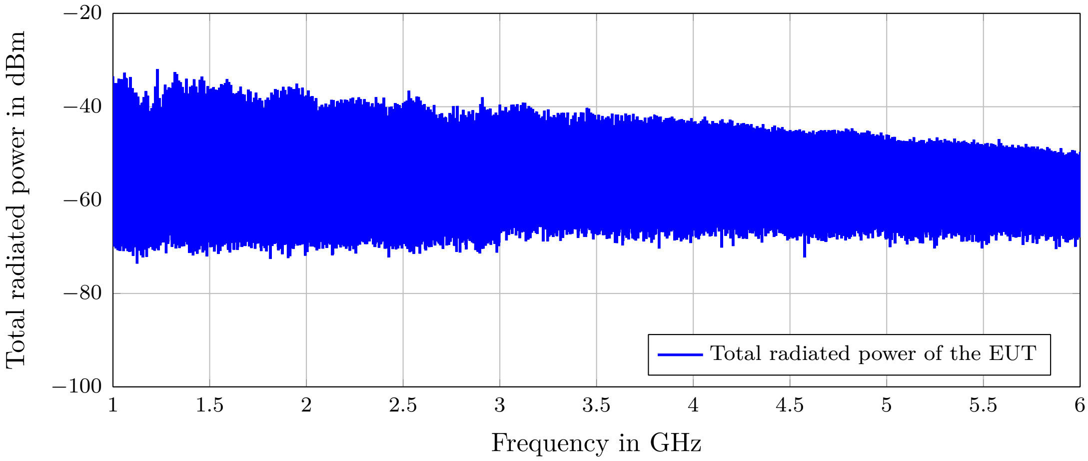

Figure 5.20: Total radiated power of the slotted enclosure with an attached wire (with 1 m length) fed by a comb generator

receiving antenna. In order to achieve the FAR conditions in the semi anechoic chamber, additional absorbers were placed on the ground. The measurement procedure is carried out according to the standard [DIN10]. The received antenna is placed at a height of 1 m with a 3 m measurement distance, taking both the horizontal and vertical polarizations into account. Three different orientations of the EUT are taken into consideration in order to measure the maximum E-field strength with a higher possibility. The measurements in the FAR were performed with an R&S ESU EMI Test Receiver using an RBW of 1 MHz and a preamplifier with a gain of 20 dB. Again, the measurements were performed for the slotted enclosure without and with an attached wire. As an example, Figure 5.21 shows the measurement setup for the FAR measurements of the EUT with an attached wire.

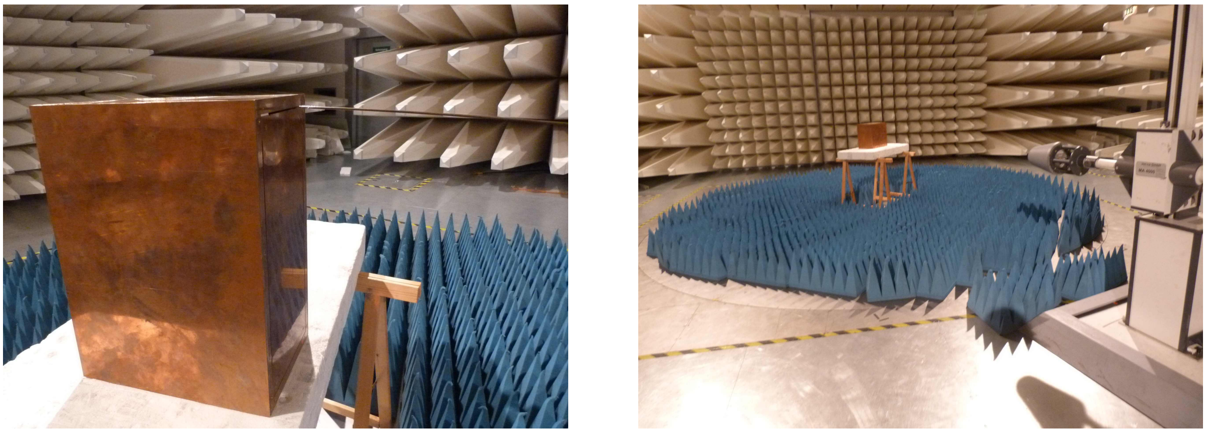
(a) Zoom view

(b) Over view

Figure 5.21: Measurement set-up of the radiated E-field strength of the slotted enclosure with an attached wire under FAR conditions.

The measured E-field strength in the FAR E_{FAR} for the slotted enclosure in Fig. 5.22 and the slotted enclosure with an attached wire in Fig. 5.23 was only considered in the frequency range from 1 GHz to 3 GHz, due to the fact that the emission level of the EUT is very low above 3 GHz and almost close to the noise level. Therefore, the measured E-field strength in the FAR above 3 GHz is not considered for further analysis.

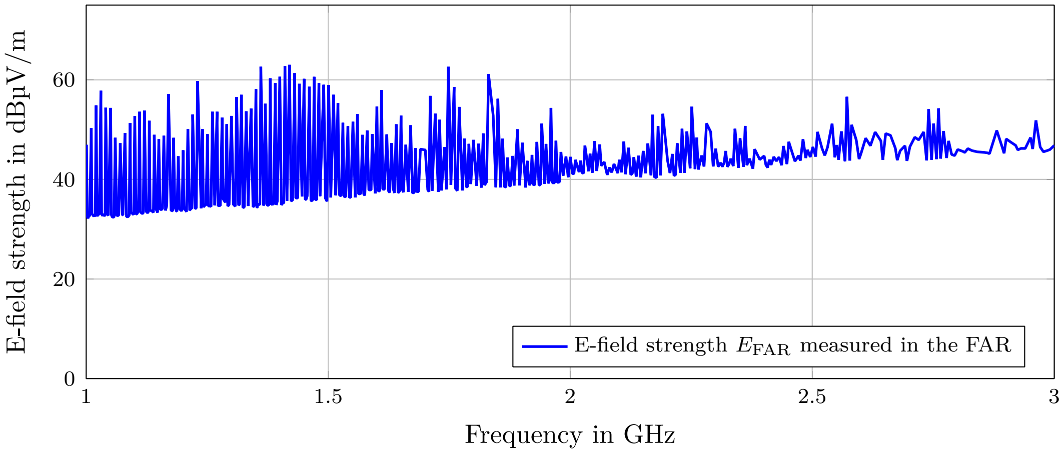

Figure 5.22: Measured E-field strength E_{FAR} in the FAR for the slotted enclosure

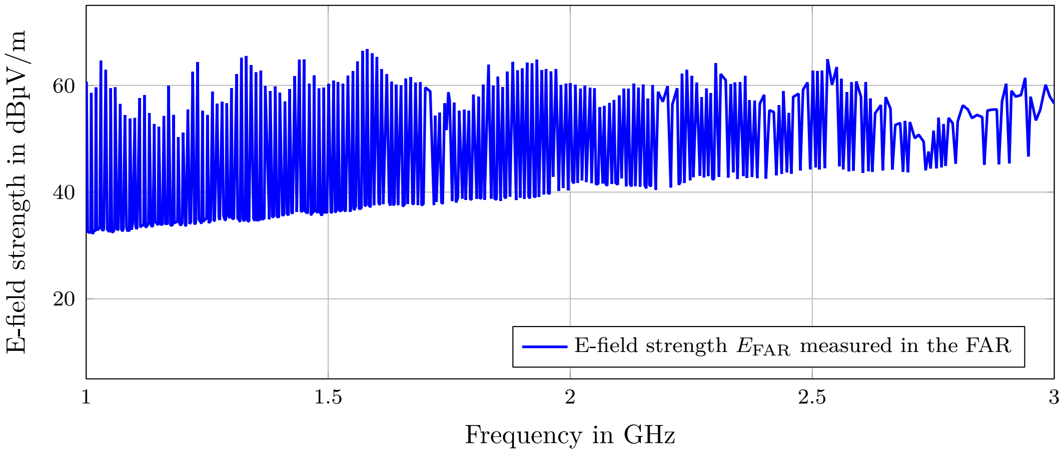

Figure 5.23: Measured E-field strength in the FAR for the slotted enclosure with an attached wire with 1 m length

5.4.2 Application of the different conversion methods

The measured results were used to assess the practical application of the procedures. As followed, the three methods are applied in details.

5.4.2.1 Measurement in the FAR

The measured electric field strength of the EUT without wires is shown in Fig. 5.24. The quantity L_{FAR} is in fact the CISPR 22 radiated emission limit for class B equipment – information technology equipment (ITE) measured in a FAR at 3 m separation [CIS05, DIN11], which is shown by the green line in Fig. 5.24. In the whole frequency range, the measured E-field strength in the FAR E_{FAR} is smaller than the existing CISPR 22 class

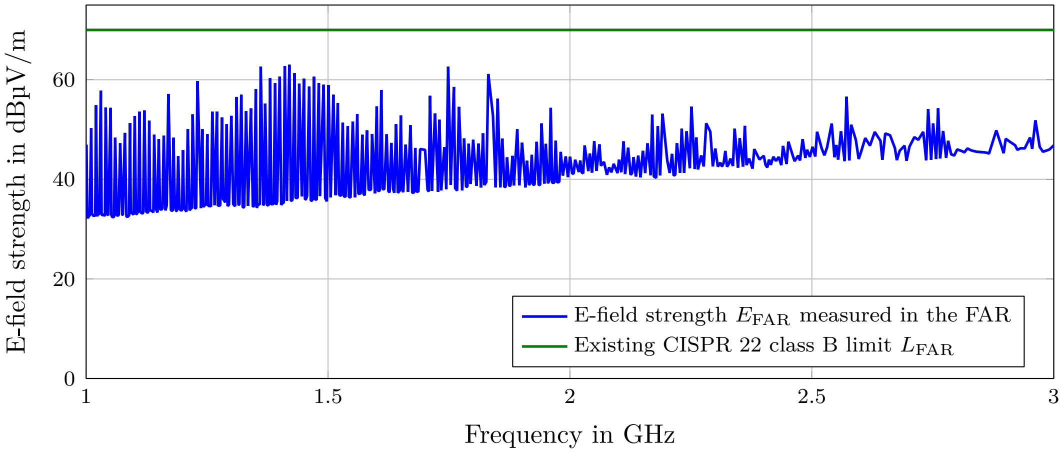

Figure 5.24: Measured E-field strength E_{FAR} in the FAR for the slotted enclosure

B limit L_{FAR}. A similar tendency could be observed for the EUT with an attached wire with 1 m length in Fig. 5.25.

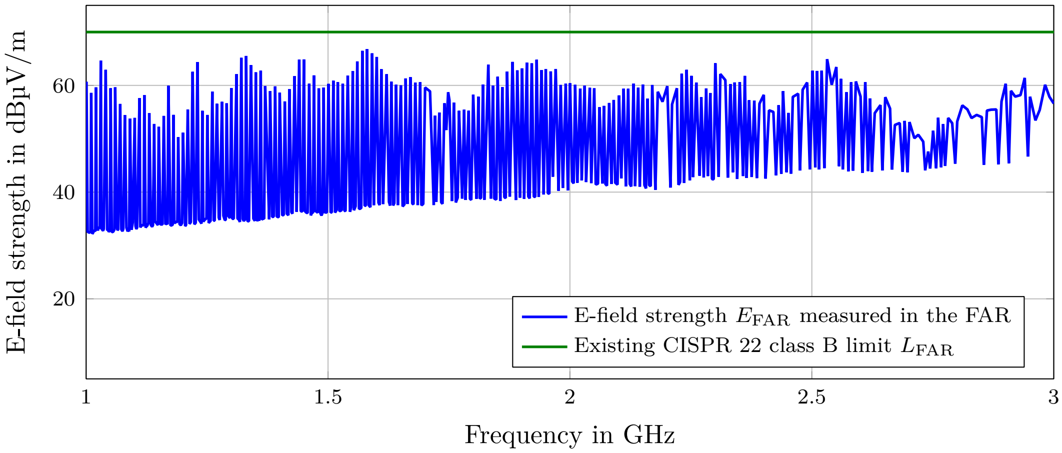

Figure 5.25: Measured E-field strength in the FAR for the slotted enclosure with an attached wire with 1 m length

5.4.2.2 Conversion of the measured radiated power to E-Field value

According to Eq. (5.4), the total radiated power measured in the MSC can be converted to an equivalent E-field strength E_{MSC}.

For the first model – the slotted enclosure with an attached wire with a length of 1 m, the result is shown in Fig. 5.27. The E-field strength E_{MSC} was obtained based on the total radiated power as shown in Fig. 5.20 and the conversion factor as shown in Fig. 5.26, which is the right side $10\log_{10}(^{D\eta}/_{4\pi r^2})$ in Eq. (5.4). The results in Fig. 5.27 shows that the converted E-field strength E_{MSC} is slightly smaller than the existing CISPR 22 class B limit L_{FAR}, except a few frequency points.

Figure 5.26: Conversion factor to convert the measured radiated power to the electric field strength for the slotted enclosure with an attached wire with a length of 1 m

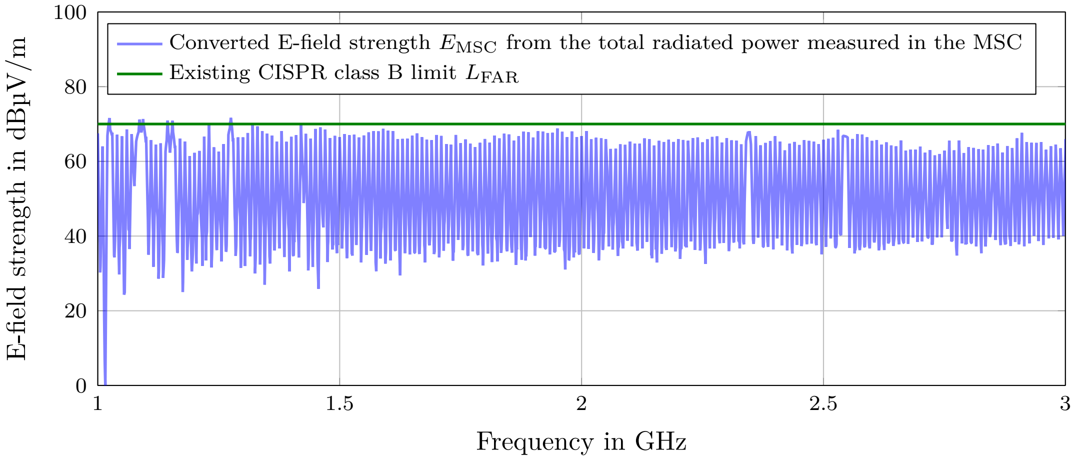

Figure 5.27: Comparison of the converted E-field strength in the MSC and the existing CISPR class B limit L_{FAR} for the slotted enclosure with an attached wire with 1 m length

A similar tendency can be observed for the second model – the slotted enclosure. According to Eq. (5.4), the total radiated power measured in the MSC as shown in Fig. 5.19 can be converted to an E-field strength E_{MSC} using the conversion factor shown in Fig. 5.28. The calculated values are shown in Fig. 5.29. It is clear that the converted E-field strength E_{MSC} in the MSC is lower than the existing CISPR 22 class B limit L_{FAR}, except a few frequency points.

5.4.2.3 Application of the proposed power limit

In Section 5.3, a proposal for a new power limit for emission measurements was shown in Fig. 5.15, which is the same curve denoted by the green curve in Fig. 5.30. This power limit is proposed, because it is more similar to the practical applications. The comparison shows that the radiated power of the box with an attached wire is slightly below the

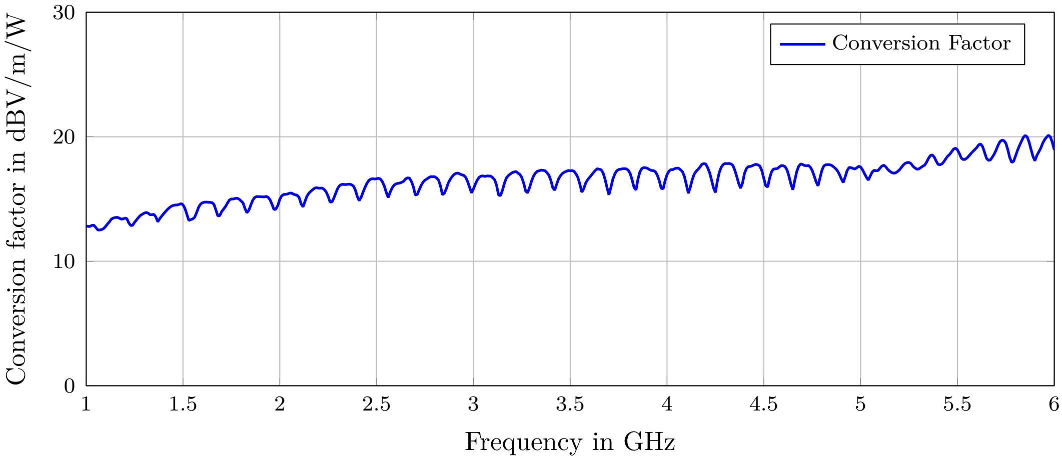

Figure 5.28: Conversion factor to convert the measured radiated power to the electric field strength for the slotted enclosure

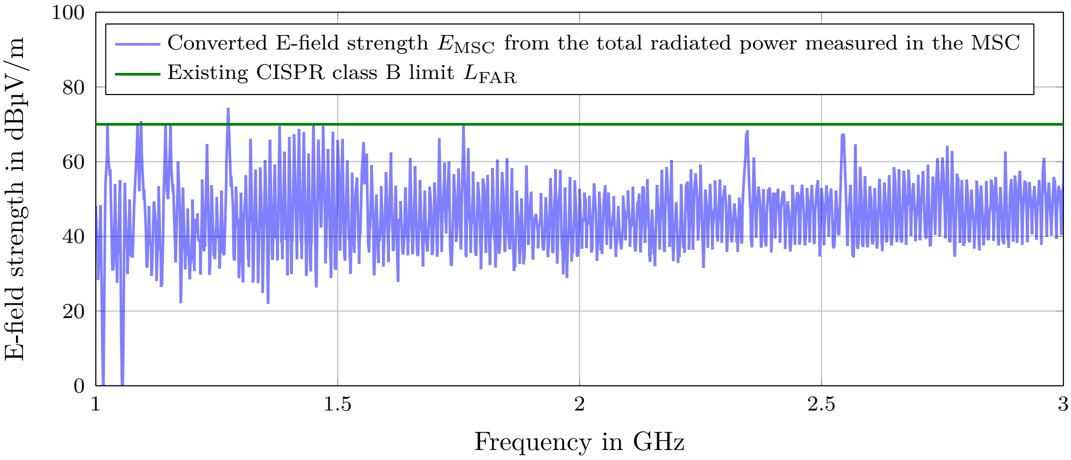

Figure 5.29: Comparison of the converted E-field strength E_{MSC} in the MSC and the existing CISPR class B limit L_{FAR} for the slotted enclosure

power limit, except a few frequency points around 1.2 GHz. A similar tendency for the slotted enclosure could be observed in Fig. 5.31. This method could be used for the further application, while the measured total radiated power can be directly compared with the new power limit.

5.5 Chapter conclusion

In this chapter, the subject of investigation is the radiated emission measurements performed in different EMC measurement facilities. Three methods are proposed. In Method 1, the conversion algorithm in CISPR 16-4-5 is applied for the stochastic model of the slotted enclosure with and without attached wires. The deviation of the FAR method and the MSC method are achieved. This method is straightforward, but not practical.

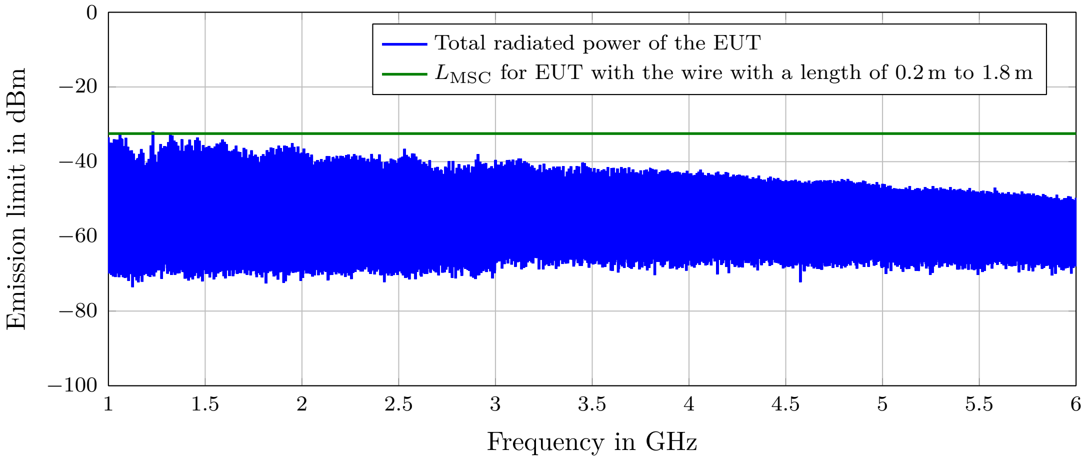

Figure 5.30: Comparison of the newly derived power limit L_{MSC} and the total radiated power of the enclosure with an attached wire with a wire length of 1 m

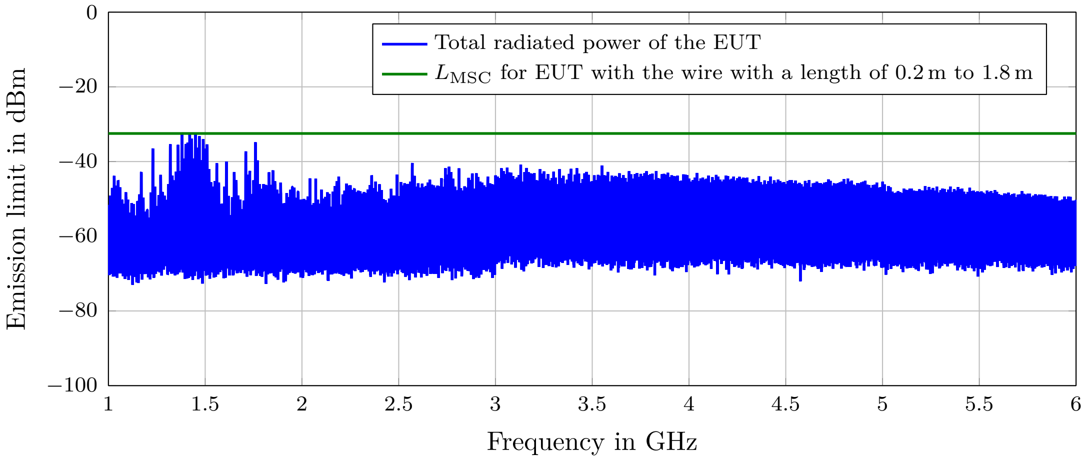

Figure 5.31: Comparison of the newly derived power limit L_{MSC} and the total radiated power of the enclosure

In comparison, Method 2 takes the directivity of the EUT and the total radiated power to obtain the equivalent E-field strength. The equivalent E-field strength could be compared with the existing E-field limit. The experimental investigation of the emission results has been carried out in the MSC measurements, as is shown in Fig. 5.27 and Fig. 5.29. However, the value of the directivity has to be determined by the numerical simulation procedure. Still, it is not practical. The disadvantage is that this procedure has to be carried out for every EUT.

Instead, one could apply the power limit as described in Method 3, which is based on the electrical size of the EUT. This approach seems very practicable, because the electrical size can be analytically determined. EUTs could be classified into different types, based on the electrical size. This makes the emission measurement procedures simpler. The proposed power limit could be compared with the measured total radiated power in the MSC. This procedure could be directly applied when performing MSC measurements.

6 Summary and Outlook

The focus of this work is to determine the radiated emission of an electrically large test object. EMC measurements are required to determine the radiated emissions. The established method – FAR can be used over 1 GHz. However, with increasing frequency, the measurement effort to determine the maximum emission is increasing as well. Alternative methods are required. The mode stirred chamber can be used to determine the total radiated power, which can not be directly compared to the established E-field limits. The conversion procedure introduced in CISPR 16-4-5 can be applied, but it is based on round robin tests and not generally usable. A direct conversion to electric field strength is only possible with the knowledge of the directivity of the EUT. Therefore, in this work, the directivity of the electrical large EUT above 1 GHz was examined and a power-based emission limit was suggested, which is the final result of this work.

Three observation methods for the determination of the radiated emission were analyzed, e. g. measurements with a planar scan (FAR method), a cylindrical scan (SAC and OATS method) and a spherical scan. Using the planar or cylindrical scan, the maximum emission level could be missed due to the complicated radiation pattern of ELEUT. Only by a spherical scan over the ELEUT the maximum emission level can be fully detected. However, this approach is very time-consuming, which is not practicable. In the MSC, the total radiated power of the EUT can be directly determined, but up to now the conversion to the equivalent electric field strength is necessary. The most important factor in the conversion procedure is the directivity of EUTs.

The directivity can be analytically determined by spherical wave theory, or standing wave antenna theory. Then the directivity for the cordless EUTs and EUTs with attached cables is investigated using these two theories. The SW theory could be applied to estimate the directivity for cordless EUTs but not applicable for EUTs with cables. Besides, the SWA theory could not be used to estimate the directivity of cordless EUTs and gives available results only in a limited range for EUTs with attached wires.

For a general approach to determine the directivity for different EUTs, numerical simulations were used in this work. The models (cordless EUTs and EUTs with attached cables) are generated by the numerical simulation technique and validated by the measurement results of real electronic devices. The influencing factors on the directivity were investigated. Compared to the directivity value in free space and above a ground plane, approximately 6 dB difference was predicted. Furthermore, $D_{\max}$ increases along with the total wire length, independently on the wire configurations.

The numerical simulation was used to obtain the directivity in terms of a statistical analysis. The statistical models were generated, by randomly changing the slots, the size of the EUT or the length of the wire. The simulated directivity agrees well with the theory in Chapter 2 and provides a good basis for further investigations.

Finally, three variants to determine the radiated emissions of ELEUT were analyzed. The methods were practically investigated based on measured values. In the first variant, the method described in CISPR 16-4-5 was applied. However, this procedure depends on round robin test, which has to be done for each EUT. Therefore, in the second variant, the radiated power was converted to an E-field strength using the previously determined statistical directivity. A conversion factor was determined which allows the direct conversion of the measured radiated power in an MSC to an electric field strength. By this, after applying the conversion factor the measured result can be compared to the E-field limit. However, the conversion method has to be carried out for every EUT. Finally, in the third variant a power limit was calculated based on the statistically determined directivity and the existing E-field limit. Because the measured power can be directly compared with the new power limit, this method is relative simple and could save measurement time.

As one final result, a power limit for a class of test objects (the EUT with a wire length from 0.2 m to 1.8 m) was proposed based on the simulations, as it is shown in Fig. 5.15. This power limit is a first step to expand the emission standards towards the definition of power limits in EMC standards. This makes it possible to apply the MSC for frequencies above 1 GHz as a referenced test method.

Besides the topics presented in this thesis, still much work has to be carried out. In the future work, the emission limit for other size of EUTs can be achieved. It is also interesting to enlarge the database through other variations to obtain a larger sample.

It is also helpful to categorize EUTs with similar characteristics into several EUT types, which could be considered independently. In general, three types of EUTs could be classified, based on the electrical size:

1. small devices, e. g., hand-held, portable, cell-phone size, etc;
2. medium devices, e. g., notebook/laptop size, tabletop devices, computer cases, coffee maker, hair dryer, possibly with attached cables;
3. large devices, e. g., floor-standing devices, refrigerator size, control cabinet, 19" racks, always with attached cables.

Then the measured total radiated power in the MSC can be compared with a newly derived power limit. This finding is very essential. The measurement procedures can be greatly simplified by using the MSC.

Bibliography

[Bal97] Balanis, Constantine A.: *Antenna Theory – Analysis and Design*. 2. New York : John Wiley & Sons, 1997. – ISBN 0–471–59268–4

[BG08] Battermann, Sven. ; Garbe, Heyno.: Subjects of discussion in radiated emission measurements above 1 GHz. In: *Advances in Radio Science* 6 (2008), Mai, S. 299–301

[Bom13] Bombadil Tom: *Latex code for generating polarized electromagnetic wave*. `https://tex.stackexchange.com/questions/113900/draw-polarized-light`. Version: Mai 2013

[Buc12] Buchholz, Sophie: Einflussfaktoren bei der Messung und Modellierung der Direktivität statistischer Strahler / Technische Universität Dresden. Dresden, September 2012. – Diplomarbeit

[CIS02] CISPR/A (Hrsg.): *IEC 61000-4-21 Ed.1, Electromagnetic Compatibility (EMC) - Part 4-21: Testing and measurement techniques - Reverberation Chamber Test Methods*. IEC/CISPR 22:2002. Genf, Schweiz: CISPR/A, 2002

[CIS05] CISPR (Hrsg.): *Information technology equipment - Radio disturbance characteristics - Limits and methods of measurement*. IEC/CISPR 22:2005. Genf, Schweiz: CISPR, Juli 2005

[CIS06a] CISPR (Hrsg.): *Specification for radio disturbance and immunity measuring apparatus and methods – Part 2-3: Methods of measurement of disturbances and immunity – Radiated disturbance measurements*. IEC/CISPR 16-2-3:2006. Genf, Schweiz: CISPR, 2006

[CIS06b] CISPR (Hrsg.): *Specification for radio disturbance and immunity measuring apparatus and methods – Part 4-5: Uncertainties, statistics and limit modelling – Conditions for the use of alternative test methods*. IEC/CISPR 16-4-5:2006. Genf, Schweiz: CISPR, 2006

[CIS06c] CISPR/A (Hrsg.): *IEC 61000-4-22 Ed.1, Radiated emissions and immunity measurements in fully anechoic rooms (FARs)*. IEC/CISPR 22:2006. Genf, Schweiz: CISPR/A, 2006

[CIS10] CISPR (Hrsg.): *Specification for radio disturbance and immunity measuring apparatus and methods – Part 2-3: Methods of measurement of disturbances and immunity – Radiated disturbance measurements*. IEC/CISPR 16-2-3:2010. Genf, Schweiz: CISPR, 2010. – 431 S.

[CIS15] CISPR (Hrsg.): *Industrial, scientific and medical equipment - Radio-frequency disturbance characteristics - Limits and methods of measurement*. IEC/CISPR 11:2015. Genf, Schweiz: CISPR, Juni 2015

[Col85] Collin, Robert E.: *Antennas and Radiowave Propagation*. McGraw-Hill College, 1985. – 508 S. – ISBN 0–07–Y66156–1

[Com09] Computer Simulation Technology ; CST AG (Hrsg.): *Microwave Studio, User Manual*. Darmstadt, Germany: CST AG, 2009. `http://www.cst.com`

[Dij07] Dijk, Nico van: *New Concepts for EMC Standards Applicable to Multimedia Products*. Eindhoven, TU Eindhoven, Dissertation, 2007

[DIN10] DIN Deutsches Institut für Normung e.V. und VDE Verband der Elektrotechnik Elektronik Informationstechnik e.V. (Hrsg.): *Industrielle, wissenschaftliche und medizinische Gerät – Funkstörungen – Grenzwerte und Messverfahren*. IEC/CISPR 11:2009, modifiziert +A1:2010. Berlin, Frankfurt: DIN Deutsches Institut für Normung e.V. und VDE Verband der Elektrotechnik Elektronik Informationstechnik e.V., Mai 2010. – auch VDE 0875-11:2010-05

[DIN11] DIN Deutsches Institut für Normung e.V. und VDE Verband der Elektrotechnik Elektronik Informationstechnik e.V. (Hrsg.): *DIN EN 55022, Einrichtungen der Informationstechnik – Funkstöreigenschaften – Grenzwerte und Messverfahren (CISPR 22:2008, modifiziert); Deutsche Fassung EN 55022:2010*. Berlin, Frankfurt: DIN Deutsches Institut für Normung e.V. und VDE Verband der Elektrotechnik Elektronik Informationstechnik e.V., November 2011. – auch VDE 0878-22:20011-11

[GB08] Garbe, Heyno ; Battermann, Sven: Converting total-radiated-power measurements to equivalent E-Field Data. In: *2008 IEEE International Symposium on Electromagnetic Compatibility*, 2008. – ISSN 2158–110X, S. 1–6

[GV09] Gonschorek, Karl-Heinz ; Vick, Ralf: Electromagnetic Compatibility for Device Design and System Integration, Springer-Verlag Berlin Heidelberg, 2009. – ISBN 978–3–642–03289–9, S. 470

[Han88] Hansen, Jesper E. (Hrsg.): *Spherical Near-field Antenna Measurements*. Institution of Engineering and Technology, 1988 (Electromagnetic Waves). – 404 S. `http:`

`//dx.doi.org/10.1049/PBEW026E`. `http://dx.doi.org/10.1049/PBEW026E`. – ISBN 9780863411106

[Har00] HARRINGTON, Timothy: Total-radiated-power-based OATS-equivalent emissions testing in reverberation chambers and GTEM cells. In: *Electromagnetic Compatibility, 2000. IEEE International Symposium on* Bd. 1, 2000, S. 23–28 vol.1

[Hil98] HILL, David A.: Electromagnetic Theory of Reverberation Chambers / National Institute of Standards and Technology. Boulder, CO, USA, 1998 (1506). – Technical Note

[Int10] INTERNATIONAL ELECTROTECHNICAL COMMISSION (Hrsg.): *IEC 61000-4-20, Testing and measurement techniques – Emission and immunity testing in transverse electromagnetic (TEM) waveguides.* 2. Genf, Schweiz: International Electrotechnical Commission, August 2010

[Int11] INTERNATIONAL ELECTROTECHNICAL COMMISSION (Hrsg.): *IEC 61000-4-21, Testing and measurement techniques – Reverberation chamber test methods.* 2. Genf, Schweiz: International Electrotechnical Commission, Januar 2011

[Kap03] KAPPEL, Udo: *Vergleichbarkeit von Verfahren zur Messung der Störfeldstärke.* Dortmund, University of Dortmund, Dissertation, August 2003. – 266 S

[Kar14] KARK, Klaus W.: *Antennen und Strahlungsfelder – Elektromagnetische Wellen auf Leitungen, im Freiraum und ihre Abstrahlung.* 5. Wiesbaden : Springer Fachmedien Wiesbaden, 2014. – 508 S. `#http://dx.doi.org/10.1007/978-3-658-03616-4#`. – ISBN 9783658036164

[KH99] KAPPEL, Udo ; HIRSCH, Holger: Statistical conversion factor between measurements of EMI in different test facilities. In: *Symposium on Electromagnetic Compatibility* Bd. 1, 1999, S. 139 – 144

[KHL00] KOEPKE, Galen ; HILL, David A. ; LADBURY, John: Directivity of the test device in EMC measurements. In: *International Symposium on Electromagnetic Compatibility* Bd. 2, 2000, S. 535–539

[Kod01] KODALI, Prasad: *Engineering electromagnetic compatibility: Principles, measurements, technologies, and computer models.* 2nd ed. New York : Institute of Electrical and Electronics Engineers, 2001. – ISBN 978–0780347434

[Kra07a] KRAUTHÄUSER, Hans-Georg: *Grundlagen und Anwendungen von Modenverwirbelungskammern.* Magdeburg, University of Magdeburg, habilitation, 2007. – 289 S

[Kra07b] Krauthäuser, Hans-Georg: On the Measurement of Total Radiated Power in Uncalibrated Reverberation Chambers. In: *IEEE Transactions on Electromagnetic Compatibility* 49 (2007), May, Nr. 2, S. 270–279. `http://dx.doi.org/10.1109/TEMC.2007.897122`. – DOI 10.1109/TEMC.2007.897122. – ISSN 0018–9375

[Kra11] Krauthäuser, Hans-Georg: Statistical Analysis of the Correlation of Emission Limits for Established and Alternative Test Sites. In: *IEEE Transactions on Electromagnetic Compatibility* 53 (2011), November, Nr. 4, S. 863 –875. `http://dx.doi.org/10.1109/TEMC.2010.2102764`. – DOI 10.1109/TEMC.2010.2102764. – ISSN 0018–9375

[Mag12] Magdowski, Mathias: *Vergleich der Einkopplung deterministischer und statistischer elektromagnetischer Felder in Leitungen*. Magdeburg, University of Magdeburg, dissertation, 2012. – 154 S

[Mag17] Magdowski, Mathias: Some Comments on the Necessity of the Reference Quantity in CISPR TR 16- 4-5, 2017

[Mar01] Mardiguian, Michel: *Controlling radiated emissions by design*. 2. Boston, Mass. : Kluwer Academic Publ., 2001. – 338 S. – ISBN 9780792379782

[MBG14] Menssen, Benjamin ; Burghardt, Felix ; Garbe, Heyno: Simulation objects to be used as unintentional radiators. In: *Electromagnetic Compatibility, Tokyo (EMC'14/Tokyo), 2014 International Symposium on*, 2014, S. 37–40

[MC05] Marvin, Andy ; Cui, Yong: ON DETERMINING THE MAXIMUM EMISSIONS OF ENCLOSURES AT FREQUENCIES ABOVE 1 GHZ, 2005

[Men15] Menke,Henri: *Latex code for generating electromagnetic wave propagation*. `https://tex.stackexchange.com/questions/229674/electromagnetic-wave-propagation-with-tikz`. Version: Februar 2015

[Pau94] Paul, Clayton R.: *Analysis of Multiconductor Transmission Lines*. New York, USA : John Wiley & Sons, 1994 (Wiley series in microwave and optical engineering). – ISBN 0–471–02080–X

[Pau06] Paul, Clayton R. ; Chang, Kai (Hrsg.): *Introduction to Electromagnetic Compatibility*. 2. Hoboken, New Jersey, USA : John Wiley & Sons, 2006 (Wiley Series in Microwave and Optical Engineering). – ISBN 978–0–471–75500–5

[Smi97] Smith, Glenn S. (Hrsg.): *An Introduction to Classical Electromagnetic Radiation*. Cambridge : Cambridge University Press, 1997. – ISBN 0521586984

[Stu81] Stutzman, Warren L. ; Thiele, Gary A. (Hrsg.): *Antenna theory and design.* New York, NY : Wiley, 1981. – 598 S.

[Tes11] Teseq (Hrsg.): *Reference Spectrum Generator 3000, Data Sheet.* Berlin, Germany: Teseq, 2011. `http://www.teseq.com/products/RSG-3000.php`

[Tes14] Teseq (Hrsg.): *Reference Spectrum Generator 2000, Data Sheet.* Berlin, Germany: Teseq, 2014. `http://www.teseq.com/products/RSG-2000.php`

[WFS01] Wang, Jianqing ; Fujiwara, Osamu ; Sasabe, Kohji: A simple method for predicting common-mode radiation from a cable attached to a conducting enclosure. In: *Microwave Conference, Asia-Pacific* Bd. 3, 2001, S. 1119–1122

[WHH02] Wilson, Perry F. ; Hill, David A. ; Holloway, Christopher: On Determining the Maximum Emissions From Electrically Large Sources. In: *IEEE Transactions on Electromagnetic Compatibility* 44 (2002), Februar, Nr. 1, S. 79 – 86

[WHK04] Wilson, Perry F. ; Holloway, Christopher L. ; Koepke, Galen H.: A Review of Dipole Models for Correlating Emission Measurements Made at Various EMC Test Facilities. In: IEEE (Hrsg.): *International Symposium on Electromagnetic Compatibility* Bd. 3. Santa Clara, CA, USA, August 2004, S. 898 – 901

[WHV16] Wang, Xiaowei ; Hirte, Matthias ; Vick, Ralf: Statistische Ermittlung der Direktivität eines elektrisch großen Prüflings mittels analytischer und numerischer Verfahren. In: *EMV. - Berlin : VDE Verl., 2016 ; Kongress: Kongress für Elektromagnetische Verträglichkeit.* Düsseldorf, Februar 2016

[Wik] Wikipedia, the free encyclopedia: *Abstract.* `https://en.wikipedia.org/wiki/Polarization_(waves)`

[Wil04] Wilson, Perry F.: Emission and immunity testing: test object electrical size and its implication. In: *Electromagnetic Compatibility, International Symposium on* Bd. 2, 2004, S. 349–352

[Wil10] Wilson, Perry F.: Radiation patterns of unintentional antennas: Estimates, simulations, and measurements. In: *2010 Asia-Pacific International Symposium on Electromagnetic Compatibility*, 2010. – ISSN 2162–7673, S. 985–989

[WV14] Wang, Xiaowei ; Vick, Ralf: Directivity Statistics of a Rectangular Enclosure With Slots. In: *U. R.S.I. Landesausschuss in der Bundesrepublik Deutschland e.V. Kleinheubacher Tagung, Miltenberg, Deutschland, 29. 09 - 01. 10. 2014*, 2014

[WV15a] Wang, Xiaowei ; Vick, Ralf: Determination of radiated emissions of an electrically large EUT: Simulation and experiment. In: *Proceedings of IEEE International Symposium on Electromagnetic Compatibility and EMC Europe. - Piscataway, NJ : IEEE*, 2015, S. 295–299

[WV15b] Wang, Xiaowei ; Vick, Ralf: Directivity and effective radius of an electrically large EUT with attached wires. In: *2015 IEEE International Symposium on Electromagnetic Compatibility (EMC)*, 2015. – ISSN 2158–110X, S. 1467–1472

[WV16] Wang, Xiaowei ; Vick, Ralf: Influencing factors on the directivity estimates of an electrically large EUT. In: *Proceedings of IEEE International Symposium on Electromagnetic Compatibility and EMC Europe 2016. - Piscataway, NJ: IEEE*, 2016, S. 859–864

[ZHG10] Zamow, Dirk ; Hamann, David ; Garbe, Heyno: Susceptibility of Electrical Systems to UWB Disturbances Due to the Layout of Exit Cables. In: *AMEREM 2010: 14th International Symposium on Antenna Technology and Applied Electromagnetics (ANTEM) and the American Electromagnetics Conference*, 2010. – ISSN 978–1–4614–9500–0

[ZHGG11] Zamow, Dirk ; Hamann, David ; Genender, Evgeni ; Garbe, Heyno: On estimating the directivity of electrically large cable dominated desktop systems. In: *EMC Europe 2011 York*, 2011, S. 482–487

A Statistical directivity of the EUT with rectangular slots

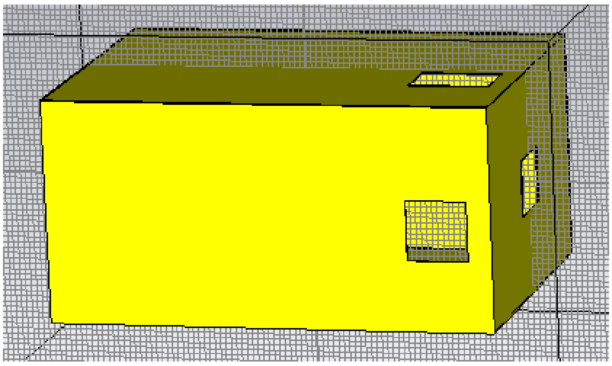

Figure A.1: Rectangular enclosure with stochastic rectangular slots stochastically distributed on the surface.

Table A.1: Statistical variation of the rectangular slots on the surface of the enclosure

Parameter	**Statistical variation range**	**Comment**
Number of slots	random number between 1 to 6	always on different planes
Length of slots	40 mm to 50 mm	
Width of slots	40 mm to 50 mm	
Position of slots		stochastic, but at least 40 mm to the boundary

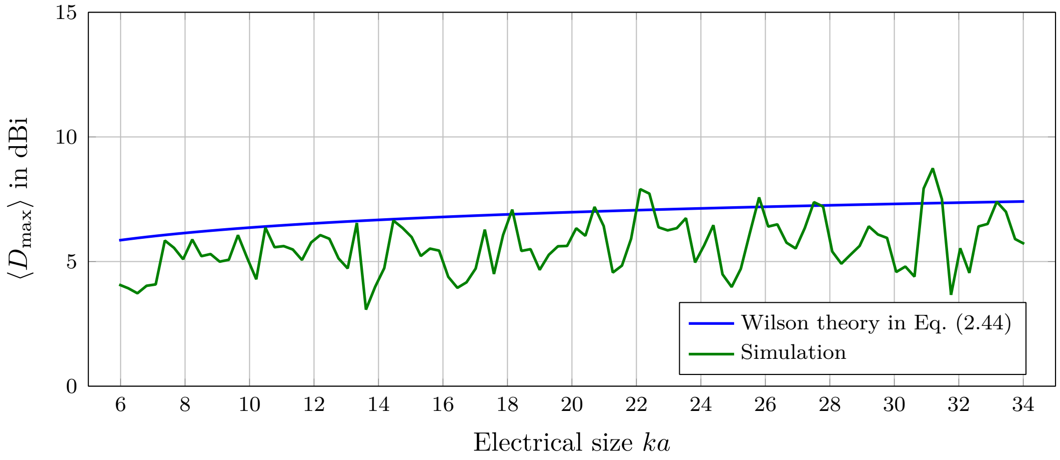

Figure A.2: Expectation value of $D_{\max}$ for the enclosure with rectangular stochastic slots.

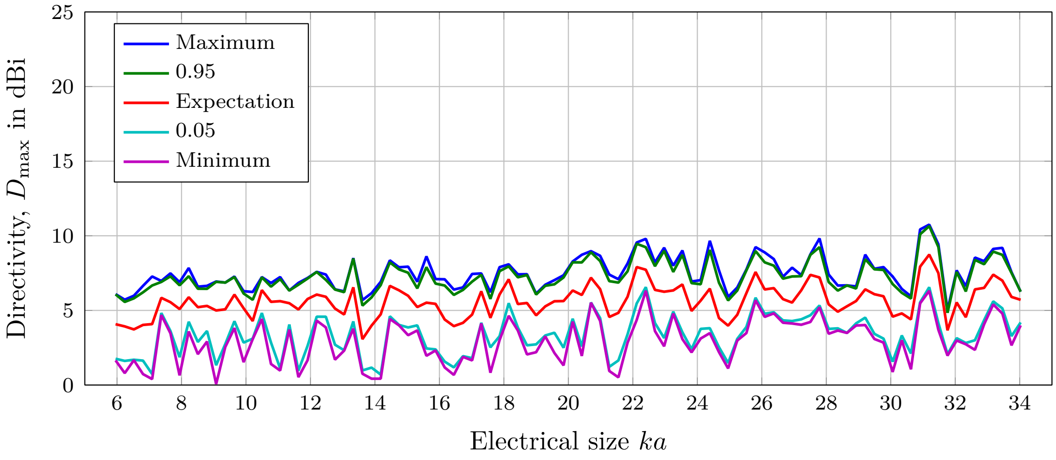

Figure A.3: Statistical distribution of the directivity for the enclosure with stochastic rectangular slots.

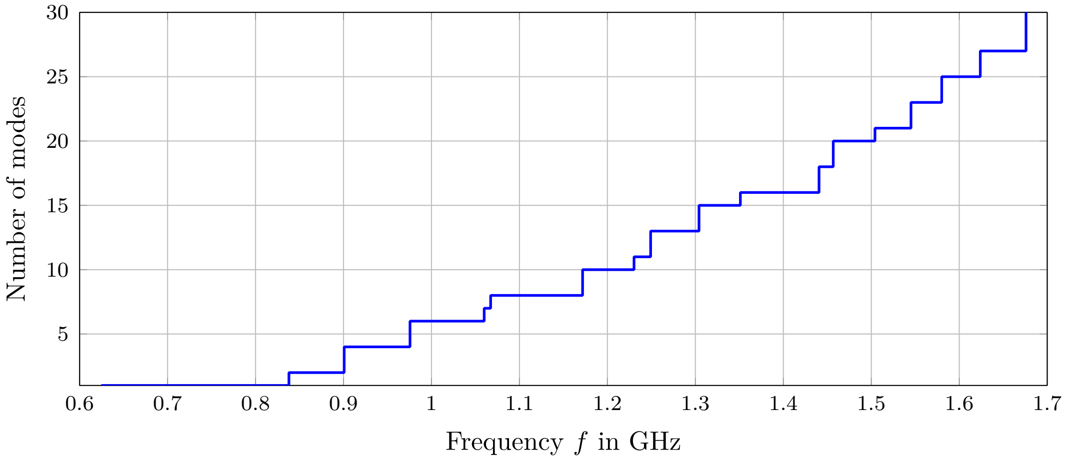

Figure A.4: The resonance modes of the enclosure in the frequency range from 0.6 GHz to 1.8 GHz.

B Current distribution and effective radius of the three wire layouts with a length of $3\,\mathrm{m}$ attached to the slotted enclosure

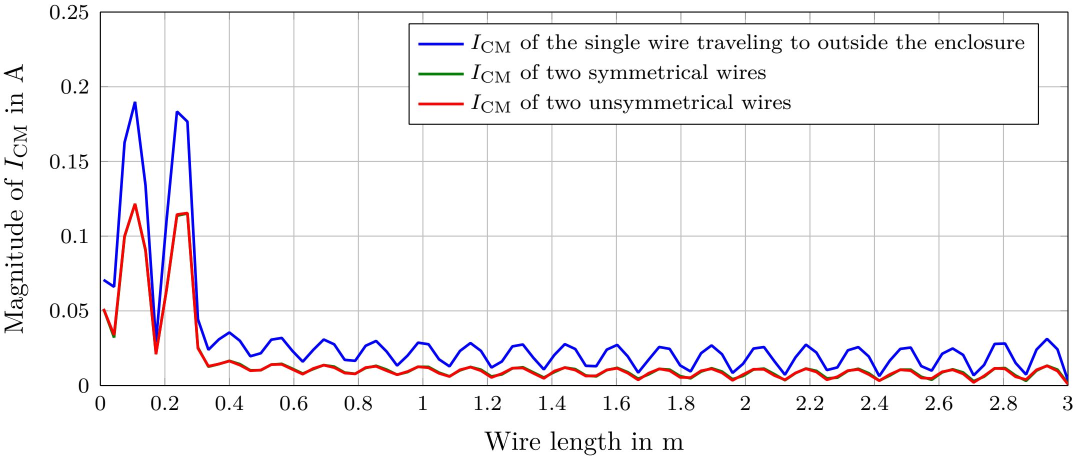

Figure B.1: Common-mode current I_{CM} as a function of the wire length up to $3\,\mathrm{m}$ for different wire layouts at $3\,\mathrm{GHz}$

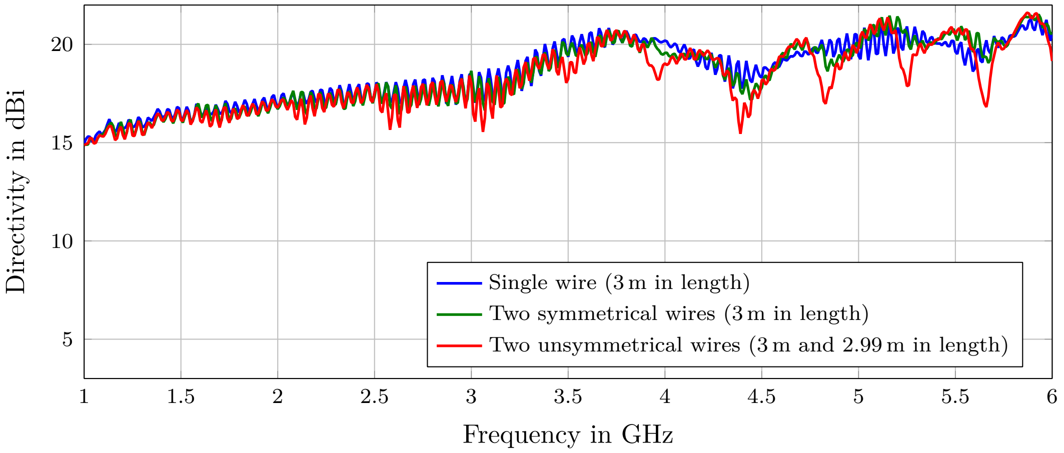

Figure B.2: Simulated directivity against the frequency for 3 different wire configurations attached to the enclosure, located 80 cm above ground.

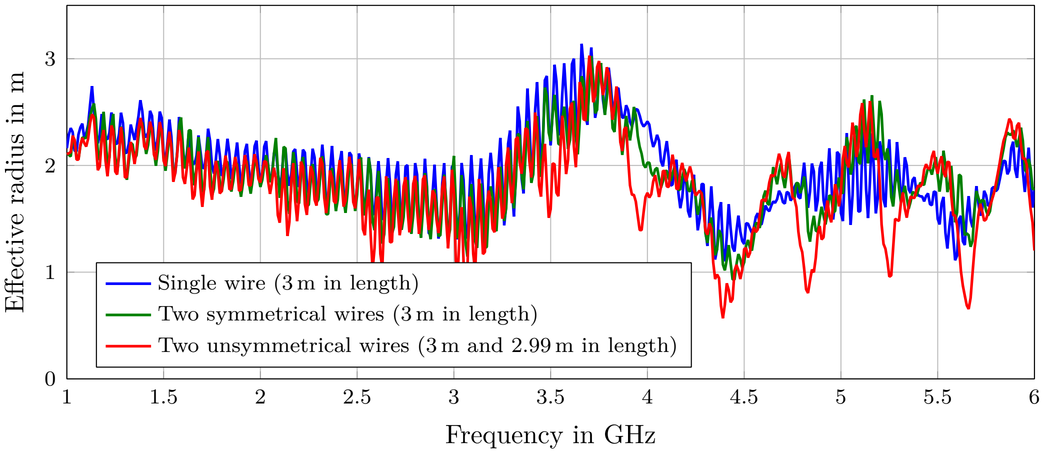

Figure B.3: Effective radius against the frequency for 3 different wire layouts according to the TWA theory

C Derivation of the directivity for standing wave antennas and traveling wave antennas

C.1 Derivation of the analytical expression for traveling wave antennas and standing wave antennas

Here, the analytical expression for SWAs and TWAs will be derived in details. The total radiation pattern $C_{\text{total}}(\theta, \varphi)$ of an antenna can be determined as the product of the element factor $C_E(\theta, \varphi)$ and the array factor $C_{\text{Gr}}(\theta, \varphi)$, which can be written as: $C_{\text{total}}(\theta, \varphi) = C_E(\theta, \varphi) \cdot C_{\text{Gr}}(\theta, \varphi)$ [Stu81]. Here, θ is the elevation angle, φ is the azimuth angle, $C_E(\theta, \varphi)$ is the pattern of an infinitesimal current element and $C_{\text{Gr}}(\theta, \varphi)$ is the result of the integral over currents, which can be considered as consisting of many current elements. The electric field strength of a SWA with the length of l_{SWA} and peak current of I_{m} can be written as

$$E_{\theta,\text{SWA}} = \mathrm{j}\omega\mu \frac{\mathrm{e}^{-\mathrm{j}kr}}{4\pi r} I_{\text{m}} l_{\text{SWA}} \left[\frac{\cos\left(\dfrac{kl_{\text{SWA}}}{2}\cos\theta\right) - \cos\left(\dfrac{kl_{\text{SWA}}}{2}\right)}{\sin\theta} \right] \tag{C.1}$$

For a TWA with the length l, the electric field strength can be written as:

$$E_{\theta,\text{TWA}} = \mathrm{j}\omega\mu \frac{\mathrm{e}^{-\mathrm{j}\beta r}}{4\pi r} I_{\text{m}} l \sin\theta \frac{\sin\left[\dfrac{\beta l}{2}(1-\cos\theta)\right]}{\dfrac{\beta l}{2}(1-\cos\theta)} \tag{C.2}$$

In this formula, the factor $\sin\theta$ shows the directivity of the element factor and the factor $\sin\left[\frac{\beta l}{2}(1-\cos\theta)\right] / \frac{\beta l}{2}(1-\cos\theta)$ is the directivity of the antenna array.

Taking the TWA as an example, the radiated power of an antenna can be obtained by the integral of the electric field over the solid angle:

$$P_r ad = \frac{1}{2\eta} \iint |E_{\theta,\text{TWA}}|^2 r^2 \sin\theta \, \mathrm{d}\theta \, \mathrm{d}\phi \tag{C.3}$$

$$
\begin{aligned}
P_rad &= \frac{1}{2\eta}\left(\frac{\omega\mu}{4\pi}I_{\mathrm{m}}l\right)^2\int_0^{2\pi}\mathrm{d}\phi\int_0^{\pi}\sin^3\theta\left[\frac{\sin\left(\frac{\beta l}{2}\left(1-\cos\theta\right)\right)}{\frac{\beta l}{2}(1-\cos\theta)}\right]^2\mathrm{d}\theta \\
&= \frac{\omega^2\mu^2 2\pi}{2\eta 16\pi^2}I_{\mathrm{m}}^2 l^2\alpha \\
&= \frac{1}{16\pi}\frac{\omega^2\mu^2}{\eta}I_{\mathrm{m}}^2 l^2\alpha
\end{aligned}
\tag{C.4}
$$

Assuming $\alpha = \int_0^{\pi}\sin^3\theta\left[\frac{\sin\left(\frac{\beta l}{2}(1-\cos\theta)\right)}{\frac{\beta l}{2}(1-\cos\theta)}\right]^2\mathrm{d}\theta$ in (C.4). Now let $\tau = \frac{\beta l}{2}(1-\cos\theta)$, then $\mathrm{d}\tau = \frac{\beta l}{2}(\sin\theta)\,\mathrm{d}\theta$, and $\cos\theta = 1-\frac{2\tau}{\beta l}$, $\sin^2\theta = 1-\cos^2\theta = 1-\left(1-\frac{2\tau}{2l}\right)^2 = \frac{4}{\beta l}\eta-\frac{4}{(\beta l)^2}\tau^2$. Then the expression of α can be written as:

$$
\begin{aligned}
\alpha &= \int_0^{\beta l}\left[\frac{4}{\beta l}\tau-\frac{4}{(\beta l)^2}\tau\right]\frac{\sin^2\tau}{\tau^2}\frac{d\tau}{\frac{\beta l}{2}} \\
&= \frac{8}{(\beta l)^2}\left(\int_0^{\beta l}\frac{\sin^2\tau}{\tau}\,\mathrm{d}\tau-\int_0^{\beta l}\sin^2\tau\,\mathrm{d}\tau\frac{1}{\beta l}\right) \\
&= \frac{4}{(\beta l)^2}\int_0^{2\beta l}\frac{1-\cos t}{t}\,\mathrm{d}t-\int_0^{\beta l}(1-\cos 2\tau)\,\mathrm{d}\tau\frac{1}{\beta l} \\
&= \frac{4}{(\beta l)^2}\mathrm{Cin}(2\beta l)-\frac{1}{\beta l}\left(\beta l-\frac{\sin 2\beta l}{2}\right) \\
&= \frac{4}{(\beta l)^2}\left[0.5772+\ln(2\beta l)-\mathrm{Ci}(2\beta l)-1+\frac{\sin(2\beta l)}{2\beta l}\right]
\end{aligned}
\tag{C.5}
$$

where Ci is the cosine integral function, which is the antiderivative of ${}^{\cos x}/_{x}$. The function Ci is an even entire function, with the relation: $\mathrm{Cin}(x) = \gamma+\ln x-\mathrm{Ci}(x)$. Because $\ln(2\beta l) = \ln\left(4\pi\frac{l}{\lambda}\right) = \ln(4\pi)+\ln\left(\frac{l}{\lambda}\right) = 2.531+\ln\left(\frac{l}{\lambda}\right)$, the total radiated power can be reformulated as:

$$
P_rad = \frac{1}{16\pi}I_{\mathrm{m}}^2 l^2\frac{\omega^2\mu^2}{\eta}\frac{4}{\omega\mu\varepsilon l^2}\left[(0.5772-1+2.531)+\ln\left(\frac{l}{\lambda}\right)-\mathrm{Ci}(2\beta l)+\frac{\sin(2\beta l)}{2\beta l}\right]
\tag{C.6}
$$

$$
= I_{\mathrm{m}}^2\frac{{}^{\mu}/_{\varepsilon}}{\sqrt{{}^{\mu}/_{\varepsilon}}}\frac{1}{4\pi}\left[(0.5772-1+2.531)+\ln\left(\frac{l}{\lambda}\right)-\mathrm{Ci}(\beta l)+\frac{\sin(2\beta l)}{2\beta l}\right]
\tag{C.7}
$$

$$= I_{\mathrm{m}}^2 \sqrt{\mu/\varepsilon} \frac{1}{4\pi} \left[(0.5772 - 1 + 2.531) + \ln \left(\frac{l}{\lambda} \right) - \mathrm{Ci}(2\beta l) + \frac{\sin(2\beta l)}{2\beta l} \right] \tag{C.8}$$

$$= \frac{120\pi}{4\pi} I_{\mathrm{m}}^2 \left[(0.5772 - 1 + 2.531) + \ln \left(\frac{l}{\lambda} \right) - \mathrm{Ci}(2\beta l) + \frac{\sin(2\beta l)}{2\beta l} \right] \tag{C.9}$$

$$= 30 I_{\mathrm{m}}^2 \left[2.108 + \ln \left(\frac{l}{\lambda} \right) - \mathrm{Ci}(2\beta l) + \frac{\sin(2\beta l)}{2\beta l} \right] \tag{C.10}$$

Using the definition of the directivity (the ratio of the maximum over the average radiated power flux density):

$$\begin{aligned} D &= \frac{U_{\max}}{P_r ad/4\pi} \\ &= \frac{4\pi}{P_r ad} \frac{1}{2\eta} |E_\theta|^2 r^2 \\ &= \frac{4\pi}{P_r ad} \frac{1}{2\eta} \frac{\omega^2 \mu^2}{16\pi^2} I_{\mathrm{m}}^2 l^2 \sin^2 \theta_{\mathrm{m}} \frac{\sin^2 \left[\frac{\beta l}{2} (1 - \cos \theta_{\mathrm{m}}) \right]}{\left[\frac{\beta l}{2} (1 - \cos \theta_{\mathrm{m}}) \right]^2} \\ &= \frac{4\pi}{P_r ad} \frac{1}{2\eta} \frac{\omega^2 \mu^2 4}{16\pi^2 \omega^2 \mu \epsilon} I_{\mathrm{m}}^2 \left[\frac{\sin \theta_{\mathrm{m}}}{1 - \cos \theta_{\mathrm{m}}} \right]^2 \sin^2 \left[\frac{\beta l}{2} (1 - \cos \theta_{\mathrm{m}}) \right] \end{aligned} \tag{C.11}$$

Here, θ_{m} corresponds to the direction of the maximum radiation. Now the trigonometric function relation is applied: $\frac{\sin^2 \theta_{\mathrm{m}}}{(1 - \cos \theta_{\mathrm{m}})^2} = \frac{\left(2 \sin \frac{\theta_{\mathrm{m}}}{2} \cos \frac{\theta_{\mathrm{m}}}{2} \right)^2}{2 \sin^2 \frac{\theta_{\mathrm{m}}}{2}} = \cot^2 \frac{\theta_{\mathrm{m}}}{2}$, because $1 - \cos \theta_{\mathrm{m}} = \frac{0.371}{l/\lambda}$, and $\frac{\beta l}{2}(1 - \cos \theta_{\mathrm{m}}) = 0.371\pi$, thus $\sin \left[\frac{\beta l}{2} (1 - \cos \theta_{\mathrm{m}}) \right] = \sin(0.371\pi) = 0.919$. Rearranging these equations in (C.10), the following expression can be obtained:

$$D = \frac{\frac{1}{2\pi} I_{\mathrm{m}}^2 \sqrt{\frac{\mu}{\varepsilon}} \cot^2 \left[\frac{1}{2} \cos^{-1} (1 - \frac{0.371}{l/\lambda}) \right] (0.919)^2}{30 I_{\mathrm{m}}^2 \left[2.108 + \ln \frac{l}{\lambda} - \mathrm{Ci}(2\beta l) + \frac{\sin(2\beta l)}{2\beta l} \right]} \tag{C.12}$$

and because $\sqrt{\mu/\varepsilon}$ is approximately equal to $120\pi\ \Omega$, therefore the directivity has the following expression:

$$D = \frac{1.69 \cot^2 \left[\frac{1}{2} \cos^{-1} \left(1 - \frac{0.371}{l/\lambda} \right) \right]}{2.108 + \ln \frac{l}{\lambda} - \mathrm{Ci}(2\beta l) + \frac{\sin(2\beta l)}{2\beta l}} \tag{C.13}$$

Here, Ci is the cosine integral. The directivity can be simplified into a more simpler form through the asymptotic approximation:

$$D = \left(9.1\frac{l}{\lambda} - 1.7\right)\left(2.1 + \ln\frac{l}{\lambda}\right)^{-1} \tag{C.14}$$

An overlapped result by (C.13) and (C.14) can be observed in Fig. C.1.

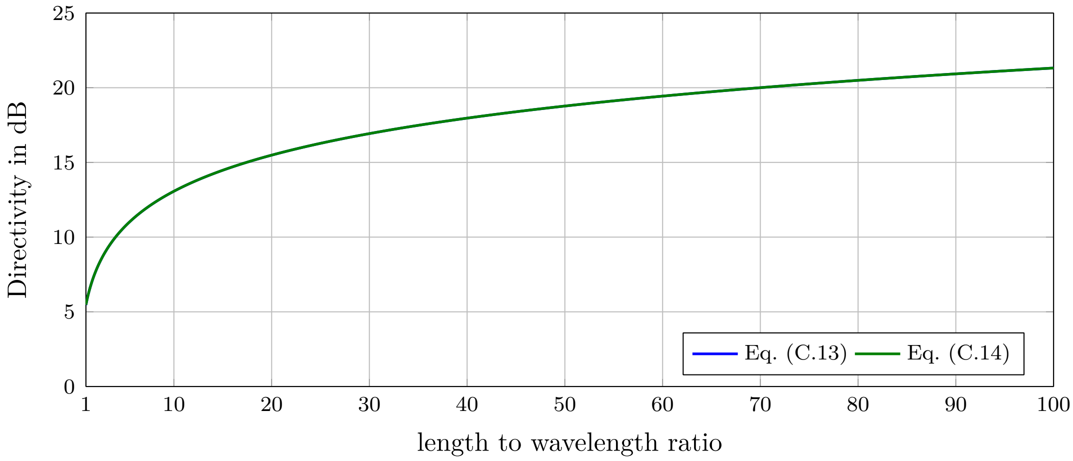

Figure C.1: Comparison of the directivity based on Eq. (C.13) and Eq. (C.14)

With a generalized coefficient C, the directivity can be classified into different cases:

$$D = C\left(9.1\frac{l}{\lambda} - 1.7\right)\left(2.1 + \ln\frac{l}{\lambda}\right)^{-1} \tag{C.15}$$

C.2 Comparison of traveling wave antennas and standing wave antennas

The coefficient C in (C.15) could take different values. Based on the radiation patterns in Fig. 2.9 and Fig. 2.10, the directivity could be determined and the coefficient C could be obtained, which can be classified into different cases:

1. in free space: $C = 1$
2. TWA horizontally placed above the PEC ground: $C = 4$
3. TWA vertically placed above the PEC ground: $C = 2\sqrt{2}$
4. $D_{\text{TWA}} = 2 \cdot D_{\text{SWA}}$ above the PEC ground

The directivity of the SWA and TWA with a length of 1 m in free space and 80 cm distance above ground is compared in Fig. C.2.

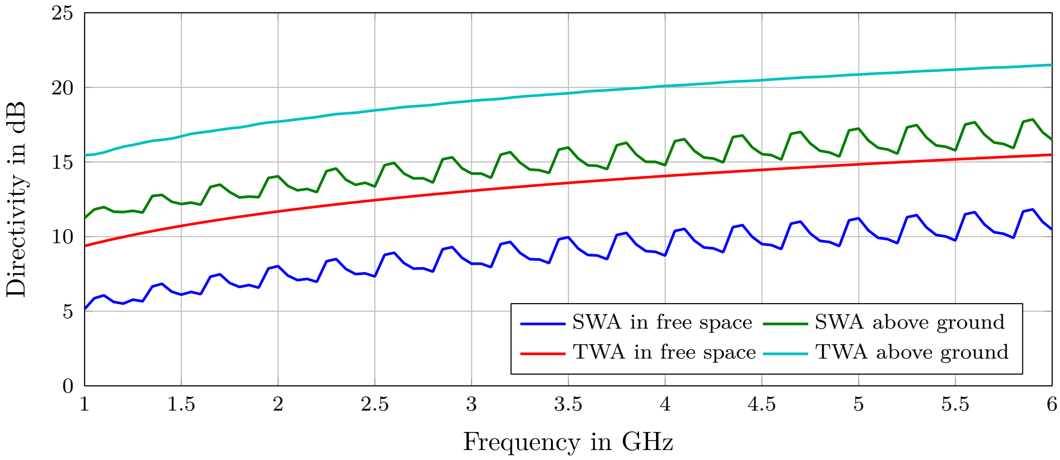

Figure C.2: Comparison of the directivity of the standing wave antenna and traveling wave antenna with the length of 1 m, located in free space and 80 cm distance above ground

The current distribution of a SWA oscillates forwards and backwards, therefore the current and E-field of the SWA is almost half of a TWA. Therefore the directivity difference is almost 3 dB between SWA and TWA with equivalent lengths of 1 m. A 6 dB difference of the directivity can be observed, when the SWA located in free space and 80 cm distance above ground, due to the fact that the ground plane doubles the electric field because of the ground reflection. This implies a constructive interference occurs because of the direct EM wave and the reflective EM wave due to the ground reflection.

D Influencing factors on directivity based on Monte Carlo simulations

Here, the influencing factors on directivity based on Monte Carlo simulation are investigated. The quantity N_{MCS} is the number of MCS, N_{obs} is the number of observation points, N_{dp} is the number of dipole source points with an observation distance R. The radius of the sphere is denoted by a and the considered frequency is indicated by f. The objective here is to analyze and quantify the influence of these different parameters, in order to minimize the uncertainties of the conversion between different test facilities.

D.1 Directivity as a function of the radius

In this part, the directivity is determined and their distribution is evaluated as a function of the radius. Here, $f = 1\,\mathrm{GHz}$ is kept constant, while changing the electrical size is realized by changing the radius a of the sphere. The observation distance is fixed, at $R = 10\,\mathrm{m}$, and with a constant number of dipoles $N_{\mathrm{dipoles}} = 50$ and the number of MCS $N_{\mathrm{MCS}} = 1000$. The *Ring* observation method is applied, which scans the EUT in a horizontal plane. The resulting CDF of $D_{\max}$ is shown in Fig. D.1. It is obvious that with increasing the radius a, $D_{\max}$ increases as well. The progression of CDF has a steep increase at the beginning and then converges to a constant value. In other words, the probability to miss the maximum emission level becomes larger when increasing the directivity. The results are in consistence with the work [Kra11]. The changing the electrical size ka corresponds to the shifting of the distribution.

D.2 Directivity as a function of the frequency

Instead of changing the radius of the sphere, another proposed method to change the electrical size is realized by changing the frequency, while keeping the radius of the sphere constant at $a = 0.27\,\mathrm{m}$, the number of dipoles is $N_{\mathrm{dipoles}} = 50$, the number of MCS is $N_{\mathrm{MCS}} = 1000$, the number of observation points is $N_{\mathrm{obs}} = 50$, and the measurement distance is $r = 10\,\mathrm{m}$ by using the *Ring* observation method. The resulting CDF is plotted in Fig. D.2, which has a similar effect as in Fig. D.1. The directivity seems proportionally

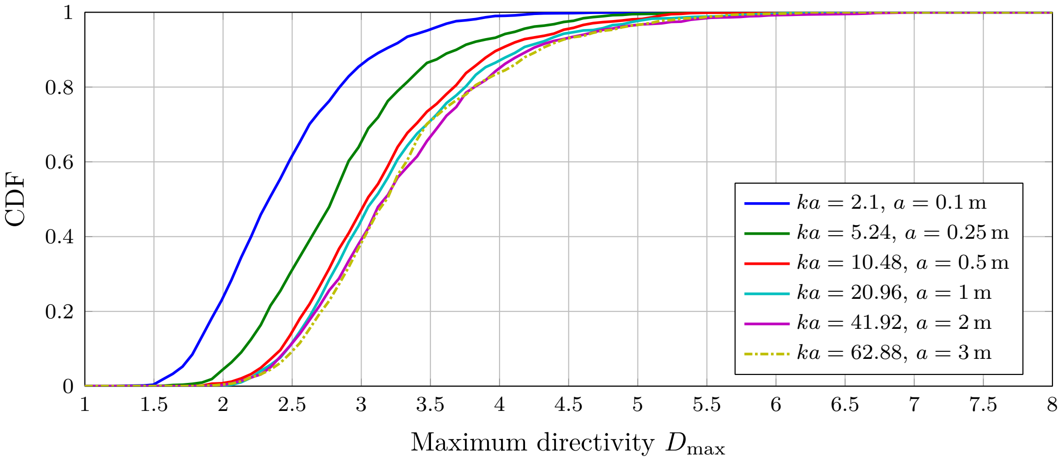

Figure D.1: CDF of the directivity dependent on the radius a, with parameters $N_{\text{dipoles}} = 50$, $N_{\text{MCS}} = 1000$, $N_{\text{obs}} = 50$, $r = 10\,\mathrm{m}$, $f = 1\,\mathrm{GHz}$, using the *Ring* observation method

convergent to a maximum value. It can be also observed that the shifting of the CDF in the diagram is approximately proportional to the shifting of the directivity. A similar result can be observed in [Kra11], the shifting of the directivity is approximately linearly changed, which could be mathematically described.

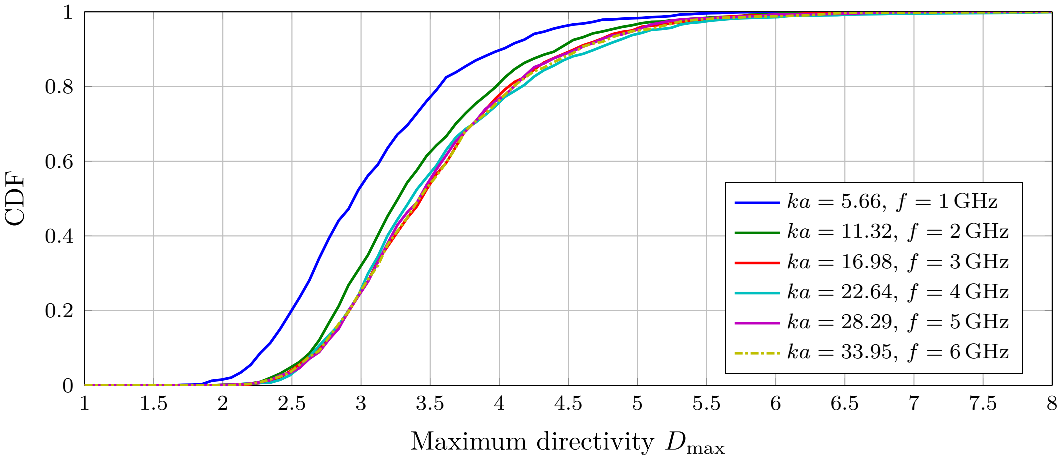

Figure D.2: CDF of the directivity in dependence of the electrical size ka, keeping the radius a constant $a_{\text{EUT}} = 0.27\,\mathrm{m}$, with parameters $N_{\text{dipoles}} = 50$, $N_{\text{MCS}} = 1000$, $N_{\text{obs}} = 50$ and $r = 10\,\mathrm{m}$, using the *Ring* observation method

D.3 Directivity as a function of the number of sampling points

The number of sampling points is an important parameter in the MCS, which corresponds to the required efforts during the measurements. The other parameters keep unchanged, with parameters $N_{\text{dipoles}} = 50$, $N_{\text{MCS}} = 1000$, $f = 1\,\mathrm{GHz}$ and $r = 10\,\mathrm{m}$. The progress of the CDF in dependence of the sampling density using the Ring observation method is shown in Fig. D.3.

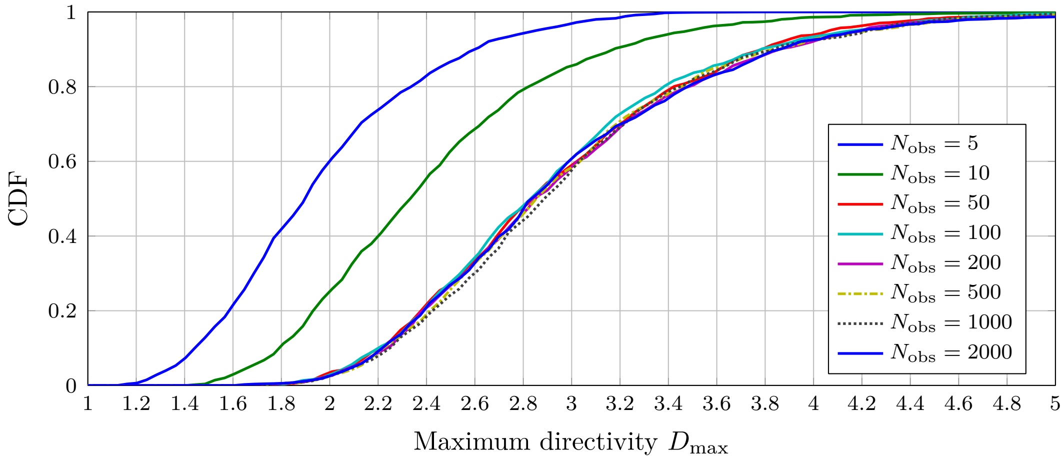

Figure D.3: CDF of the directivity in dependence of the number of sampling points, with parameters $N_{\text{dipoles}} = 50$, $N_{\text{MCS}} = 1000$, $f = 1\,\text{GHz}$, $r = 10\,\text{m}$, using the *Ring* observation method

The results are obtained by keeping all other parameters constant, the frequency is at 1 GHz with 50 dipoles superimposed to form the EUT, the radius of the EUT is $a = 0.27\,\text{m}$ and the MCS is performed 1000 times. It can be observed that the number of sampling points increases with the radius of the EUTs. More sampling points are required for larger radii of the EUT, which has almost a proportional relation. This implies that the uncertainties of different measurement methods can be reduced by properly increasing the sampling density.

D.4 Directivity as a function of the number of dipole sources

Another important influencing factor is the number of emission sources N_{dp} per EUT. The other parameters keep constant. The frequency is at 1 GHz, the number of MCS is $N_{\text{MCS}} = 1000$, the radius of the EUT is $a = 0.27\,\text{m}$ and the observation distance is 10 m. It is shown in Fig. D.4 that $D_{\max}$ increases with N_{dp}, which is convergent to a maximum value very fast.

D.5 Directivity as a function of the number of Monte Carlo simulations

The influence in dependence of number of MCS is also considered, with other parameters constant, $N_{\text{dipoles}} = 50$, $N_{\text{obs}} = 50$ using Ring observation method, $f = 1\,\text{GHz}$, $r = 10\,\text{m}$,

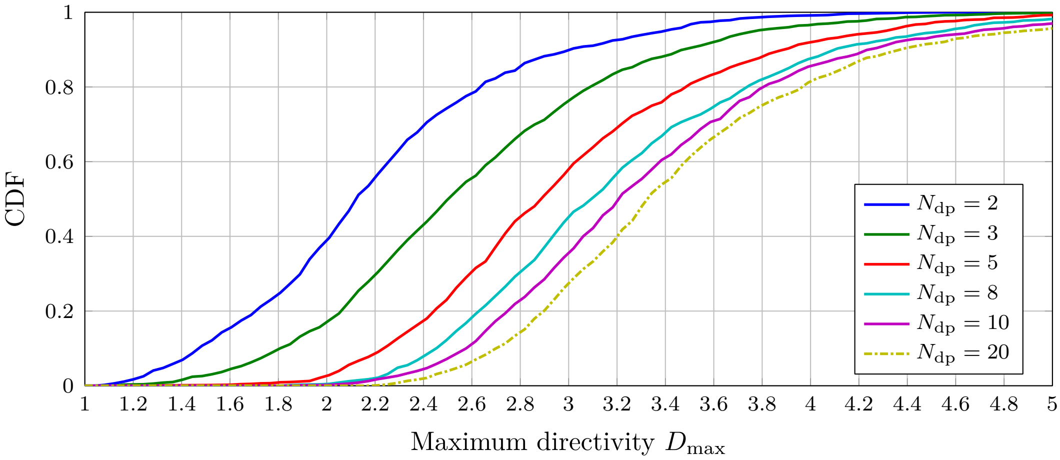

Figure D.4: CDF of the directivity, in dependence of the number of dipole sources, with parameters $N_{\mathrm{MCS}} = 1000$, $f = 1\,\mathrm{GHz}$, $r = 10\,\mathrm{m}$, $a_{\mathrm{EUT}} = 0.27\,\mathrm{m}$, using the *Ring* observation method

and $a_{\mathrm{EUT}} = 0.27\,\mathrm{m}$. The result is shown in Fig. D.5. It is noticeable that with increasing the number of MCS, the CDF of the directivity is changing slightly with a certain fluctuation. In order to obtain a more smooth curve, a larger number of MCS is preferred.

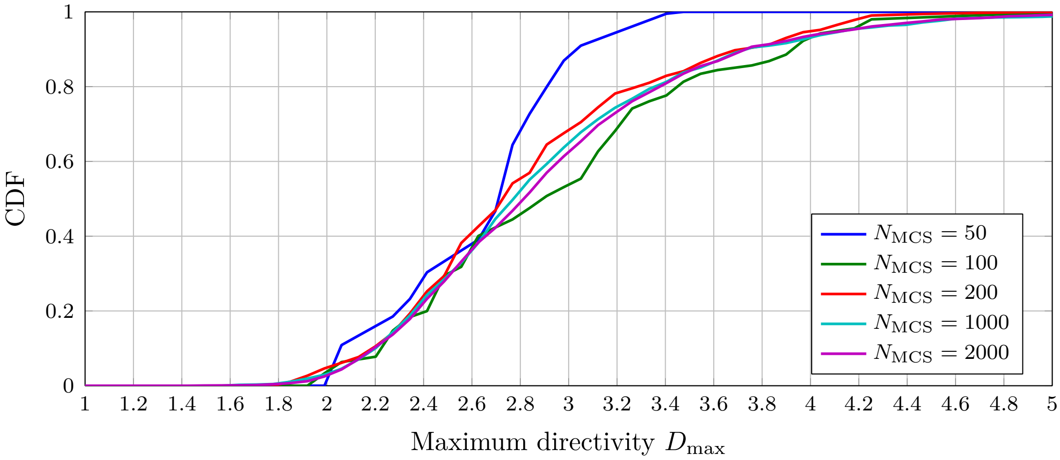

Figure D.5: CDF of the directivity in dependence of the number of MCS, with parameters $N_{\mathrm{dipoles}} = 50$, $N_{\mathrm{obs}} = 50$, $f = 1\,\mathrm{GHz}$, $r = 10\,\mathrm{m}$, $a_{\mathrm{EUT}} = 0.27\,\mathrm{m}$, using *Ring* observation method

D.6 Directivity comparison of three observation methods

In this part, three observation methods are applied. The *Sphere* observation method deals with the sampling on a spherical surface, representing a quasi-real measurement. The *Cylinder* observation method takes the sampling on a cylindrical surface into account, representing a measurement in an OATS. And the *Ring* observation method considers the sampling on a ring plane, standing for a FAR measurement. With other parameters constant, $N_{\mathrm{dp}} = 50$, $N_{\mathrm{MCS}} = 1000$, $N_{\mathrm{obs}} = 50$, $r = 10\,\mathrm{m}$, $a_{\mathrm{EUT}} = 0.27\,\mathrm{m}$, the resulting D_{max} has been determined with these three observation methods, which is shown in Fig. D.6.

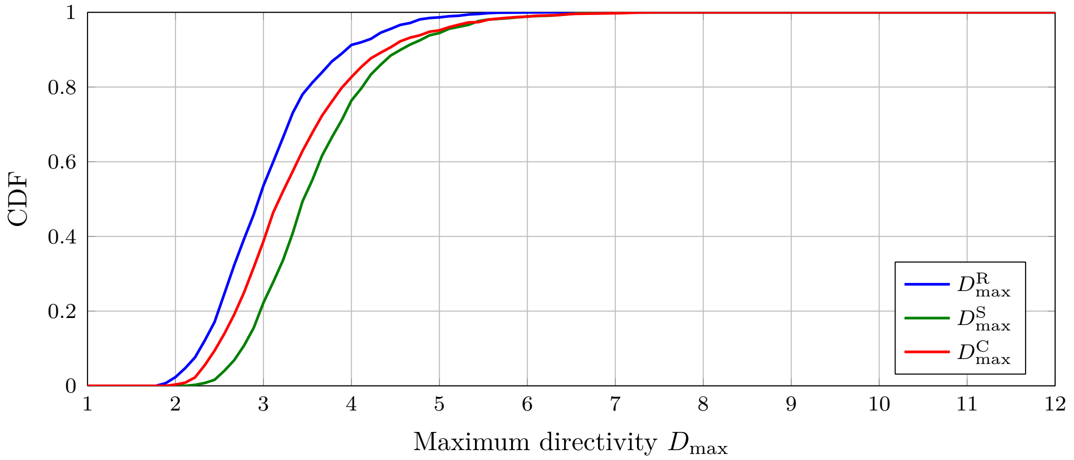

Figure D.6: Comparison of the directivity progression with *Sphere*, *Cylinder* and *Ring* observation methods, with parameters $N_{\mathrm{dipoles}} = 50$, $N_{\mathrm{MCS}} = 1000$, $N_{\mathrm{obs}} = 50$, $r = 10\,\mathrm{m}$, $a_{\mathrm{EUT}} = 0.27\,\mathrm{m}$

It can be seen that the directivity $D^{\mathrm{R}}_{\mathrm{max}}$ obtained by the *Ring* method is expected to be smaller than the directivity $D^{\mathrm{S}}_{\mathrm{max}}$ determined by the *Sphere* method. The reason lies in that in general the maximum field strength is not always on the ring plane. The directivity $D^{\mathrm{C}}_{\mathrm{max}}$ based on the *Cylinder* method locates between these two boundaries, so that $D^{\mathrm{R}}_{\mathrm{max}} < D^{\mathrm{C}}_{\mathrm{max}} < D^{\mathrm{S}}_{\mathrm{max}}$, which is consistent with the observation in [Kra11].

In a short summary, the electrical size *ka* is the decisive factor to determine the sampling density. It also shows that the selection of sampling methods, the number of small sources and the number of MCS has a considerable effect on the accuracy of the measurement results.

E Reference antenna measurement

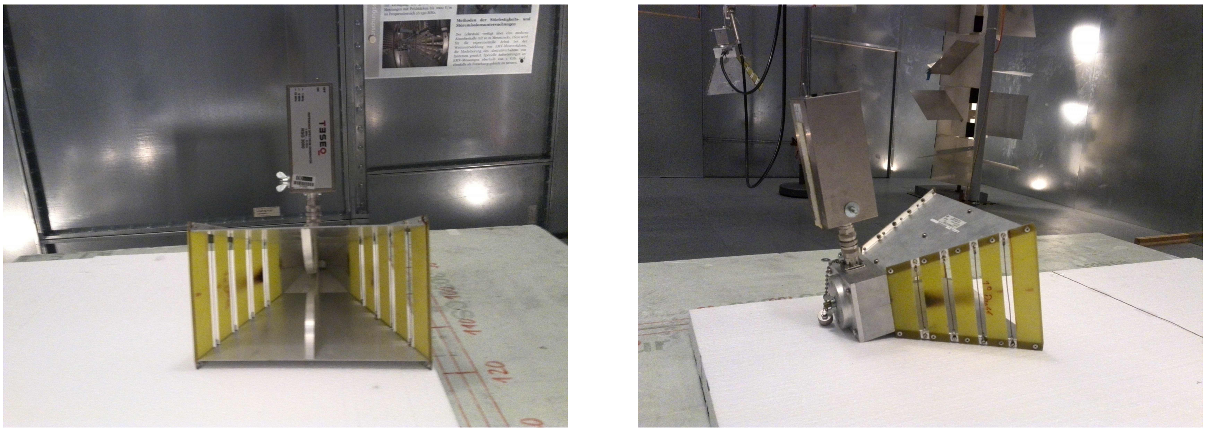

(a) Front view

(b) Side view

Figure E.1: A horn antenna as the reference antenna during the measurement in the MSC at the Otto von Guericke university in Magdeburg.

F Analytical solution for the model consisting of the slotted enclosure and the attached wire

F.1 Analytical solution of the E-field strength based on the current distribution

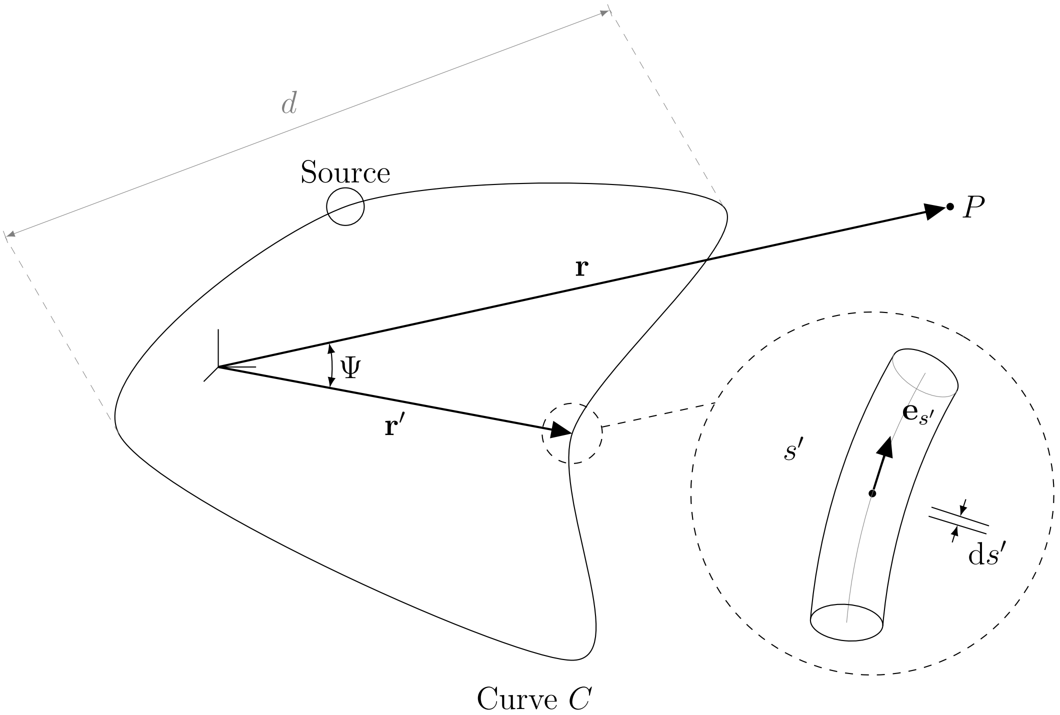

Figure F.1: Geometry of an arbitrary radiation source

Based on the current distribution, the electric field strength can be obtained by:

$$\mathbf{E}(r) = \frac{-\mathrm{j}\omega\mu_0}{4\pi r}\,\mathrm{e}^{-\mathrm{j}kr}\int\limits_C I(s')\,\mathrm{e}^{\mathrm{j}k\mathbf{e}_r\cdot\mathbf{r}'}\left[\mathbf{e}_{s'} - \mathbf{e}_r\left(\mathbf{e}_r\cdot\mathbf{e}_{s'}\right)\right]\mathrm{d}s' \tag{F.1}$$

Using $s' = z$, $\mathbf{r}' = z\mathbf{e}_z$:

$$\mathbf{E}(r) = \frac{-\mathrm{j}\omega\mu_0}{4\pi r}\,\mathrm{e}^{-\mathrm{j}kr}\left[\mathbf{e}_z - \mathbf{e}_r\left(\mathbf{e}_r\cdot\mathbf{e}_z\right)\right]\int\limits_{z_1}^{z_2} I(z)\,\mathrm{e}^{\mathrm{j}kz(\mathbf{e}_r\cdot\mathbf{e}_z)}\,\mathrm{d}z \tag{F.2}$$

The unit vector for a straight wire according to [Smi97] is $[\mathbf{e}_z - \mathbf{e}_r\left(\mathbf{e}_r\cdot\mathbf{e}_z\right)] = -\sin(\theta)\mathbf{e}_\theta$, and the inner product $\mathbf{e}_r \cdot \mathbf{e}_z = \cos\theta$,

$$E_\theta(r) = \frac{\mathrm{j}k\eta}{4\pi r}\,\mathrm{e}^{-\mathrm{j}kr}\sin\theta \int\limits_{z_1}^{z_2} I(z)\,\mathrm{e}^{\mathrm{j}kz\cos\theta}\,\mathrm{d}z \tag{F.3}$$

F.2 Coefficients for triangular functions of currents

Table F.1: Coefficients of the current distribution

Frequency in GHz	C_1^1	C_1^2	C_2^1	C_2^2
1	0.018	0.002	-0.030	-0.033
1.05	0.014	-0.017	0.004	-0.034
1.1	0.047	-0.010	0.006	-0.015
1.15	0.033	0.013	-0.035	-0.046
1.2	0.020	-0.036	-0.001	-0.037
1.25	0.038	-0.012	-0.013	-0.008
1.3	0.020	0.007	-0.020	-0.030
1.35	0.020	-0.025	0.005	-0.046
1.4	0.046	-0.017	-0.022	-0.008
1.45	0.013	-0.002	-0.023	-0.030
1.5	0.017	-0.190	0.004	-0.030
1.55	0.050	-0.012	-0.007	-0.014
1.6	0.016	-0.005	-0.036	-0.043
1.65	0.019	-0.032	-0.003	-0.024
1.7	0.035	-0.009	-0.016	-0.009
1.75	0.018	0.002	-0.026	-0.037
1.8	0.024	-0.042	-0.003	-0.030
1.85	0.029	-0.012	-0.026	-0.006
1.9	0.009	-0.006	-0.002	-0.028
1.95	0.020	-0.021	0.003	-0.029
2	0.045	-0.013	-0.029	-0.010

Table F.1: (continued)

Frequency in GHz	C_1^1	C_1^2	C_2^1	C_2^2
2.05	0.005	-0.016	-0.026	-0.031
2.1	0.020	-0.028	-0.004	-0.016
2.15	0.034	-0.008	-0.022	-0.010
2.2	0.008	-0.016	-0.030	-0.041
2.25	0.020	-0.036	-0.011	-0.008
2.3	0.019	-0.009	-0.025	-0.007
2.35	0.006	-0.011	-0.018	-0.028
2.4	0.026	-0.036	-0.005	-0.017
2.45	0.020	-0.012	-0.036	-0.007
2.5	0.002	-0.020	-0.017	-0.023
2.55	0.022	-0.027	-0.007	-0.010
2.6	0.027	-0.009	-0.037	-0.011
2.65	-0.004	-0.032	-0.022	-0.023
2.7	0.015	-0.026	-0.015	0.002
2.75	0.012	-0.008	-0.028	-0.009
2.8	0.0008	-0.026	-0.018	-0.027
2.85	0.018	-0.031	-0.020	0.006
2.9	0.003	-0.01	-0.028	-0.007
2.95	0.001	-0.024	-0.012	-0.017
3	0.024	-0.029	-0.017	0.001
3.05	-0.002	-0.015	-0.040	-0.009
3.1	-0.004	-0.030	-0.012	-0.004
3.15	0.013	-0.018	-0.020	0.005
3.2	-0.001	-0.013	-0.033	-0.012
3.25	-0.005	-0.037	-0.012	-0.000
3.3	0.005	-0.014	-0.021	0.010
3.35	-0.005	-0.013	-0.022	-0.008

Table F.1: (continued)

Frequency in GHz	C_1^1	C_1^2	C_2^1	C_2^2
3.4	0.001	-0.033	-0.011	-0.005
3.45	0.005	-0.017	-0.030	0.015
3.5	-0.014	-0.016	-0.020	-0.002
3.55	0.000	-0.025	-0.010	0.006
3.6	0.003	-0.013	-0.030	0.010
3.65	-0.023	-0.020	-0.018	0.000
3.7	-0.004	-0.018	-0.009	0.014
3.75	-0.005	-0.008	-0.021	0.007
3.8	-0.016	-0.022	-0.015	-0.002
3.85	-0.004	-0.020	-0.011	0.022
3.9	-0.012	-0.005	-0.018	0.009
3.95	-0.013	-0.018	-0.008	0.004
4	-0.002	-0.017	-0.015	0.022
4.05	-0.023	-0.002	-0.016	0.010
4.1	-0.013	-0.012	-0.001	0.011
4.15	-0.006	-0.005	-0.011	0.016
4.2	-0.023	-0.005	-0.013	0.006
4.25	-0.012	-0.011	0.004	0.017
4.3	-0.008	0.001	-0.007	0.014
4.35	-0.017	-0.006	-0.005	0.006
4.4	-0.010	-0.010	0.002	0.022
4.45	-0.013	0.009	-0.005	0.013
4.5	-0.014	-0.002	0.003	0.007
4.55	-0.007	-0.001	0.000	0.017
4.6	-0.017	0.01	-0.002	0.008
4.65	-0.009	-0.0002	0.009	0.007
4.7	-0.005	0.004	0.002	0.011

Table F.1: (continued)

Frequency in GHz	C_1^1	C_1^2	C_2^1	C_2^2
4.75	-0.014	0.005	0.001	0.005
4.8	-0.006	0.001	0.013	0.011
4.85	-0.003	0.009	0.002	0.008
4.9	-0.008	0.004	0.005	0.003
4.95	-0.002	0.005	0.008	0.010
5	-0.003	0.011	0.002	0.000
5.05	-0.004	0.003	0.006	-0.001
5.1	-0.001	0.005	0.004	0.004
5.15	-0.004	0.007	0.004	-0.002
5.2	0.001	0.001	0.007	-0.000
5.25	0.002	0.003	0.003	0.002
5.3	-0.001	0.003	0.004	-0.001
5.35	0.004	0.002	0.003	0.001
5.4	0.001	0.003	-0.001	-0.001
5.45	-0.003	0.001	0.001	-0.001
5.5	0.001	0.002	-0.000	-0.001
5.55	-0.001	0.000	-0.001	-0.002
5.6	-0.001	-0.001	0.001	-0.001
5.65	-0.001	-0.000	0.008	0.006
5.7	-0.009	-0.001	0.000	0.001
5.75	-0.001	-0.001	0.001	0.002
5.8	-0.000	0.000	0.000	0.003
5.85	-0.002	0.002	-0.001	0.002
5.9	-0.002	0.001	0.001	0.002
5.95	-0.002	0.003	0.002	0.002
6	-0.001	0.002	0.002	0.002

G Simulated E-field strength in the FAR for the stochastic model of the enclosure with stochastically varying slots and $1\,\mathrm{m}$ wire

```
        Frequency / GHz                Emax = E_ref / dBV/m
----------------------------------------------------------------------
                       1                       19.850056
                    1.05                       17.893005
                     1.1                       19.936017
                    1.15                       20.913531
                     1.2                       19.048336
                    1.25                       20.180337
                     1.3                       20.871827
                    1.35                        18.68461
                     1.4                       19.798668
                    1.45                       20.757648
                     1.5                       19.390531
                    1.55                       20.324568
                     1.6                       21.408048
                    1.65                        20.12101
                     1.7                       20.687642
                    1.75                       21.683785
                     1.8                       19.833556
                    1.85                       20.353289
                     1.9                       21.281433
                    1.95                       19.899104
                       2                       20.898868
                    2.05                        22.34373
                     2.1                        20.69675
                    2.15                       21.591766
                     2.2                       22.828976
                    2.25                       20.635161
                     2.3                       21.400424
                    2.35                       22.489405
                     2.4                       20.693875
                    2.45                       21.677088
                     2.5                       22.988446
                    2.55                       21.767177
                     2.6                       22.510169
```

2.65	23.435718
2.7	21.764936
2.75	22.198431
2.8	23.016387
2.85	21.12733
2.9	22.115841
2.95	23.112769
3	21.630614
3.05	22.79973
3.1	23.803395
3.15	21.932278
3.2	22.742361
3.25	23.316021
3.3	21.207
3.35	22.519991
3.4	23.023371
3.45	21.508493
3.5	23.394108
3.55	23.639054
3.6	22.153833
3.65	23.836626
3.7	23.326579
3.75	21.235824
3.8	23.505332
3.85	22.853354
3.9	20.996978
3.95	24.064955
4	23.528328
4.05	21.719198
4.1	24.574002
4.15	23.656553
4.2	21.303762
4.25	24.15827
4.3	22.922496
4.35	21.067128
4.4	24.264921
4.45	23.106661
4.5	21.710894
4.55	24.926731
4.6	23.268414
4.65	21.945664
4.7	24.652282
4.75	22.404877
4.8	21.854543
4.85	24.388157
4.9	22.170129
4.95	22.663663

```
                       5                       24.862833
                    5.05                       22.679315
                     5.1                       23.299682
                    5.15                       24.551537
                     5.2                       22.006721
                    5.25                       23.477549
                     5.3                        23.86922
                    5.35                       21.281255
                     5.4                       24.150015
                    5.45                        23.94767
                     5.5                       21.629136
                    5.55                       24.880039
                     5.6                       23.984047
                    5.65                       21.185257
                     5.7                       24.825713
                    5.75                       23.100067
                     5.8                       20.848196
                    5.85                       24.996783
                     5.9                       22.805403
                    5.95                       21.438603
                       6                       25.262898
```

```
        Frequency / GHz                E_FAR / dBV/m
----------------------------------------------------------------------
                       1                       18.925893
                    1.05                       16.794725
                     1.1                       19.152975
                    1.15                       20.334962
                     1.2                       18.074821
                    1.25                       19.223794
                     1.3                       20.389573
                    1.35                       17.793025
                     1.4                        19.08844
                    1.45                       20.513769
                     1.5                       18.604717
                    1.55                       19.873944
                     1.6                       21.327927
                    1.65                       19.657575
                     1.7                       20.149348
                    1.75                       21.421932
                     1.8                       19.316425
                    1.85                       19.893229
                     1.9                       20.930632
```

1.95	19.214091
2	20.534425
2.05	21.690856
2.1	19.921136
2.15	21.321648
2.2	22.183701
2.25	19.67926
2.3	20.875718
2.35	21.776939
2.4	19.83866
2.45	21.125954
2.5	22.385189
2.55	20.902623
2.6	21.801419
2.65	22.785836
2.7	20.880659
2.75	21.637569
2.8	22.051061
2.85	20.252367
2.9	21.786884
2.95	22.187006
3	20.647814
3.05	22.721507
3.1	22.931126
3.15	20.808161
3.2	22.66639
3.25	22.503383
3.3	20.21224
3.35	22.137014
3.4	22.103662
3.45	20.435616
3.5	22.924241
3.55	22.717994
3.6	21.016479
3.65	23.270036
3.7	22.330919
3.75	20.280291
3.8	22.883739
3.85	21.72003
3.9	20.16709
3.95	23.401855
4	22.308174
4.05	21.144148
4.1	23.867799
4.15	22.354758
4.2	21.020701
4.25	23.263884

4.3	21.483862
4.35	20.530201
4.4	23.176224
4.45	21.594224
4.5	21.277658
4.55	23.574449
4.6	21.68922
4.65	21.686769
4.7	23.231272
4.75	20.60523
4.8	21.650861
4.85	22.833572
4.9	20.331163
4.95	22.2885
5	23.161593
5.05	20.681404
5.1	22.777339
5.15	22.941603
5.2	20.020097
5.25	22.651398
5.3	22.063952
5.35	19.714003
5.4	22.89931
5.45	21.849747
5.5	20.757354
5.55	23.357072
5.6	21.692707
5.65	20.96353
5.7	23.120004
5.75	20.61659
5.8	20.596082
5.85	22.919253
5.9	20.042966
5.95	21.023195
6	22.764472